

# Aerosol processes relevant for the Netherlands

J. M. J. Aan de Brugh

## **Thesis committee**

### **Promotor**

Prof. dr. M. C. Krol  
Professor of Air Quality and Atmospheric Chemistry  
Wageningen University

### **Co-promotor**

Dr. M. Schaap  
Researcher Air Quality  
TNO, Earth, Environment and Life Sciences  
Research Group Climate, Air and Sustainability

### **Other members**

Prof. dr. ir. W. de Vries, Wageningen University  
Prof. M. Kanakidou, University of Crete, Greece  
Dr. E. G. Nemitz, Centre for Ecology and Hydrology, Midlothian, Great Britain  
Dr. G. J. H. Roelofs, Utrecht University, The Netherlands

This research was conducted under the auspices of the SENSE Research School

# Aerosol processes relevant for the Netherlands

J. M. J. Aan de Brugh

## **Thesis**

submitted in fulfilment of the requirements of the degree of doctor  
at Wageningen University  
by the authority of the Rector Magnificus  
Prof. dr. M. J. Kropff,  
in the presence of the  
Thesis Committee appointed by the Academic Board  
to be defended in public  
on Friday 22 February 2013  
at 4 p.m. in the Aula.

J. M. J. Aan de Brugh  
Aerosol processes relevant for the Netherlands  
175 pages

PhD thesis, Wageningen University, Wageningen, NL (2013)  
With references, with summaries in Dutch and English

ISBN 978-94-6173-421-1

# Contents

---

<b>Summary</b>	<b>9</b>
<b>Samenvatting</b>	<b>13</b>
<b>1 Introduction</b>	<b>17</b>
1.1 Aerosols, health and climate . . . . .	18
1.2 The aerosol life cycle . . . . .	20
1.3 Research in this thesis . . . . .	25
<b>2 Measurements and models</b>	<b>29</b>
2.1 Measuring aerosols . . . . .	30
2.2 Modelling aerosols . . . . .	31
2.2.1 Modal representation of aerosols . . . . .	32
2.2.2 Aerosol optics . . . . .	34
2.2.3 Use of different models . . . . .	36
<b>3 The European aerosol budget in 2006</b>	<b>39</b>
3.1 Introduction . . . . .	40
3.2 Model and measurements . . . . .	42
3.2.1 TM5 model description . . . . .	42
3.2.2 Aerosol module description . . . . .	42
3.2.2.1 Aerosol dynamics . . . . .	43
3.2.2.2 Ammonium and nitrate . . . . .	44
3.2.2.3 Dry deposition . . . . .	44
3.2.2.4 Wet deposition . . . . .	45
3.2.2.5 Emission . . . . .	45
3.2.2.6 Aerosol optics . . . . .	47
3.2.3 In-situ measurements . . . . .	48
3.3 Results and discussion . . . . .	49
3.3.1 Concentration distribution . . . . .	49
3.3.2 Model evaluation . . . . .	51
3.3.2.1 Annual means . . . . .	51
3.3.2.2 Time series January 2006 . . . . .	55
3.3.3 The aerosol budget . . . . .	55
3.3.4 Optical analysis . . . . .	62

3.3.5	Uncertainty analysis . . . . .	66
3.3.5.1	Wet deposition . . . . .	66
3.3.5.2	Forest fires . . . . .	67
3.4	Conclusions . . . . .	69
<b>4</b>	<b>Modelling the partitioning of ammonium nitrate in the convective boundary layer</b>	<b>71</b>
4.1	Introduction . . . . .	72
4.2	Materials and methods . . . . .	74
4.2.1	Observations . . . . .	75
4.2.2	The model . . . . .	76
4.2.2.1	Meteorological module . . . . .	77
4.2.2.2	Chemical module . . . . .	77
4.2.2.3	Optical module . . . . .	78
4.3	Results and discussion . . . . .	82
4.3.1	ISORROPIA only . . . . .	82
4.3.2	Column model results . . . . .	84
4.3.2.1	Tuning the meteorology . . . . .	84
4.3.2.2	Partitioning at the surface . . . . .	84
4.3.2.3	Aerosol nitrate profiles . . . . .	87
4.3.2.4	Optical analysis . . . . .	90
4.3.3	Sensitivity of optical properties . . . . .	92
4.3.4	Correcting the instant equilibrium . . . . .	94
4.4	Conclusions . . . . .	95
<b>5</b>	<b>A large-eddy simulation of the phase transition of ammonium nitrate in a convective boundary layer</b>	<b>97</b>
5.1	Introduction . . . . .	98
5.2	Numerical simulation . . . . .	100
5.3	Results . . . . .	103
5.3.1	Vertical profiles . . . . .	107
5.3.2	Sensitivity to the partitioning timescale . . . . .	109
5.3.3	Probability density functions . . . . .	110
5.3.4	Effects of a colder boundary layer on the partitioning . . .	113
5.4	Discussion . . . . .	114
5.5	Conclusion . . . . .	116
<b>6</b>	<b>The Generic Aerosol Optics Toolbox: an aerosol optics module for any atmospheric model</b>	<b>117</b>
6.1	Introduction . . . . .	118
6.2	Theory . . . . .	120
6.2.1	Effective-medium theory . . . . .	120
6.2.2	Optical properties of aerosols . . . . .	121
6.2.3	The Mie-curve . . . . .	122
6.3	Implementation . . . . .	126
6.3.1	Lookup table generator . . . . .	127

---

6.3.2	Coupling to a model . . . . .	130
6.4	Applications . . . . .	132
6.5	Conclusions . . . . .	134
<b>7</b>	<b>General discussion and outlook</b>	<b>135</b>
7.1	General findings . . . . .	136
7.1.1	European aerosol budget and uncertainties . . . . .	136
7.1.2	Delay in ammonium nitrate partitioning . . . . .	137
7.1.3	Influence on the partitioning of ammonium nitrate by turbulence . . . . .	138
7.1.4	Implementation of aerosol optics in models . . . . .	138
7.2	Challenges . . . . .	139
7.2.1	Wet removal of aerosols . . . . .	139
7.2.2	More dynamic aerosol modes . . . . .	140
7.2.3	Displacement between nitrate and chloride . . . . .	140
7.2.4	Modelling the partitioning timescale . . . . .	141
7.3	Perspective . . . . .	141
	<b>Bibliography</b>	<b>143</b>
	<b>Publications</b>	<b>165</b>
	<b>Acknowledgements</b>	<b>167</b>
	<b>Index</b>	<b>171</b>
	<b>SENSE certificate</b>	<b>173</b>
	<b>Support</b>	<b>175</b>



# Summary

---

Particulate matter (or aerosols) are particles suspended in the atmosphere. Aerosols are believed to be the most important pollutant associated with increased human mortality and morbidity. Therefore, it is important to investigate the relationship between sources of aerosols (such as industry) and the concentration of harmful aerosols at ground level. Furthermore, aerosols influence the climate system by scattering and absorbing solar radiation and by influencing cloud properties. The total climate effect of aerosols is poorly understood compared to the climate effect of greenhouse gases. Therefore, climate studies also benefit from a better understanding of aerosols.

The goal of this thesis is to investigate the spatial distribution of aerosols over Europe with focus on the Netherlands. The aerosol life cycle and effects are calculated with numerical simulations. Performing numerical simulations of aerosols is very challenging, because, in contrast to gas molecules, each individual aerosol differs in size, composition and microphysical properties. Without simplifications, a model has to track each individual particle, which would take far too much computational time, even for modern supercomputers. The challenge is to design simplifications in such a way that the life cycle of aerosols and the effects of aerosols on human health and climate are still properly represented.

Many model studies are supported by measurements. Both the measurements and the models can have different purposes. Using the correct combination of different models and observations is key for studies on aerosols. A different combination of models and observations is required to accomplish the different sub goals of this thesis. These sub goals are:

- Investigation of the aerosol life cycle over Europe
- Improvement of the understanding of gas-aerosol phase transition of ammonium nitrate and aerosol optics
- Improvement of representation of aerosols and their effects in models

The life cycle of aerosols in Europe is investigated in chapter 3. The full life cycle of aerosols has been implemented in a global transport model. It is concluded that Europe is a net source of anthropogenic (man-made) aerosols and a net sink of natural aerosols. The most important sink of anthropogenic aerosols is removal by clouds and rain, while natural aerosols are removed predominantly

by dry deposition processes. By comparing model results with observations, it is concluded that the largest uncertainties are caused by the parameterisation of wet removal processes and by missing emissions.

In the Netherlands, emissions of nitrogen oxides and ammonia are high because of the high population density and intensive agriculture. After oxidation of nitrogen oxides to nitric acid, ammonium nitrate aerosols can be formed. This aerosol is special, because it can evaporate under warm and dry conditions and condense back to the aerosol phase under cold and moist conditions. Like the case of clouds, the phase equilibrium changes with altitude as the atmospheric temperature decreases with altitude. The phase of ammonium nitrate is poorly detected by many measurement instruments, because the gas-aerosol partitioning can change inside the instrument. Partly due to the scarcity of reliable measurements, the phase transition of ammonium nitrate is poorly implemented in large-scale models.

Because ammonium nitrate aerosol and its phase transition is important for the aerosol budget of the Netherlands, this process has further been investigated in case studies. The goal of case studies is to gain detailed insight in the aerosol processes and, ultimately, to develop better parameterisations for large-scale models. These case-studies are performed with more detailed small-scale models. In these models, not the full aerosol life cycle is simulated but only the processes that are being investigated. A large advantage, however, is that these models have a higher resolution both in the spatial and the temporal domain. As a result, the important processes can be resolved more precisely.

Chapter 4 presents a case study where the interaction between ammonium nitrate phase transition and mixing in the lower atmosphere (boundary layer) is investigated for a warm day in spring. During an intensive measurement campaign near the Cabauw tower in the Netherlands, measurements of ammonium nitrate have been performed. Importantly, the gas and the aerosol phases have been separated with a special instrument so that both concentrations are measured without errors due to phase transition inside the instrument. It is shown that the observed partitioning between gas and aerosol ammonium nitrate deviates significantly from the thermodynamic equilibrium. The hypothesised explanation for this mismatch is that aerosol-rich air from higher altitudes (where the aerosol phase is preferred due to lower temperatures) is transported to the surface, increasing the aerosol-phase fraction of ammonium nitrate at the surface. This implies that the thermodynamic equilibrium is not instantaneously restored at the surface. A simulation of ammonium nitrate partitioning in the boundary layer has been performed with a simplified column model. The match between model results and observations improved drastically when applying a delay timescale up to two hours for the gas-aerosol equilibrium.

The interaction between turbulence and ammonium nitrate partitioning is further investigated in a more detailed model study (chapter 5). In this model, turbulent motions are explicitly resolved. As highlighted above, downward motions are associated with higher aerosol concentrations, because the phase equilibrium of ammonium nitrate is shifted towards the aerosol phase at higher altitudes. Therefore, turbulent motions induce a fluctuating concentration of aerosol ammonium nitrate with updrafts containing lower aerosol ammonium nitrate concentrations and sub-

sidence motions containing enhanced aerosol ammonium nitrate concentrations. It is discussed that these fluctuations in observations may provide information about the speed of gas-aerosol partitioning, which is very difficult to measure directly.

Throughout chapters 3 to 5, several ideas for model improvements have been posed. These ideas originate both from knowledge gained in the studies and from further challenges that are discovered. One such improvement for models is a computationally efficient and adequate representation of the optical properties of aerosols. Implementation of aerosol optics has been quite challenging, because the physics of aerosol optics is very complicated. Chapter 6 presents a package that allows easy implementation of aerosol optics in atmospheric models that represent aerosols.

Aerosol modelling is a very challenging task and can be developed much further. In this thesis, important steps have been taken to improve knowledge about aerosols. Future research should proceed by unravelling remaining aerosol mysteries, such as those presented in the final chapter (7) of this thesis.



# Samenvatting

---

Fijnstof (of aërosolen) zijn deeltjes die in de atmosfeer zweven. Aërosolen worden beschouwd als de luchtverontreiniging die het meest verantwoordelijk is voor verhoogde ziekte en sterfte onder mensen. Daarom is het belangrijk om het verband tussen bronnen van aërosolen (zoals industrie) en de concentraties van schadelijke aërosolen op leefniveau te onderzoeken. Aërosolen beïnvloeden ook het klimaat door zonnestraling te verstrooien en te absorberen en door de eigenschappen van wolken te beïnvloeden. Het totale klimaateffect van aërosolen wordt relatief slecht begrepen vergeleken met het klimaateffect van broeikasgassen. Daarom zullen klimaatstudies ook voordeel hebben van een betere kennis over aërosolen.

Het doel van dit proefschrift is het onderzoeken van de ruimtelijke verdeling van aërosolen boven Europa met speciale aandacht voor Nederland. De levenscyclus en de effecten van aërosolen worden berekend met numerieke simulaties. Het uitvoeren van numerieke simulaties van aërosolen is zeer uitdagend, want, in tegenstelling tot gasmoleculen is ieder individueel deeltje anders qua grootte, samenstelling en microfysische eigenschappen. Zonder vereenvoudigingen zou een model ieder individueel deeltje moeten volgen, hetgeen veel te veel computerkracht zou kosten, zelfs voor moderne supercomputers. De uitdaging is om de vereenvoudigingen zodanig te ontwerpen dat de levenscyclus van aërosolen en de effecten van aërosolen op de menselijke gezondheid en het klimaat toch goed worden berekend.

Veel modelstudies worden ondersteund door metingen. Zowel de metingen als de modellen kunnen verschillende doelen hebben. Voor aërosolstudies is het belangrijk om de juiste combinatie van modellen en metingen te gebruiken. Voor de verschillende subdoelen in dit proefschrift zijn verschillende combinaties van metingen en modellen gewenst. Deze subdoelen zijn als volgt:

- Onderzoek naar de levenscyclus van aërosolen in Europa
- Het beter begrijpen van de faseovergang van ammoniumnitraat tussen gas en deeltjes en het beter begrijpen van aërosoloptica
- Het verbeteren van de representatie van aërosolen en de effecten van aërosolen in modellen

De levenscyclus van aërosolen in Europa wordt onderzocht in hoofdstuk 3. Hiervoor is de volledige levenscyclus van aërosolen geïmplementeerd in een mondiaal

transportmodel. Geconcludeerd is dat Europa en netto bron is van antropogene (door de mens gemaakte) aërosolen en een netto put van natuurlijke aërosolen. Antropogene aërosolen worden het effectiefst verwijderd door wolken en regen, terwijl natuurlijke aërosolen vooral verwijderd worden door droge depositieprocessen. Door modelresultaten met metingen te vergelijken is de conclusie getrokken dat de grootste onzekerheden in het model worden veroorzaakt door de parameterisatie van natte verwijdering en door onbekende emissies.

In Nederland zijn de emissies van stikstofdioxide en ammoniak hoog door de hoge bevolkingsdichtheid en de intensieve landbouw. Als stikstofdioxide worden geoxideerd tot salpeterzuur, dan kunnen er aërosolen van ammoniumnitraat ontstaan. Deze aërosolen zijn speciaal, want ze kunnen verdampen als het warm en droog is en weer condenseren op deeltjes als het weer kouder en vochtiger wordt. Net als bij wolken is het evenwicht tussen de fases afhankelijk van de hoogte, omdat de temperatuur van de atmosfeer afneemt met de hoogte. De faseovergang van ammoniumnitraat wordt door veel meetinstrumenten matig opgevangen, omdat er verdere faseovergang kan plaatsvinden binnen het meetinstrument zelf. Mede dankzij de schaarste aan betrouwbare metingen is de faseovergang van ammoniumnitraat nog niet zo goed geïmplementeerd in grootschalige modellen.

Omdat ammoniumnitraataërosolen en de faseovergang van ammoniumnitraat zo belangrijk zijn voor het aërosolbudget van Nederland, wordt dit proces verder onderzocht in specifieke studies. Het doel van specifieke aërosolstudies is om gedetailleerd inzicht in specifieke processen te verkrijgen en uiteindelijk om betere parameterisaties voor grootschalige modellen te ontwerpen. Zulke specifieke studies worden uitgevoerd met meer gedetailleerde, kleinschaligere modellen. In deze modellen wordt niet de volledige levenscyclus van aërosolen gesimuleerd, maar alleen de processen die op dat moment onderzocht worden. Een groot voordeel van deze kleinschalige modellen is dat ze een hogere resolutie hebben, zowel in de ruimte als in de tijd. Daarom kunnen de belangrijke processen preciezer worden opgelost.

Hoofdstuk 4 presenteert een studie naar de interactie tussen de faseovergang van ammoniumnitraat en het mengen van de lucht in de onderste laag van de atmosfeer (de grenslaag), voor een warme lentedag. Tijdens een intensieve meetcampagne rondom de toren in Cabauw (Nederland), zijn metingen naar ammoniumnitraat verricht. Bij deze metingen zijn de gasfase en de deeltjesfase gescheiden met een speciaal instrument, zodat beide concentraties gemeten kunnen worden, zonder fouten door verdere faseovergangen binnen het meetinstrument. De studie laat zien dat de verdeling tussen gas- en deeltjesfase die aan de grond gemeten is significant afwijkt van het thermodynamische evenwicht. De hypothese luidt dat dit verschil wordt veroorzaakt doordat lucht met veel ammoniumnitraat in deeltjesvorm vanaf hogere hoogtes (waar door de lagere temperatuur de deeltjesfase gunstiger is) naar beneden wordt getransporteerd, waardoor er aan de grond relatief meer ammoniumnitraat op deeltjes wordt geobserveerd. Dit impliceert dat het thermodynamische evenwicht niet instantaan wordt hersteld aan de grond. De faseovergang van ammoniumnitraat in de grenslaag is gesimuleerd met een eenvoudig kolommodel. De overeenkomst tussen de modelresultaten en de observaties verbeterde drastisch als er een vertraging tot twee uur werd toegepast voor het fase-evenwicht van ammoniumnitraat.

De interactie tussen turbulentie en de faseovergang van ammoniumnitraat is verder onderzocht in een gedetailleerdere modelstudie (hoofdstuk 5). In dit model worden de turbulente bewegingen expliciet opgelost. Zoals hierboven al opgemerkt is de concentratie ammoniumnitraat in deeltjes hoger in neergaande luchtstromen, omdat het fase-evenwicht naar de deeltjesfase is verschoven op hogere hoogtes. Daarom zorgen turbulente bewegingen voor fluctuaties in de concentratie ammoniumnitraat op deeltjes, met opwaartse luchtstromen met lagere concentraties ammoniumnitraat in de deeltjesfase en zakkende luchtstromen met hogere concentraties ammoniumnitraat in de deeltjesfase. Er wordt bediscussieerd dat fluctuaties in gemeten concentraties ammoniumnitraat informatie zouden kunnen bevatten over de snelheid waarop het fase-evenwicht zich instelt. Deze snelheid is moeilijk direct te meten.

In hoofdstukken 3 tot en met 5 zijn verschillende ideeën voorgesteld om modellen te verbeteren. Deze ideeën komen zowel door de verbeterde kennis die in de studies is opgedaan als door de verdere uitdagingen die zijn ontdekt. Eén zulke modelverbetering is een goede en efficiënte manier om de optische eigenschappen van aerosolen te berekenen. De implementatie van aerosooptica in modellen is altijd al uitdagend geweest, omdat de natuurkunde van deeltjesoptica zeer ingewikkeld is. Hoofdstuk 6 presenteert een softwarepakket dat het eenvoudig maakt om aerosooptica te implementeren in atmosferische modellen met aerosolen.

Het modelleren van aerosolen is zeer uitdagend en kan nog verder worden ontwikkeld. In dit proefschrift zijn belangrijke stappen genomen om de kennis over aerosolen te verbeteren. In de toekomst moet men verder gaan met het ontrafelen van verdere aerosolmysterieën. Deze mysterieën worden gepresenteerd in het laatste hoofdstuk (7) van dit proefschrift.



# 1

---

## Introduction

This thesis presents numerical studies about particulate matter, also referred to as aerosols. Aerosols are solid or liquid particles that are suspended in the atmosphere. Their size ranges from a few nanometres up to tens of microns, which makes them larger than gas molecules, but still light enough to remain suspended in air. The chemical composition of aerosols varies enormously. Over oceans, most aerosol particles consist of wind-blown sea salt and similarly, natural dust particles originate from deserts. Natural and man-made fires produce smoke which contains soot and organic matter. Aerosols are also formed by condensable gas molecules in the atmosphere. These so-called secondary aerosols often consist of inorganic salt or low-volatile organic components. Below, we will review the main reasons to study aerosols. In short, aerosols are believed to be the most important pollutant for adverse human health effects. Moreover, aerosols influence the climate system directly by scattering and absorbing solar radiation and indirectly by influencing cloud properties.

In the Netherlands, the combination of a high population density and intensive farming leads to large emissions of nitrogen oxides (from traffic) and ammonia (from agriculture). After chemical reactions in the atmosphere, these gases often end up as ammonium nitrate aerosols. These inorganic aerosols are semi-volatile, which means that these aerosols may evaporate at sufficiently high temperatures. This interesting property leads to an intriguing interplay between gas-aerosol phase transition and air motion in the lower atmosphere, a topic studied in chapters 4 and 5.

## 1.1 Aerosols, health and climate

Exposure to particles has been associated with severe health effects including enhanced mortality, cardiovascular, respiratory and allergic diseases (Pöschl, 2005; Bernstein et al., 2004). Atmospheric particles are believed to be the most important air pollutant responsible for these health effect. Even short-term exposure has been associated with increased mortality and morbidity (Brunekreef and Holgate, 2002; Dockery et al., 1993; Pope et al., 1995). Vulnerable people, such as elderly, young children and people with pre-existing lung issues experience increased adverse health effects from aerosols (Pope, 2000; Alessandrini et al., 2010).

Ultrafine particles are suspected to be particularly hazardous to human health, because they are sufficiently small to penetrate the membranes of the respiratory tract and enter the blood circulation or be transported along olfactory nerves into the brain (Pöschl, 2005; Stone and Donaldson, 1998). Fine particles cause inflammation and oxidative stress to a greater extent than coarse particles, because of their larger surface area per unit mass (Brown et al., 2001; Li et al., 2002; Alessandrini et al., 2009). Exposure to traffic-related air pollutants (black smoke and nitrogen dioxide) is expected to shorten life expectancy (Hoek et al., 2002). Natural aerosols, like sea salt, are expected to be less harmful due to their chemical composition and their relatively large size.

The aerosol concentration is often quantified up to a certain size threshold, ignoring the mass of the aerosols with a diameter larger than a predefined limit.

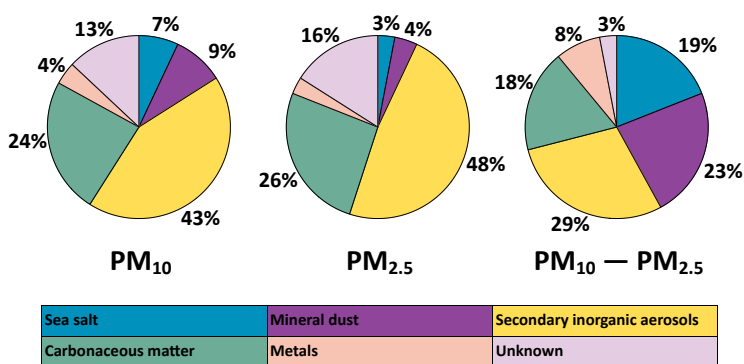


**Figure 1.1:** Figure from Schaap et al. (2010): Chemical composition of particulate matter finer than 10  $\mu\text{m}$ , finer than 2.5  $\mu\text{m}$ , and difference between the two, measured at the Cabauw tower (the Netherlands) in 2007–2008.

Commonly-used size limits are 10  $\mu\text{m}$  and 2.5  $\mu\text{m}$ . When applying these size limits, the measured aerosols are called PM<sub>10</sub> or PM<sub>2.5</sub>, which stands for particulate matter finer than 10 or 2.5 micrometres in diameter. Comparison between the chemical compositions of PM<sub>10</sub> and PM<sub>2.5</sub> provides information about the different aerosol types. Such an analysis (shown in Fig. 1.1) taken from (Schaap et al., 2010) clearly shows that sea salt and mineral dust reside on coarse aerosols and that secondary inorganic aerosols and carbonaceous aerosol reside primarily on fine aerosols.

The European Union has developed an extensive body of legislation which establishes health-based standards and objectives for a number of pollutants in air, both for gas-phase pollutants and for particulate matter. In 2005, the standards for particulate matter were based on PM<sub>10</sub> concentrations. The yearly average concentration of PM<sub>10</sub> is not allowed to exceed 40  $\mu\text{g}\text{m}^{-3}$  and the daily-averaged concentration of PM<sub>10</sub> is not allowed to exceed 50  $\mu\text{g}\text{m}^{-3}$  for more than 35 days per year. Because fine particulate matter is more harmful than coarse particulate matter, a new standard was developed for PM<sub>2.5</sub>. From 2015 onwards, the yearly-averaged concentration of PM<sub>2.5</sub> is not allowed to exceed 25  $\mu\text{g}\text{m}^{-3}$ . Note that legislation primarily targets the total aerosol mass. Except for a few heavy metals, no standard exist for the concentration of specific aerosol components, such as black carbon. These air quality standards are continuously in development and a better knowledge about the aerosol life cycle and the effect of aerosols on human health is required for an adequate definition of these standards.

Another effect of aerosols is that they influence the climate by altering the radiation budget of the earth through scattering and absorption of solar radiation (Hess et al., 1998; Haywood and Boucher, 2000; IPCC, 2007). Over polluted continental regions, the direct forcing of sulphate alone can be as large as that of the combined greenhouse gases, but opposite in sign (e.g. Charlson et al., 1992;

Kiehl and Briegleb, 1993). In the last decade, the influence on the radiation budget of a number of other aerosol components, like organic carbon, black carbon and mineral dust, has also been shown (IPCC, 2007).

Aerosols influence the climate system also indirectly by altering cloud properties (Rosenfeld et al., 2008; Kaufman et al., 2002). Additional cloud condensation nuclei (aerosols) slow the conversion of cloud drops into raindrops by nucleating larger number concentrations of smaller drops, which are slower to coalesce into raindrops, suppressing precipitation from shallow clouds (Rosenfeld et al., 2008). This influences the lifetime and the albedo (whiteness) of a cloud throughout its life cycle, altering the influence of clouds on the climate system. Scattering aerosols may also exert an indirect effect on climate. The increase in diffuse radiation enhances photosynthesis (Mercado et al., 2009), increasing the carbon dioxide uptake by plants and thereby reducing the greenhouse effect.

Aerosols are involved in many climate feedback loops, both positive and negative, of which many are related to the interaction between aerosols and radiation (Carslaw et al., 2010). Biogenic emissions of organic aerosols have a cooling effect due to scattering of solar radiation and addition of cloud condensation nuclei. These emissions are expected to increase by rising temperature and carbon dioxide concentration. Deposition of aerosol material on vegetation can, depending on their fertilising properties, increase or decrease the emission of biogenic organic aerosols, influencing the climate system (Pöschl, 2005). Aerosols can also have a warming effect. Deposition of carbonaceous aerosols on snow decreases the snow albedo (Carslaw et al., 2010). Absorption of radiation by black carbon in the atmosphere also has a warming effect (Chung and Seinfeld, 2005). Furthermore, eutrophication effects of aerosols may decrease photosynthesis and biogenic aerosol emissions, warming the climate (Pöschl, 2005).

The current estimates show that aerosols have a net cooling effect on climate. However, the uncertainties associated with the forcing estimates are large. Hence, the aerosol effect has masked the real climate sensitivity towards an increase in greenhouse gases to an unknown extent (Anderson et al., 2003). A better understanding of the role of aerosols in our atmosphere and improving its description in models is necessary to reduce uncertainties.

## 1.2 The aerosol life cycle

Aerosols enter the atmospheric in two different ways. Primary aerosols are directly emitted into the atmosphere, while secondary aerosols emerge by clustering of gas molecules. Figure 1.2 displays the main sources of primary and secondary aerosols. Primary emissions are indicated by direct arrows from the bottom row (sources) to the top row (aerosols). Secondary aerosols emerge indirectly by emission of gas species that subsequently cluster into particles or condense onto pre-existing particles. Production of secondary aerosols is displayed in Fig. 1.2 by a pathway from the bottom row (sources) via the middle row (gas species) to the top row (aerosols). In many cases, the emitted gas molecules only cluster into aerosols after being fully or partially oxidised in the atmosphere. This oxidation happens

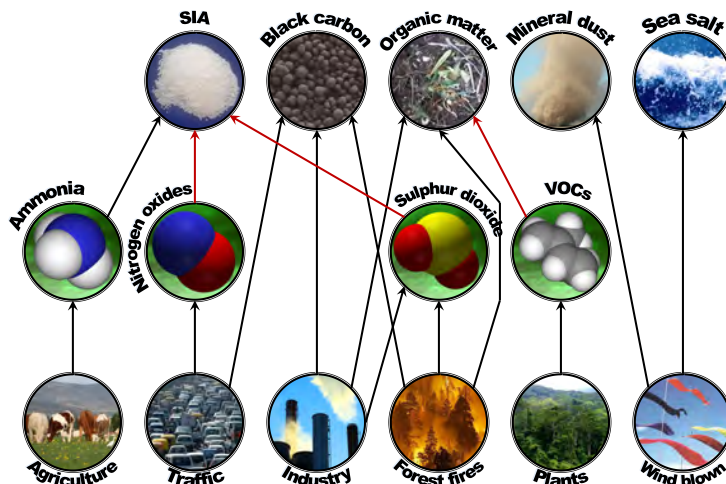


**Figure 1.2:** Main emission sources (lower row) of gases (middle row) and aerosols (upper row) and transitions between gases to aerosols. Red arrows involve oxidation. SIA stands for secondary inorganic aerosols and VOCs stand for volatile organic compounds.

naturally by the oxidising agents in the atmosphere such as the hydroxyl radical (OH), ozone ( $O_3$ ) and the nitrate radical ( $NO_3$ ).

A more detailed study on the origin of particulate matter in the Netherlands has been performed by Hendriks et al. (2012) in a model study (see Fig. 1.3). Clear is the large contribution of anthropogenic sources, especially agriculture and road transport. Note that although mineral dust is generally a natural aerosol component, previously deposited mineral dust can be resuspended into the atmosphere by anthropogenic activities. This explains the large contribution of road transport to the mineral dust in the Netherlands in Fig. 1.3. Naturally emitted Saharan dust is attributed as ‘outside domain’ in this model study, because the Sahara is outside their model domain.

Primary anthropogenic aerosols have a short production pathway (direct emission) and their emissions are concentrated in industrialised areas. Therefore, the concentrations of these aerosols are very high in these industrialised areas and are much lower in the rural environment. Primary natural aerosols have larger source areas, so the concentrations do not show such a hot-spot structure as for primary anthropogenic aerosols. The concentration of mineral dust in Europe shows a clear gradient with high concentrations in the south and low concentration in the north, because a main source of mineral dust is the Sahara desert. Sea salt concentrations are high exclusively above open sea and on coastal areas. Secondary aerosols show a smoother concentration field, because the emitted precursor gases have been transported and diffused before they cluster or condense into aerosols.

Emitted primary aerosols exist in all size ranges. Sea salt and mineral dust are relatively coarse ( $\sim \mu\text{m}$ ), while emitted carbonaceous aerosols from forest fires and traffic are much finer (10–100 nm) (Stier et al., 2005). Aerosols grow through

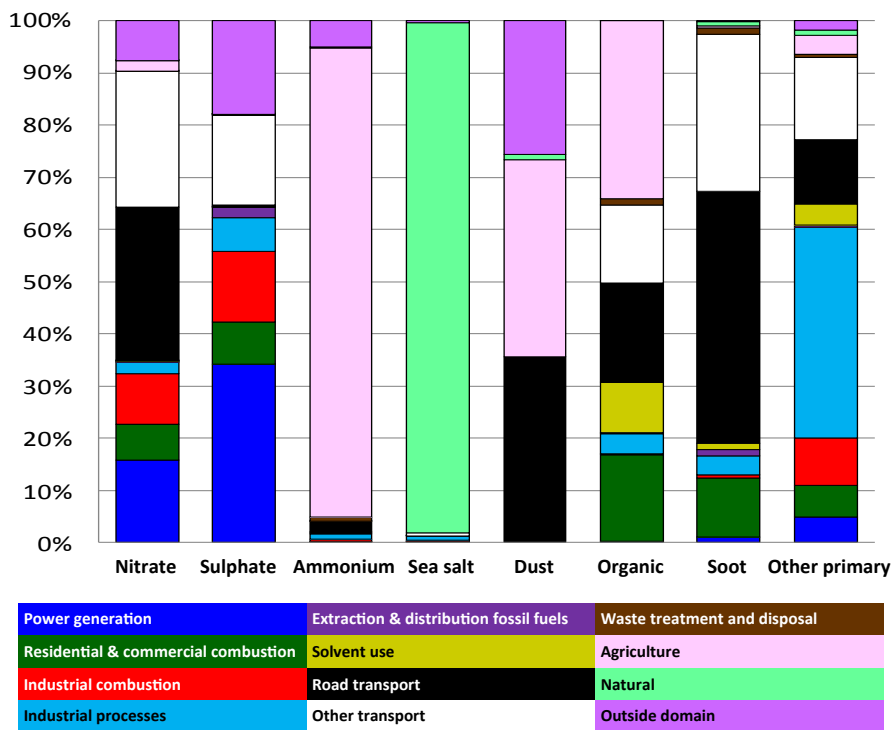


**Figure 1.3:** Figure from Hendriks et al. (2012): Modelled source contributions for different aerosol components in the Netherlands.

condensation of secondary aerosol material and by coagulation among aerosols. Condensation and coagulation also influence the mixing state of aerosols. Secondary aerosol material can condense on primary aerosols resulting in aerosols with a core of primary material (e.g. black carbon) coated with secondary material (e.g. ammonium sulphate). Coagulation between aerosols of different origin results in mixed aerosols consisting of several materials.

Both the size and the mixing state, which evolve during the life cycle of aerosols, influence the microphysical properties of the aerosols and thereby the efficiency at which further processes take place. For example, diffusive deposition removes predominantly the fine particles and gravity-driven sedimentation removes predominantly the coarse particles, so particles in the size range in between reside the longest in the atmosphere (Seinfeld, 1986). Furthermore, coating of water-insoluble particles with a layer of water-soluble material enhances hygroscopic growth and wet deposition.

Low-volatile gas molecules, like sulphuric acid, can cluster into new particles. Nucleation of new particles is hard to detect with common measurements instruments, because these particles are in the order of a nanometre in size. In polluted areas, most of those nanoparticles are taken up by other aerosols before they grow to a detectable size. In size-segregated observations of aerosols, nucleation events can be detected by an increase in fine particles, followed by a steady growth of these particles in time. These events are usually only observed in pristine areas with a lot of forest, like at the SMEAR II station (Hari and Kulmala, 2005) in Hyytiälä, Finland (Sihto et al., 2006, 2009). At the Cabauw tower (The Netherlands), nucleation events have been observed above the boundary layer (Wehner et al., 2010) during the EUCAARI campaign (Kulmala et al., 2009).

Figure 1.4 displays size ranges and solubility classes of aerosols from several sources. The transitions during the residence in the atmosphere are displayed with arrows. Insoluble aerosols become soluble by condensation of soluble matter or by coagulation with a soluble aerosol. This process is called aging and is displayed with blue arrows in Fig. 1.4. Soluble aerosols grow efficiently by further condensation of secondary matter and by coagulation with other aerosols. This growth is displayed with the green arrow in Fig. 1.4. However, coarse particles grow much less efficiently because the frequency of collisions is lower and the relative surface area for condensation is smaller. Note that no growth is displayed for insoluble aerosols because coagulation among insoluble aerosols is relatively inefficient. Under normal conditions, insoluble aerosols age to soluble aerosols before they have grown significantly. In Fig. 1.4, a measurement of the aerosol size distribution at Cabauw is included. The size axis of this graph also applies for the approximate size ranges of the displayed aerosols. The measurement technique is further explained in Sect. 2.1.

Aerosols are removed from the atmosphere when they are impacted at the surface or in the canopy. Where gas-phase species only exhibit diffusive deposition, aerosols can be removed both by diffusive deposition and by gravity-driven sedimentation. As mentioned above, the size of the aerosols is very important for both of these deposition processes. Where fine aerosols are more prone to diffusive deposition, coarse aerosols are removed more efficiently by sedimentation. Aerosols

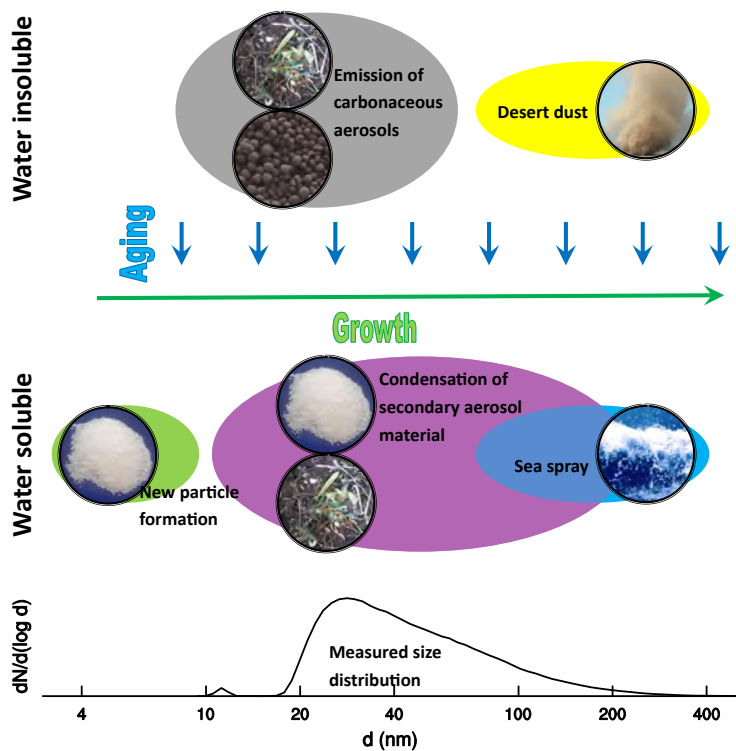


**Figure 1.4:** Display of aerosol sources and dynamic processes in a size and solubility domain. Displayed size ranges are rough approximations. A measured aerosol size distribution is added at the bottom.

---

with a moderate size ( $0.1 - 1.0 \mu\text{m}$ ) are removed the slowest by the two combined processes and therefore have the longest lifetime.

Clouds and rain also play a dominant role in aerosol removal. The model study in chapter 3 concludes that clouds and rain are the main sink for anthropogenic aerosols in Europe. Especially large convective clouds can efficiently remove aerosols from the entire atmospheric column. Wet deposition is challenging for modellers because the microphysical interaction between droplets and particles is quite complicated. Coarse-resolution models have additional difficulties with parameterising clouds and removal of aerosols in clouds, because these models cannot explicitly resolve the clouds. Moreover, wet deposition affects aerosols at high altitudes, where no continuous in-situ measurement are performed.

The lifetime of aerosols in the atmospheric is approximately one week. This implies that the transport pathways relevant for a local aerosol budget can be up to a few thousands of kilometres long. Long-range transport can be responsible for dust events. During these events, dust from the Sahara is transported all the way to the Netherlands. Also, emissions from a large forest fire in Russia in 2006 travelled all the way to Western Europe with easterly winds. As explained in chapter 3, this event caused significantly enhanced concentrations of carbonaceous aerosols for a large part of Europe.

### 1.3 Research in this thesis

Aerosols form a challenge for both models and measurements because aerosols vary widely in size and composition. Any measurement or model representation is an approximation of the real situation, because the full representation would require a description of the status of each individual particle. For gas-phase species, on the other hand, the concentration fully describes the situation, because each individual gas molecule of one specie is identical. For both observations and models, it is unrealistic to acquire a full description of the situation with respect to aerosols. Observations would have to analyse the microstructure of each individual particle, which is impossible. Models would have to track and describe the full microstructural parameters of each individual particle, which is also impossible.

It is however important to properly represent aerosols in air quality and climate models, because they play a vital role in climate and the toxicity of air. To make computational modelling feasible, several assumptions and approximation have to be applied. The challenge is to define these assumptions and approximations in such a way that the aerosol life cycle and the aerosol properties that affect human health and climate are represented in the model.

The aerosol size distribution is an important aspect as it influences the efficiency of microphysical aerosol processes (such as coagulation), the efficiency of deposition processes, the interaction between aerosols and radiation, and the ability of aerosols to act as cloud condensation nuclei. The aerosol mixing state, i.e. the degree to which different aerosol components reside on the same particles, also influences the aerosol life cycle and optical properties of aerosols. The life cycle is influenced, because coexistence of soluble material on aerosols with insoluble material causes

the insoluble material to be more susceptible to wet removal and further growth to larger sizes. The optical properties, which are complicated and highly nonlinear, also depend on the mixing state (see Sect. 2.2.2 and chapter 6).

The goal of this thesis is to investigate aerosols in Europe and in particular the Netherlands. Chapter 3 of the thesis investigates the aerosol budget in Europe. Quantification of the aerosol budget helps to understand the relationship between aerosol emissions and the concentration of aerosol on ground level, so that effective mitigation strategies can be defined. By comparison of model results to observations, it is concluded that the most uncertain aerosol processes are wet removal and emissions. Another difficult issue is the representation of ammonium nitrate aerosol, an aerosol type that is implemented in large-scale models only to a small degree of detail. Comparison with observations is difficult, because ammonium nitrate is also very difficult to measure (see Sect. 2.1 and chapters 3 and 4). The reason why ammonium nitrate is so difficult to measure and to simulate is that it can undergo a reversible, temperature-dependent phase transition to gas-phase ammonia and nitric acid.

In western Europe, secondary inorganic aerosols (which includes ammonium nitrate) and organic matter are the most abundant aerosol species (Putaud et al., 2004). In the Netherlands, secondary inorganic aerosols are particularly important because the ammonia emissions are very high compared to the rest of Europe due to intensive livestock (Buijsman et al., 1987). In the Netherlands, nearly half (42%–48%) of the fine aerosol (PM<sub>2.5</sub>) mass consists of secondary inorganic aerosols (Weijers et al., 2011) (see also Fig. 1.1). Both the direct and the indirect climate effect of secondary inorganic aerosols are large in the Netherlands. Secondary inorganic aerosols are the dominant anthropogenic aerosol species in the size range with maximum light scattering (0.4–1.0 μm) (ten Brink et al., 1997). Also, these aerosols are effective cloud condensation nuclei, because of their size and water solubility.

Because ammonium nitrate is so important for the Netherlands, it is vital to better understand the phase transition between gas-phase ammonia and nitric acid and aerosol ammonium nitrate. This process has been further investigated in smaller-scale models in chapters 4 and 5. The goal of these chapters is to enhance the knowledge about this process and its influence on modelled and observed quantities. Therefore, measurements can better be interpreted, parameterisation in models can be improved and mismatches between models and observations can better be explained.

As stated in Sect. 1.1, aerosols influence the climate system by scattering and absorbing solar radiation. In order to properly calculate the radiative forcing of aerosols, it is vital to understand the relationships between aerosols and radiation. Knowledge of these relationships is also necessary to interpret remote-sensing data (see Sect. 2.1). The physics that describes the relationship between aerosols and radiation is very complicated and modelling teams developing air-quality and climate models are largely oriented at other process description than the aerosol optical properties, so high-level expertise on this subject is often lacking. Arbitrary parameterisation for aerosol optics can impede model intercomparison. Therefore, chapter 6 presents a generic toolbox for aerosol optics that can be implemented

in any model that represents aerosols. The calculations use Mie-scattering theory and the assumptions on the representation of the aerosols in the model are well-documented in the software package and its documentation.

Chapters 3 to 6 are based on scientific articles that are either published or under review in scientific journals. They focus on the following general research questions:

- What are the main features of the European aerosol budget and what are the main sources of uncertainties in large-scale aerosol modelling? (chapter 3)
- How can a delayed gas-aerosol equilibrium for ammonium nitrate improve the match between modelled and observed ammonium nitrate concentrations? (chapter 4)
- How is the partitioning of nitrate between the gas and aerosol phase influenced by turbulent motions in a well-developed convective boundary layer? (chapter 5)
- How can aerosol optics be implemented properly without taking too much computational time in such a way that the same module can easily be adapted to different models? (chapter 6)



# 2

---

Measurements and models

The research in this thesis is performed mainly with numerical models, supported and validated with observations. Continuous observations for long periods are used in chapter 3 to validate our large-scale model calculations. Intensive campaign-based measurements are used for model evaluation and setup for case studies. To better appreciate aerosol observations, some basic aerosol measurement techniques are outlined in Sect. 2.1.

The main focus of this thesis is on the models themselves. Aerosols can be represented in models in many different ways, depending on the goal of the research. The models and the representations of aerosols in the different models are introduced in Sect. 2.2.

## 2.1 Measuring aerosols

In-situ measurements of aerosols are performed at ground-based measurement stations. A large network of measuring stations is the European Monitoring and Evaluation Programme (EMEP; Lazaridis et al., 2002; EMEP, 2008). These stations provide data for a host of pollutants. Measurements can be performed by filtering aerosols from an air stream and analysing the abundances of chemical substances that are present in the filtered material. This gives a total mass concentration of aerosol components in the atmosphere. To acquire the concentration of the most relevant particles, a size filtering can be applied. As discussed in Sect. 1.1, fine aerosols are more important for health than coarse aerosols. For a measurement of just the fine particles, coarse aerosols are filtered out by inserting a plate in such a way that the air stream is deflected at  $90^\circ$ . Due to their inertia, coarser particles will be impacted on the surface of the plate, while finer particles remain suspended in the air. The properties of the plate and the flow rate determine the cut-off size, which is defined as the aerodynamic diameter of which 50% of the particles pass. A common cut-off size is  $10\ \mu\text{m}$ , in which case the aerosols that pass are called  $\text{PM}_{10}$  (particulate matter finer than  $10\ \mu\text{m}$ ).

Unfortunately, measurements of secondary aerosol components are prone to sampling artefacts. Filter measurements are uncertain due to potential losses of ammonium nitrate and absorption of nitric acid and organic compounds (Vecchi et al., 2009). The abovementioned volatilisation and absorption artefacts cause the sampling of nitrate and ammonium to be difficult (Yu et al., 2006; Zhang and McMurry, 1992; Cheng and Tsai, 1997). Continuous measurements of total (gas plus aerosol phase) ammonium ( $\text{NH}_3 + \text{NH}_4^+$ ) and total nitrate ( $\text{HNO}_3 + \text{NO}_3^-$ ) are more widespread and therefore often used to validate large-scale models. Correct separation between aerosol and gas phase is only possible with denuders in combination with a filter pack or a Steam Jet Aerosol Collector (Slanina et al., 2001; Schaap et al., 2002; Trebs et al., 2004). For continuous measurements, these labour intensive are rarely used. Therefore, reliable measurements of aerosol ammonium nitrate are often campaign-based like EUCAARI-LONGREX (Kulmala et al., 2009) and the IMPACT-campaign at the Cabauw tower in the Netherlands (Morgan et al., 2010).

As mentioned in Sect. 1.3, the characterisation of the aerosol size distribution is

---

very important, both for health aspects and for climate effects of aerosols. This information can be obtained by size-resolved particle counters, such as the Scanning Mobility Particle Sizer (SMPS; Zieger et al., 2011; ten Brink et al., 1983; Wang and Flagan, 1990). The mobility size spectrometer consists of a sequential set-up of an impactor, neutraliser, differential mobility analyser (DMA) and a condensation particle counter (CPC). In the DMA, aerosol particles are classified according to their electrical mobility. The analyser consists of a cylinder with a negatively charged rod at the centre. Only aerosols in a narrow range of mobility exit through the output slit, where they enter the CPC, which determines the particle concentration of that size. The size of the particles reaching the output slit is being determined by the control rod voltage and the flow within the DMA. Before entering the DMA, aerosols are brought to a bipolar charge equilibrium using a  $^{85}\text{Kr}$  bipolar charger (neutraliser). In charge equilibrium, the fraction of particles with a single elementary charge is known for all sizes (Wiedensohler, 1988). Particles with diameters larger than about 800 nm are removed by a 0.0457 centimetre-diameter-orifice aerosol inlet in order to facilitate multiple charge correction. Because the aerosols are in charge equilibrium, the total number of particles can be calculated.

Information about aerosols can also be acquired by remote sensing. The interaction between aerosols and solar radiation is measured through ground-based networks (e.g. AERONET; Holben et al., 2001) and satellite-based sensors (e.g. MODIS; Justice et al., 1998). The obtained remote-sensing data provide information for the entire atmospheric column. Information on the entire column is of great importance to evaluate models as they complement traditional ground-based observations.

## 2.2 Modelling aerosols

As stated in Sect. 1.3, computational modelling of aerosols is only possible with several simplifications. A commonly-used simplification is the bulk approach. This approach discards all aspects of aerosol size and shape, so that only the amount of aerosol material per unit of volume air is represented. In many cases, the aerosols are assumed to be externally mixed. This implies that each individual particle consists of only a single component. With this assumption, sources and sinks of different aerosol components can be assumed independent of each other.

One of the disadvantages of the bulk approach is that it does not represent the aerosol size distribution. Several processes, such as deposition, depend on the aerosol size. A better representation of the aerosol size distribution therefore seems beneficial. A simple extension on the bulk approach is a bin scheme. In this approach, aerosols are represented by multiple tracers, each representing a size section (bin) of the aerosol distribution. In this way, different physical behaviour (e.g. deposition) of the different bins can be implemented in models.

### 2.2.1 Modal representation of aerosols

Though a bin scheme represents the aerosol size distribution, it remains rather static as the sizes of the bins are fixed. Many bins are required to represent a smooth aerosol size distribution, which leads to a large number of concentrations that have to be tracked in the model. A smooth aerosol size distribution can be modelled by using a so-called modal size distribution. A mode is a broad size section that can vary. This way, it is possible to model aerosols of any size with a limited number of scalars. Furthermore, aerosol processes that influence the size, such as coagulation and condensation, can be more properly modelled.

A popular modal aerosol module is M7 (Vignati et al., 2004). This aerosol scheme distinguishes seven modes with different sizes and water solubilities. These modes specify the aerosol mixing state and the aerosol size distribution. Each mode is assumed to be a population of aerosols that are internally mixed. This means that all aerosol components in a mode are distributed the same over all the particles in that mode, while different modes are assumed to be externally mixed (components of different modes do not reside on the same aerosol). This mixing state is important for aerosol processes such as solubility and interaction with radiation (see Sect. 1.3). However, it is difficult to validate whether the modelled mixing state is correct, because the mixing state is hard to derive from observations.

Each mode is assumed to be a lognormal size distribution that together represent the entire aerosol size distribution. Such a lognormal distribution is determined with three variables: the total number concentration ( $N$ ), the median size ( $\bar{r}_g$ ) and the geometric standard deviation ( $\sigma$ ). Note that  $\bar{r}_g$  actually means the geometric mean of the size. This is equal to the median size in a lognormal distribution. The lognormal distribution is given in Seinfeld (1986):

$$\frac{dN}{d \ln r} = \frac{N}{\sqrt{2\pi} \ln \sigma} \cdot e^{-\frac{(\ln r - \ln \bar{r}_g)^2}{2 \ln^2 \sigma}} \quad (2.1)$$

An advantage of a lognormal distribution is that, if the perspective is transformed to aerosol mass or surface area, it is again a lognormal distribution. Here, the lognormal distribution is expressed from the perspective of the number concentration ( $N$ ). For several size-dependent aerosol processes, the distribution should be transformed to a perspective of aerosol mass ( $\sim r^3$ ) or aerosol surface area ( $\sim r^2$ ). These perspectives are the second and third moments of the distribution respectively.

$$\frac{dN_\gamma}{d \ln r} \equiv r^\gamma \frac{dN}{d \ln r} \quad (2.2)$$

This formula defines the  $\gamma^{\text{th}}$  moment of the distribution. As stated above, this is also a lognormal distribution. Compared to the zeroth moment (Eq. 2.1), the median size ( $\bar{r}_{g\gamma}$ ) and the magnitude change, but the geometric standard deviation remains the same. The amplification of the magnitude is the arithmetic mean of  $r^\gamma$ .

$$\bar{r}_{g\gamma} = \bar{r}_g e^{\gamma \ln^2 \sigma} \quad (2.3)$$

$$\bar{r}^\gamma = \bar{r}_g^{-\gamma} e^{\frac{\gamma^2 \ln^2 \sigma}{2}} \quad (2.4)$$

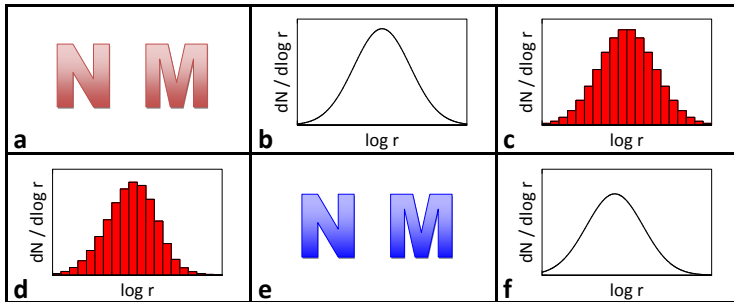


**Figure 2.1:** Diagram describing how a size-dependent process is resolved on an assumed lognormal aerosol mode. Panel a: variables describing the mode before the process. Panel b: Assumed lognormal distribution before the process. Panel c: Binned size distribution before the process. Panel d: Binned size distribution after the process. Panel e: Variables describing the mode after the process. Panel f: Assumed lognormal distribution after the process.

In M7, the size distribution of a mode is fully determined with the number concentration and the mass concentrations of the components (e.g. sulphate, black carbon, sea salt). To obtain the lognormal distribution, the relationship between the number (zeroth moment) and the mass (third moment) is used. Furthermore, it is assumed that all aerosols are spherical.

$$\sum_i \frac{M_i}{\rho_i} = \frac{4}{3}\pi N \bar{r}^3 = \frac{4}{3}\pi N \bar{r}_g^3 e^{\frac{9 \ln^2 \sigma}{2}} \quad (2.5)$$

Unfortunately, this equation still has two unknowns:  $\bar{r}_g$  and  $\sigma$ . For a unique solution, one more assumption has to be made. In M7, the standard deviation ( $\sigma$ ) is assumed fixed, so that  $\bar{r}_g$  can be solved from Eq. 2.5.

The lognormal distribution of the modes is used when the aerosols are subject to size-dependent processes, such as sedimentation. This is illustrated in Fig. 2.1. Before the process, the mode is represented with the number concentration and the mass concentrations (panel a). The aerosol module assumes a lognormal distribution with a prescribed standard deviation that correspond to these concentrations (panel b). For the size-dependent process, the lognormal distribution is discretised in size bins (panel c). The process is resolved for each of these size bins independently. In this example, the coarser aerosols are removed more efficiently than the fine aerosols (panel d). By summing up the numbers and masses of all these bins, new values for the number and mass concentrations are obtained (panel e). A new lognormal distribution with the same standard deviation is assumed for the next size-dependent process (panel f). The size distribution that the model assumes for the next size-dependent process (panel f) is not equal to the size distribution that is calculated after the process (panel d). This numeric diffusion is inevitable because the aerosol size distribution has to be determined from just the number and mass concentrations.

### 2.2.2 Aerosol optics

As stated in Sect. 1.1, aerosols affect the climate by scattering and absorbing solar radiation. To quantify this direct climate effect in models, it is important to properly calculate the aerosol optical properties in these models. Furthermore, optical calculations in models can be utilised to interpret remote-sensing measurements (see Sect. 2.1) or to use these measurements to validate the model.

The radiative properties of aerosols are generally summarised in three variables: the extinction cross section ( $\sigma_{\text{ext}}$ ), the single-scattering albedo ( $a$ ) and the asymmetry parameter ( $g$ ). These three variables indicate how efficiently radiation is absorbed and scattered by aerosols and to what extent forward scattering is preferred over backwards scattering. Most radiation models, such as TUV (Madronich, 1987), implement the aerosol effect on radiation with these three variables.

Calculation of optical properties can be done to different extents of complexity, depending on how aerosols are represented in the model. Models with a bulk aerosol approach may use a fixed optical activity per unit of mass for each aerosol component. Models with a bin scheme or a modal approach can take the size-dependence into account. Besides the size distribution, the mixing state is important as well.

The interaction between homogeneous spherical particles and electromagnetic radiation is defined in Mie-theory (Mie, 1908). Models implementing size-dependent aerosol optics use this theory or an approximation of it. Because Mie-theory is defined for homogeneous spherical particles, the models that use it assume implicitly that aerosols are homogeneous and spherical. Though this homogeneous sphere approximation is generally quite accurate, it was pointed out that this could lead to an underestimation in the aerosol radiative forcing close to black-carbon sources (Kahnert, 2010a).

Mie-theory describes how efficiently radiation is absorbed and scattered by spherical particles. Important parameters are the wavelength of the light ( $\lambda$ ), the radius of the spherical particle ( $r$ ) and the complex refractive index ( $m$ ). Mie-theory can be defined as two functions, one for absorption ( $M_a$ ) and one for scattering ( $M_s$ ), of which the latter also depends on the scattering angle,  $\varphi$  (see Fig. 2.2).

$$P_{\text{abs}} = I_0 \cdot M_a(m, r, \lambda) \quad (2.6)$$

$$\frac{dP_{\text{sca}}}{d\varphi} = I_0 \cdot M_s(m, r, \lambda, \varphi) \quad (2.7)$$

Here,  $I_0$  is the incoming light intensity at wavelength  $\lambda$  (in  $\text{Wm}^{-2}\text{nm}^{-1}$ ),  $P_{\text{abs}}$  is the power of absorbed light (in  $\text{Wnm}^{-1}$ ). The scattered light is expressed as the differential power with respect to the scattering angle (in  $\text{Wnm}^{-1}\text{rad}^{-1}$ ). Note that this quantity is already integrated over the azimuthal angle.

The variables that are used to describe the optical properties of aerosols are the extinction cross section, the single scattering albedo and the asymmetry parameter. These variables can be obtained from the Mie-formulas (Eqs. 2.6 and 2.7). The extinction cross section and the single-scattering albedo can be obtained straight forward after calculating the total scattering cross section by integrating Eq. 2.7

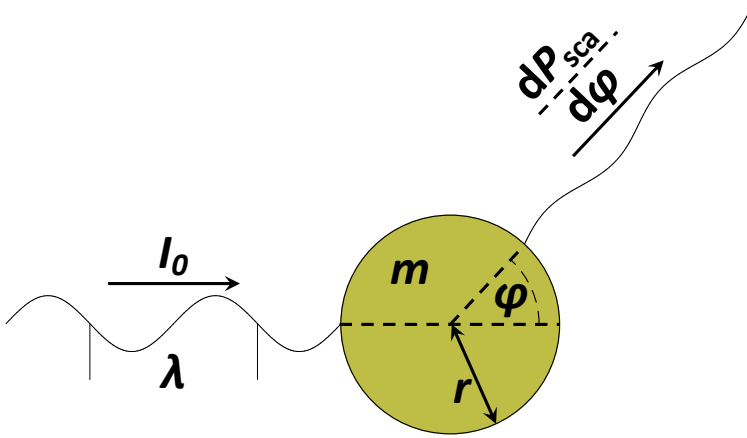


**Figure 2.2:** Diagram of a light beam that is scattered by a homogeneous spherical particle in a specific angle. All relevant parameters are highlighted with symbols.

over the scattering angle. The asymmetry parameter can also be obtained from Eq. 2.7. In fact, it is a simplification from the angle-distribution that is described in Mie-scattering. The asymmetry parameter is defined as the average cosine of the scattering angles of all scattered radiation and is calculated as follows:

$$g \equiv \frac{\int_0^\pi \cos \varphi \cdot \frac{dP_{sca}}{d\varphi} \cdot d\varphi}{\int_0^\pi \frac{dP_{sca}}{d\varphi} \cdot d\varphi} \quad (2.8)$$

In one-dimensional radiation models, the asymmetry parameter is interpreted as a distribution between two possible scattering directions: forward and backward, the only two possible direction in a one-dimensional model. The distribution between forward and backward scattering is such that the average cosine of the scattering angle is still equal to  $g$ .

$$\sigma_{sca,f} = \frac{1}{2}(1 + g)\sigma_{sca} \quad (2.9)$$

$$\sigma_{sca,b} = \frac{1}{2}(1 - g)\sigma_{sca} \quad (2.10)$$

Here the subscripts ‘f’ and ‘b’ stand for forward and backward.

The optical activity of aerosols per unit mass strongly depends on the aerosol size distribution. Aerosols with diameter between 0.4 and 1.0  $\mu\text{m}$  scatter visible light the most efficiently per unit of aerosol mass. Models that do not resolve the aerosol size cannot perform Mie-calculation that make any sense, unless they utilise other methods to acquire information about the size distribution (e.g. using observations). Most models nowadays, however, use a size-resolved representation of aerosols (e.g. with M7) because of the size-dependence of other aerosol processes. Aerosol modules like M7 also include a representation of the aerosol water uptake. Aerosol water uptake influences the aerosol size and composition and is therefore

important for the aerosol optical properties. With such a modern aerosol module, a proper calculation of the aerosol optical properties is possible in many models.

### 2.2.3 Use of different models

A study focussing on the aerosol budget over Europe is presented in chapter 3. Aerosols are simulated in different kinds of models, varying in complexity and scale. Large-scale models, such as TM5 (see chapter 3), are designed to reproduce observations or to predict large-scale changes induced by changing circumstances (e.g. global warming or emission scenarios). In these kinds of models, a compromise has to be found between computational efficiency and the accuracy by which the aerosol processes are represented. The end result is more important than neat representations of all individual processes. All processes have to be implemented in the model, also when detailed knowledge of the process is lacking. In such a case, a parameterisation may be based on empirical formulas or on approximations. The uncertainty of these parameterisations can be high. For further model development and for the interpretation of the results, it is important that uncertain parameterisations of difficult processes are documented very well. Comparison of model results with observations is very important in large-scale models, because this assesses the model's ability to represent the large-scale situation. A study focussing on the aerosol budget over Europe is presented in chapter 3.

Large-scale models are less effective in unravelling individual processes, because the uncertainty of that individual process is always masked by the uncertainties of other relevant processes. In large-scale models, where all processes are relevant, this masking uncertainty may be quite significant. Smaller-scale models, such as a column model or a large-eddy simulation (chapters 4 and 5) are better at analysing individual processes, because the uncertainties caused by other processes can be reduced for multiple reasons. First, smaller-scale models have a finer spatial and temporal resolution. Therefore, processes that are theoretically well-described can be more properly resolved, reducing their uncertainties. Second, it is easier to reduce the number of relevant processes. For instance, if cloud processes cause a large uncertainty, it is beneficial to avoid clouds in the simulation (a golden day). This is better possible in smaller-scale models, because one cloudless day in one location is more realistic than a cloudless month for entire Europe. Another way to reduce uncertainties by other processes is by avoiding implementation of these processes using observations. Instead of implementing the process, the result of that process can be obtained from observations and applied to the model. This requires a data set for the entire (temporal and spatial) model domain, which is possible more easily for small-scale models. Note that this use of observations is only possible if the process that is being analysed has no influence on the observed quantity.

There is another aspect where end-result-oriented models differ from process-oriented models. Process-oriented models can be simplified further than what is realistic, creating so-called idealised model setups. As mentioned above, it is not realistic to have a month without clouds for whole Europe. However, if such an analysis is desired, the situation can be simulated in a model by turning off clouds.

The disadvantage is that there are no observations for such a case, so comparison with observations is impossible.

In this thesis, three different models are being used. In chapter 3, a large-scale model (TM5) is used, a clear example of an end-result focussed model. In this chapter, comparison between model and observations plays an important role. In chapter 4, a single-column model is used. This model has a high vertical resolution so that boundary-layer processes that are not resolved in TM5 can be properly simulated. Furthermore, observations are used to force the model to represent certain observed quantities well. Chapter 5 is an example of an idealised model setup. Here, only turbulence and phase transition of nitrate are simulated. All other processes are avoided so that these two processes can be analysed in much detail. The disadvantage is that comparison to observations is difficult. With the combination of large-scale and small-scale analysis, this thesis provides additional knowledge about microphysical processes including an indication for the relevance for the impact on the scale of the Netherlands or Europe.



# 3

---

## The European aerosol budget in 2006

This paper presents the aerosol budget over Europe in 2006 calculated with the global transport model TM5 coupled to the size-resolved aerosol module M7. Comparison with ground observations indicates that the model reproduces the observed concentrations quite well with an expected slight underestimation of  $PM_{10}$  due to missing emissions (e.g. resuspension). We model that a little less than half of the anthropogenic aerosols emitted in Europe are exported and the rest is removed by deposition. The anthropogenic aerosols are removed mostly by rain (95%) and only 5% is removed by dry deposition. For the larger natural aerosols, especially sea salt, a larger fraction is removed by dry processes (sea salt: 70%, mineral dust: 35%). We model transport of aerosols in the jet stream in the higher atmosphere and an import of Sahara dust from the south at high altitudes. Comparison with optical measurements shows that the model reproduces the Ångström parameter very well, which indicates a correct simulation of the aerosol size distribution. However, we underestimate the aerosol optical depth. Because the surface concentrations are close to the observations, the shortage of aerosol in the model is probably at higher altitudes. We show that the discrepancies are mainly caused by an overestimation of wet-removal rates. To match the observations, the wet-removal rates have to be scaled down by a factor of about 5. In that case the modelled ground-level concentrations of sulphate and sea salt increase by 50% (which deteriorates the match), while other components stay roughly the same. Finally, it is shown that in particular events, improved fire emission estimates may significantly improve the ability of the model to simulate the aerosol optical depth. We stress that discrepancies in aerosol models can be adequately analysed if all models would provide (regional) aerosol budgets, as presented in the current study.

### 3.1 Introduction

Aerosols have a large impact on the behaviour of our atmosphere as they influence the earth's radiation budget both directly through interaction with solar radiation (Hess et al., 1998; Haywood and Boucher, 2000; IPCC, 2007) and indirectly through altering the properties and life cycle of clouds (Rosenfeld et al., 2008; Kaufman et al., 2002). The aerosol-climate interactions are complex and the aerosol forcing is much less certain compared to the radiative effect of greenhouse gases. Hence, the combined direct and indirect aerosol effect may have masked the climate sensitivity towards an increase in greenhouse gases to an unknown extent (Anderson et al., 2003).

Exposure to particles has been associated with adverse health effects and particles are believed to be the most important air pollutant responsible for these health effects. Short-term exposure has been associated with increased human morbidity and mortality (Brunekreef and Holgate, 2002; Dockery et al., 1993; Pope et al., 1995). Although most health studies have quantified relationships between the total aerosol mass ( $PM_{10}$  or  $PM_{2.5}$ ) and health effects, some studies indicate that also the chemical composition of aerosols (Hoek et al., 2002) and particle size (Stone and Donaldson, 1998) might play a significant role. To reduce the adverse health effects, air quality standards for particulate matter have been implemented

---

in many countries. To design effective mitigation strategies, governments need to know the relationship between sources and concentrations of particulate matter. Within Europe, these relationships are traditionally obtained through source-receptor calculations (Seibert and Frank, 2004). Another way to investigate these relationships is a budget analysis as pointed out in this paper.

To better understand the relationship between the emission of aerosols and their precursors on the one hand, and the observed distribution of aerosols on the other hand, numerical models have been developed that describe the aerosol life cycle (Wilson et al., 2001; Bauer et al., 2008; de Meij et al., 2006). This presents an extremely challenging task as one needs to accurately model a host of sources, formation and transformation pathways as well as removal processes to assess aerosol composition, size distribution and mixing state. Together they determine the optical properties of aerosols as well as their ability to act as cloud condensation nuclei (CCN). Thus, to describe the full life cycle of aerosols one needs reliable (size-resolved) emission inventories and parameterisations to supply the necessary boundary conditions for the models (Vignati et al., 2010a; Dentener et al., 2006). Furthermore, one needs to represent the complex aerosol dynamics (Stier et al., 2005; Vignati et al., 2004; Wilson et al., 2001; Lee and Adams, 2010; Korhonen et al., 2008). Also, it is necessary to couple the aerosol dynamics to atmospheric chemistry to account for secondary aerosol formation, semi-volatile species and the involvement of aerosols in numerous chemical cycles. Finally, one needs to consider size and composition resolved aerosol removal by wet and dry deposition processes. In the assessment of the aerosol budget, the key uncertainties arise from inaccurate emission estimates (Dentener et al., 2006; Vignati et al., 2010b) and uncertainties in the wet-removal process (Chin et al., 2000).

In a model intercomparison study, Textor et al. (2006) highlighted the poor agreement among models concerning aerosol processes, and specifically the wet removal of aerosols. The parameterisations in models are probably often tuned to produce a reasonable comparison with (satellite) observations. Unfortunately, model specific tuning often remains undocumented and arbitrarily tuning of models can have led to the huge diversity in the analysed simulations. Textor et al. (2006) showed that methodologies to analyse and compare different models are indispensable to improve our ability to model the aerosol distribution. One method that provides details about the processes that matter for aerosol modelling is a budget analysis. Budget analysis also helps to understand differences between models. An aerosol budget analysis with a bulk aerosol approach has been described in Kanakidou (2007).

The aim of this paper is threefold. First, we will present a description of the TM5 model coupled to the size-resolved aerosol module M7 and compare model results with observations. Second, we will analyse the European aerosol budget and quantify the aerosol import and export terms in the boundary layer and the free atmosphere. Thirdly, we will highlight some uncertainties that are associated with aerosol modelling. Specifically, we will address the wet-removal parameterisation in our model and focus on an anecdotic improvement of the fire-related emissions during a biomass burning episode in April–May 2006 in Eastern Europe.

## 3.2 Model and measurements

The quantification of the aerosol budget over Europe is performed with the global transport model TM5 (Krol et al., 2005) coupled to the aerosol dynamics module M7 (Vignati et al., 2004). To calculate the aerosol budget in the model, Europe is defined from 34° N to 62° N and from 12° W to 36° E. We examine the import, export, emission and deposition of aerosols as well as chemical processes that influence particulate matter. Below we describe the main characteristics of the model with a focus to the aerosol description as well as the observations used for evaluation.

### 3.2.1 TM5 model description

The global horizontal resolution of the offline chemistry transport model TM5 is 6° longitude by 4° latitude. The vertical grid comprises 25 hybrid  $\sigma$ -pressure levels ranging from surface up to in the stratosphere. As the region of interest is Europe, we used TM5's two-way nested zoom capability (Krol et al., 2005; Berkvens et al., 1999) to acquire a higher resolution over Europe. The zoomed region is defined from 12° N to 66° N and from 21° W to 39° E, with a resolution of  $1^\circ \times 1^\circ$ . Note that our definition of Europe to calculate the budget is only a part of this zoomed region. A transitional zone from 2° N to 74° N and from 36° W to 54° E, with a resolution of  $3^\circ \times 2^\circ$  is used to smoothen the transition (Krol et al., 2005). The vertical resolution remains the same.

The global time resolution is 90 min. TM5 uses operator splitting, in which each process (e.g. advection, chemistry) has a time step of 45 min. This time resolution is refined four times in the zoom region and twice in the transitional region.

TM5 uses pre-processed meteorological data from the European Centre for Medium-Range Weather Forecasts (ECMWF) (Segers et al., 2002; Bregman et al., 2003). This data includes pressure, temperature, moisture, wind fields and cloud information. TM5 operates with full chemistry and aerosols, simulating the processes: emission (Dentener et al., 2006; IPCC, 2000), deposition (Ganzeveld et al., 1998; Guelle et al., 1998), advection (Prather, 1986; Russell and Lerner, 1981), convection (Tiedtke, 1989), diffusion (Louis, 1979; Holtslag and Boville, 1993), chemistry (Houweling et al., 1998; Williams and van Noije, 2008) and photolysis (Krol and van Weele, 1997; Landgraf and Crutzen, 1998). The version used is subversion (SVN) revision 2887.

### 3.2.2 Aerosol module description

All aerosol processes including wet and dry removals are calculated in the model using the size resolved number and masses given by the aerosol dynamics module M7 (Vignati et al., 2004).

**Table 3.1:** *The seven modes in M7, their solubilities, size ranges and chemical compounds. Chemical compounds are abbreviated: Sulphate ( $SO_4^{2-}$ ), Black carbon (BC), Organic matter (POM), Mineral dust (DU), Sea salt (SS)*

#	Mode	Abbr.	Size range (d)	Compounds
1	Nucleation Soluble	nus	< 10 nm	$SO_4^{2-}$
2	Aitken Soluble	ais	10 – 100 nm	$SO_4^{2-}$ , BC, POM
3	Accumulation Soluble	acs	100 nm – 1 $\mu$ m	$SO_4^{2-}$ , BC, POM, DU, SS
4	Coarse Soluble	cos	> 1 $\mu$ m	$SO_4^{2-}$ , BC, POM, DU, SS
5	Aitken Insoluble	aii	10 – 100 nm	BC, POM
6	Accumulation Insoluble	aci	100 nm – 1 $\mu$ m	DU
7	Coarse Insoluble	coi	> 10 $\mu$ m	DU

### 3.2.2.1 Aerosol dynamics

During the chemistry step of TM5, M7 is called to simulate the aerosol microphysics. M7 distinguishes seven classes (modes) of aerosols of different size and solubility. The properties of M7’s aerosol modes are listed in Table 3.1. There are four size classes for soluble aerosols and three for insoluble aerosols. Chemical compounds can be present in various modes. For each mode, one number tracer and several tracers for the chemical compounds are subject to transport in the model for a total of twenty-five tracers.

M7 considers the modes as log-normal size distributions (von Salzen, 2006) with defined median radius ( $\bar{r}$ ) and spread ( $\sigma$ ). Although aerosols may not be spherical, they are assumed spherical in the model. The size distribution of a mode looks like (Seinfeld, 1986):

$$\frac{dN}{d \ln r} = \frac{N}{\sqrt{2\pi} \ln \sigma} \cdot e^{-\frac{(\ln r - \ln \bar{r})^2}{2 \ln^2 \sigma}} \quad (3.1)$$

Here,  $r$  is the size,  $N$  is the total aerosol number concentration,  $\bar{r}$  is the median radius and  $\sigma$  is the geometric standard deviation.

A mode consists of a number concentration and several component masses that are internally mixed ( $N, [M]$ ) (Stier et al., 2005). Given the modal component masses and their densities, the total volume ( $V$ ) can be calculated. This volume is represented by a log-normal distribution as in Eq. 3.1. To derive this distribution, M7 assumes a constant standard deviation, which allows the volume per aerosol ( $\frac{V}{N}$ ) to determine the median radius ( $\bar{r}$ ). The standard deviation is set to 2.00 for the coarse modes and to 1.59 for the other modes (Vignati et al., 2004). The median  $\bar{r}$  is given by (Seinfeld, 1986):

$$\bar{r} = \sqrt[3]{\frac{3V}{4\pi N} \cdot e^{-\frac{9 \ln^2 \sigma}{2}}} \quad (3.2)$$

M7 handles the formation of new particles (binary nucleation) (Vehkamäki et al.,

2002), the coagulation of particles and the condensation of sulphuric acid to existing particles. M7 ensures that the modes keep their inherent solubility by moving coated particles to the soluble (mixed) mode. The size classes are preserved by transferring mass of growing aerosols to the next mode. M7 diagnostically calculates the water attached to the soluble particles (Vignati et al., 2004).

### 3.2.2.2 Ammonium and nitrate

In Table 3.1, two compounds that are important for the aerosol budget over Europe (Putaud et al., 2004) are missing: ammonium ( $\text{NH}_4^+$ ) and nitrate ( $\text{NO}_3^-$ ). Observations show that nitrate is very abundant, especially in the western European cold season (Schaap et al., 2002; Mehlmann and Warneck, 1995). There is a temperature-dependent equilibrium between gas phase nitric acid ( $\text{HNO}_3$ ) and nitrate, dissolving into and evaporating out of the aerosol. This equilibrium also depends on the available aerosol sulphate ( $\text{SO}_4^{2-}$ ) and gas phase ammonia ( $\text{NH}_3$ ). M7 is not designed to model semi-volatile aerosol components. We use the Equilibrium Simplified Aerosol Model (EQSAM) version 3. (Metzger et al., 2002a,b) to calculate the partitioning of ammonium nitrate between the gas and aerosol phase with the total available sulphate (of all modes). EQSAM uses a bulk aerosol approach, so it does not define in which aerosol size category the ammonium nitrate gathers. We assume that the ammonium nitrate and the water absorbed by it resides in the soluble accumulation mode. Test simulations with ISORROPIA and GMXe (Nenes et al., 1998; Pringle et al., 2010) confirm that virtually all ammonium nitrate mass is in the soluble accumulation mode. EQSAM limits the relative humidity to 99% to exclude cloud formation (Metzger et al., 2002a). The aerosol associated water mass, can be sufficiently accurately reproduced by EQSAM with respect to other global model uncertainties (Metzger et al., 2002b).

### 3.2.2.3 Dry deposition

While gas-phase chemicals exhibit diffusive dry deposition (Ganzeveld et al., 1998; Hicks et al., 1986), aerosols are removed by diffusive dry deposition and gravity-driven sedimentation (Slinn and Slinn, 1980; Kerckweg et al., 2006). Both deposition pathways depend on the size of the aerosols.

To calculate the deposition velocities for the tracers in each mode, the log-normal distribution is used to distribute the mass and number tracers into twenty-three size bins. Each of these bins is subject to a bin-dependent deposition velocity, recalculated every three hours depending on e.g. atmospheric stability and surface type (Ganzeveld et al., 1998).

After accounting for dry deposition in each bin, the log-normal distribution is reconstructed. For simplicity, the modes remain log-normal with a fixed standard deviation. Hereby, aerosol mass moves from a size range with a slower deposition velocity to a size range with a faster deposition velocity. This introduces a bias that hard to avoid, but might accelerate loss by deposition.

Apart from surface deposition, the coarse mode aerosols exhibit a non-negligible fall velocity due to gravitational settling in the atmosphere. This sedimentation process is modelled by calculating 3-D fields of the fall velocities for each mode

(Slinn and Slinn, 1980). Sedimentation removes preferably the larger particles, which results in smaller fall velocities for the aerosol numbers than for aerosol masses. The sedimentation process also changes the median radii of the M7 modes.

### 3.2.2.4 Wet deposition

Wet deposition is split in deposition from stratiform and convective precipitation. For stratiform precipitation, in-cloud scavenging and below-cloud scavenging is handled separately. Below-cloud scavenging of gases is linearly related to the surface rain flux, using a gas-to-droplet transfer coefficient based on the Reynolds and Sherwood numbers of the falling rain droplets. For aerosols, the scavenging parameterisation from Dana and Hales (1976) is used and calculated for each aerosol mode separately. In-cloud scavenging is modelled in two phases: the mass transfer of soluble gases and aerosol to the liquid phase and the formation of rain droplets (Roelofs and Lelieveld, 1995). In convective precipitation, aerosols are assumed to be removed very efficiently (similar to  $\text{HNO}_3$ ). The removal rate is modelled as a simple function that depends on the convective precipitation at the surface (Vignati et al., 2010b).

TM5 assumes well-mixed grid cells. However, the time scale of wet removal can become faster than the mixing time scale of the grid cell. Therefore, the wet-deposition yield will increase for larger grid boxes. This is a significant issue as multiple resolutions are used within the same simulation. This issue is treated pragmatically by introducing a time parameter  $\tau_{\text{nomix}}$ , in which the in-cloud, below-cloud and cloudless fractions of a grid cell are treated quasi-independently (Vignati et al., 2010b). This way, the wet removal in large grid cells is slowed down, reducing the resolution dependence. Applying the wet removal on a fraction of the gridbox has always been a challenge for modellers, as outlined in a study on  $^{210}\text{Pb}$  (Balkanski et al., 1993).

### 3.2.2.5 Emission

Emission data used in the model are those recommended for the AEROCOM (Dentener et al., 2006) model intercomparison studies and from the IPCC (IPCC, 2000). For biomass burning emissions, we use climatologic inventories from the global fire emission database (GFED 2) (Randerson et al., 2006; van der Werf et al., 2006) with prescribed height distribution (Dentener et al., 2006). In these data, it is predefined in which modes the aerosols are emitted. Aerosol mass emissions have an assumed lognormal distribution with a median radius ( $\bar{r}$ ) (Table 3.2) in their inventories. This median radius is used to calculate the total emitted aerosol number with a mode-dependent standard deviation.

Ammonia is emitted mainly by domestic animals and synthetic fertilisers. Other sources of ammonia are biomass burning, the oceans, crops, human population and pets and natural soils (Bouwman et al., 1997).

Oxidised sulphur is emitted by industry, fossil fuel combustion (Cofala et al., 2005), biomass burning (Randerson et al., 2006; van der Werf et al., 2006) and volcanoes (Andres and Kasgnoc, 1998; Halmer et al., 2002). Part (2.5%) of the

**Table 3.2:** *Implemented aerosol emissions with the predefined M7 modes and median emission radii.*

Compound	Category	Percentage	Mode	$\bar{r}$ ( $\mu\text{m}$ )
$\text{SO}_4^{2-}$	Fossil fuel (Domestic and road transport)	50	ais	0.03
$\text{SO}_4^{2-}$	Fossil fuel (Domestic and road transport)	50	acs	0.075
$\text{SO}_4^{2-}$	Biomass burning	50	ais	0.03
$\text{SO}_4^{2-}$	Biomass burning	50	acs	0.075
$\text{SO}_4^{2-}$	Industry	100	acs	0.075
BC	Fossil fuel	100	aii	0.015
BC	Biomass burning	100	aii	0.04
POM	Fossil fuel	65	ais	0.015
POM	Fossil fuel	35	aii	0.015
POM	Biomass burning	65	ais	0.04
POM	Biomass burning	35	aii	0.04
POM	Secondary organic aerosol	100	ais	0.01*
DU	Wind blown	**	aci	***
DU	Wind blown	**	coi	***
SS	Wind blown	**	acs	0.08
SS	Wind blown	**	cos	0.63

\* SOA is assumed to condensate on existing aerosols so particle numbers are only created when needed to prevent unrealistic situations.

\*\* Emissions in different modes are independent.

\*\*\* Variable radius, included in the AEROCOM emission file.

sulphur is emitted directly in the particulate form ( $\text{SO}_4^{2-}$ ) (Stier et al., 2005; Dentener et al., 2006). The particulate sulphate emissions from biomass burning and fossil fuel combustion are divided equally over the Aitken and accumulation mode, while industrial sulphate emissions are all in the accumulation mode (Dentener et al., 2006).

Carbonaceous compounds are emitted by fossil fuel, biofuel (Bond et al., 2004) and biomass burning (Randerson et al., 2006; van der Werf et al., 2006). These particles are only emitted in the Aitken mode. The black carbon is always emitted as insoluble particles, while 65% of the particulate organic matter (POM) is emitted in the soluble mode (Stier et al., 2005). Production of secondary organic aerosols is modelled as a direct emission. In reality, secondary organic aerosols from e.g. terpenes are involved in the formation and the early growth of new particles (Sihto et al., 2006, 2009) and they condensate on existing particles. In our model, however, these organic compounds are directly added as particulate organic matter mass in the soluble Aitken mode (Kanakidou et al., 2005). However, to avoid unrealistic situations, particles of 10 nm are added when there are no other emissions in the soluble Aitken mode. It is assumed that the organic matter involved in nucleation has been coagulated efficiently. Furthermore, through coagulation of the Aitken mode particles, we mimic the condensation of these organic compounds to the accumulation mode.

For dust, we used pre-calculated AEROCOM data (Dentener et al., 2006). The emission sizes are variable and are pre-calculated as well. Dust is emitted both in the insoluble accumulation mode and the Insoluble coarse mode. Sea salt emissions are calculated online as function of the ten-meter wind speed as described in Vignati et al. (2010a) and Gong (2003). Sea salt is emitted in both the soluble accumulation mode and the soluble coarse mode.

### 3.2.2.6 Aerosol optics

We calculate the AOD in our model from the aerosol concentrations using Mie scattering theory (Mie, 1908; Barber and Hill, 1990). An aerosol contributes to the AOD, depending on its wet radius ( $r_w$ ), its complex refractive index ( $m$ ) and the wavelength ( $\lambda$ ).

The size of the wet droplets ( $r_w$ ) is calculated from the median wet radius ( $\bar{r}_w$ ) and the fixed standard deviation ( $\sigma$ ). The refractive index ( $m$ ) of aerosol compounds, including water, are based on ECHAM-HAM (Kinne et al., 2003), OPAC (Hess et al., 1998) and Segelstein (Segelstein, 1981).

We compute for each time step, for each grid cell and for each aerosol mode an effective refractive index based on the chemical composition. We do not employ a simple volume-weighted mean of the refractive indices of the chemical compounds, which is known to give inaccurate results. Rather, we use proper effective medium theory from Maxwell-Garnett (Maxwell-Garnett, 1904) and Bruggeman (Bruggeman, 1935).

Mie-scattering calculations demand a significant computational burden and simplifying the Mie-scattering theory causes significant errors (Boucher, 1997). To tackle this problem, we pre-calculated a lookup table. The input parameters of

this lookup table (refractive index and size) are sampled with forty times fifteen values for the refractive index (real  $\times$  imaginary) and a hundred values for the size parameter  $\frac{r_w}{\lambda}$ . With interpolation, the discretisation error is expected to be low (at most a few percent).

By calculating the AOD at several wavelengths, we can determine the Ångström parameter (Russell et al., 2010) with the following general relationship between AOD and wavelength (Ångström, 1929):

$$\tau = \beta \lambda^{-\alpha} \quad (3.3)$$

Here,  $\tau$  is the AOD,  $\beta$  is a prefactor,  $\lambda$  is the wavelength and  $\alpha$  is the Ångström parameter. The prefactor  $\beta$  is a measure for the overall AOD and the Ångström parameter is a measure for the wavelength-dependence of the AOD. Verification on the Ångström parameter enables to check whether the aerosol distribution is dominated by fine ( $\alpha > 1.3$ ) or coarse ( $\alpha < 1.3$ ) particles.

### 3.2.3 In-situ measurements

The modelled concentrations are compared to in-situ measurements from the EMEP network (EMEP, 2008) (<http://www.emep.int>), which provides data for a host of air pollutants (Lazaridis et al., 2002; EMEP, 2008). We used the yearly averaged data for particulate matter, aerosol composition and aerosol precursors. The averaged data for 2006 were used for the stations that produced valid data during at least 10% of the time. For the vast majority of the used data points (94%), this valid-data percentage was above 50%. Verification of the model results against measurements for PM and its components is hampered by potential artefacts in the sampling. PM filter measurements are uncertain due to potential losses of ammonium nitrate and absorption of nitric acid and organic compounds (Vecchi et al., 2009). The abovementioned volatilisation and absorption artefacts cause the sampling of nitrate and ammonium to be difficult (Yu et al., 2006; Zhang and McMurry, 1992; Cheng and Tsai, 1997). Correct sampling is only possible with denuder filter packs. However, these labour intensive methods are hardly used in Europe (Schaap et al., 2002). Hence, we use aerosol nitrate and ammonium data from inert filters, although we acknowledge that they are prone to losses at temperatures above 20°C (Schaap et al., 2004b). Most data on nitrate and ammonium, however, are given as the sum of gas and aerosol concentration. Gas phase concentrations for ammonia and nitric acid obtained with a filter pack are used here when reported by EMEP.

Observations of sulphur and nitrogen compounds are reported as masses S and N rather than total mass. Sea-salt concentrations are evaluated with observed sodium (Na) concentrations. Throughout this paper, we will express any sulphur compounds, nitrogen compounds or sea salt as masses S, N and Na. For the conversion of total sea salt to sodium, we use a conversion factor of 0.306 (Millero, 2004).

Unfortunately, measurements of carbonaceous compounds of 2006 are very scarce. Therefore, we will use measurements from the EMEP EC-OC campaign in 2002–2003 (Yttri et al., 2007). In the EMEP campaign, organic carbon (OC)

is measured, while TM5 simulates organic matter (POM). In the analysis, a factor 1.4 is used to convert the observations of organic carbon to organic matter to account for the non-carbon part of the organic matter.

There are also insufficient observations of mineral dust aerosol. Mineral dust is a mixture of many components, so it is very difficult to measure it reliably, especially when only a small fraction of the total aerosol mass is dust, which is the case in the majority of Europe.

We compare the modelled aerosol optical depth (AOD) to European observations from the Aerosol Robotic Network (AERONET) (Holben et al., 2001). These are measured by the sun-powered CIMEL Electrique 318A spectral radiometer that points systematically to the sun in a programmed routine (<http://aeronet.gsfc.nasa.gov>).

In the model, the AOD is calculated at the wavelengths ( $\lambda$ ) at which the AERONET stations measure. We sample the observed AOD-values with 1.5-h intervals, where multiple measurements within one interval are averaged. This adapts the time resolution of the observations to that of the model.

We also analyse the ability of the model to simulate the Ångström parameter. The Ångström parameter is reported by AERONET as well. In our model, we use a function fit of Eq. 3.3 to obtain the Ångström parameter.

### 3.3 Results and discussion

In this section, we first examine the modelled surface concentrations of the aerosol components and precursor gases in Europe, as well as AOD and Ångström parameter. Next, we compare these results with observations followed by the European budget of aerosol compounds and precursors. To address the model's ability to simulate the full aerosol burden we evaluate the modelled AOD and Ångström parameter with observations. Finally, we will address two main uncertainties, namely wet removal and biomass burning emissions.

#### 3.3.1 Concentration distribution

The annual average concentration distribution of aerosol chemical compounds and their precursors are shown in Fig. 3.1. The AOD and the Ångström parameter are shown in Fig. 3.2.

Nitrogen and sulphur oxides show a hot-spot structure with high concentrations in industrialised regions with  $\text{SO}_x$  ( $\text{SO}_2$ ,  $\text{H}_2\text{SO}_4$ ) more in Eastern Europe and  $\text{NO}_y$  ( $\text{NO}$ ,  $\text{NO}_2$ ,  $\text{NO}_3$ ,  $\text{HNO}_4$ ,  $\text{N}_2\text{O}_5$ , PAN) more in the Western Europe. We clearly model an ammonia hot spot in the Netherlands, which is due to high population of livestock (Buijsman et al., 1987). Nitric acid shows high concentrations over sea. In reality, nitric acid may react with sea salt and displace chloride (Glasgow, 2008; Schaap et al., 2004a). This reaction is not implemented in the model, since it has only a small effect on the aerosol distribution over land.

In contrast to primary gaseous pollutants, secondary inorganic aerosols have smoother distributions as they are of secondary origin. The ammonium concentration shows features of both nitrate, which peaks in north-western Europe and in

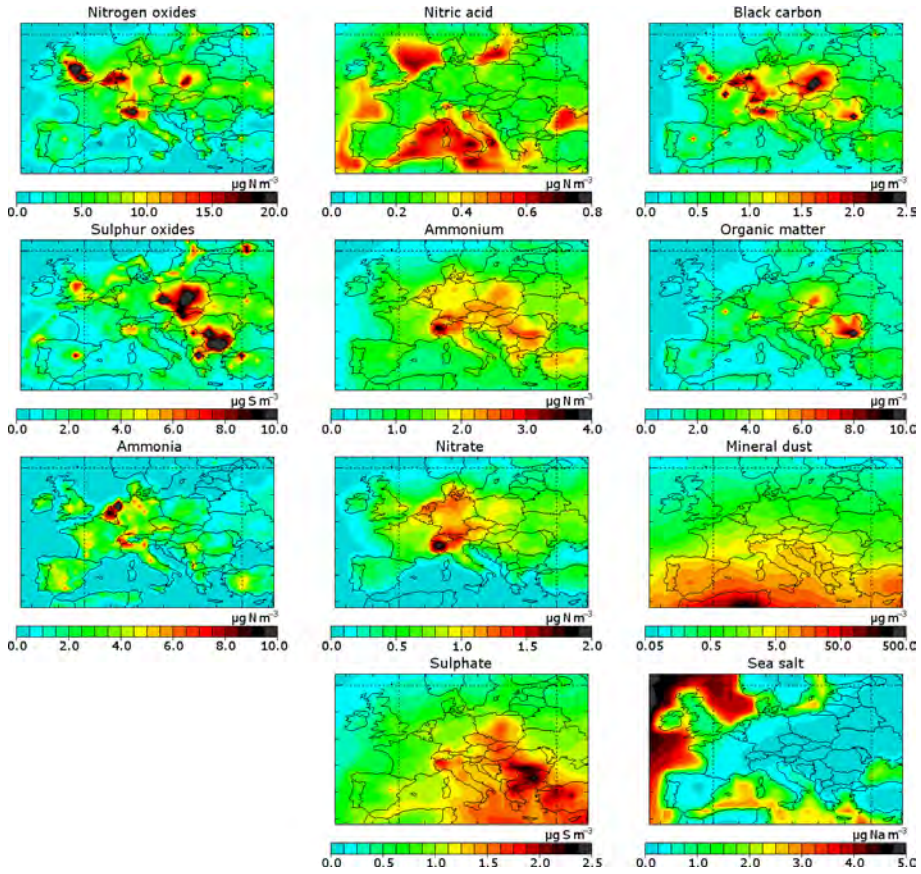


**Figure 3.1:** Modelled surface concentrations of the aerosol tracers and precursor gases. Note that the colour scale used for mineral dust is logarithmic. Nitrogen oxides include  $\text{NO}$ ,  $\text{NO}_2$ , Peroxyacetyl nitrate (PAN),  $\text{NO}_3$ ,  $\text{HNO}_4$  and  $\text{N}_2\text{O}_5$ , but no nitric acid or aerosol nitrate. Sulphur oxides include  $\text{SO}_2$  and  $\text{H}_2\text{SO}_4$ , but no aerosol sulphate. All values are averaged over 2006.

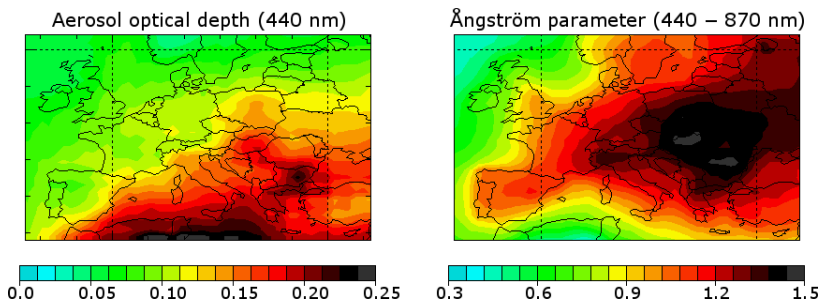


**Figure 3.2:** Modelled optical properties of the atmospheric column averaged over 2006.

the Po Valley, and sulphate, which shows highest concentrations in south-eastern Europe. This is because both nitric acid and sulphuric acid are neutralised by ammonium.

Primary anthropogenic carbonaceous aerosols show high concentrations in densely populated and industrialised regions. As for primary gaseous pollutants ( $\text{NO}_y$  and  $\text{SO}_x$ ), this results in a hot-spot structure. For black carbon and organic matter, the hot spots are located at different positions. However, the hot spot structures of  $\text{NO}_y$  and black carbon only differ slightly (more  $\text{NO}_y$  in England and more black carbon in Poland).

Mineral dust shows a sharp gradient from the Sahara to the north with significant concentrations over the Mediterranean countries. North of the Alps, mineral dust concentrations are low. As expected, sea-salt concentrations are highest above open sea. Above land, significant sea salt-concentrations are only present in coastal areas.

The calculated annual mean AOD is highest in the south and south-eastern Europe with values above 0.15. Mineral dust and sulphate appear to be the most dominant contributors to the AOD, since the AOD is high at locations where mineral dust or sulphate is abundant (see Figs. 3.1 and 3.2). The Ångström parameter is low over the sea and over northern Africa, because sea salt and desert dust are mostly coarse mode aerosols. Over land, the fine anthropogenic aerosols dominate, resulting in high Ångström parameters.

### 3.3.2 Model evaluation

Model results of particulate matter compounds and precursor gases have been compared with in-situ observations. When comparing with size-segregated observations (e.g.  $\text{PM}_{10}$ ), the log-normal distribution of M7 is used to calculate which fraction of the modelled aerosol mass is below the size limit. First, we will compare annually averaged concentrations. Later on, we will analyse a few time series of  $\text{PM}_{10}$  for January 2006. We chose to evaluate January, because the surface concentrations are the most sensitive to synoptic events in winter.

#### 3.3.2.1 Annual means

The most important results of the comparison of annually averaged aerosol and precursor concentrations are shown in Fig. 3.3. Figure 3.4 shows the results per country represented in a graphic way.

Total reduced nitrogen (ammonia and ammonium) is slightly overestimated. Aerosol ammonium is represented quite well, but ammonia is overestimated. It is well-known that modelling ammonia is challenging due to the importance of local effects (Dentener and Crutzen, 1994). Still, the Dutch ammonia hot spot is caught remarkably well in the model. Interestingly, TM5 overestimates ammonia while many other models underestimate ammonia concentrations (Schaap et al., 2004a). An issue is that the night-time concentrations estimated by the model are too high. These concentrations are very sensitive to the stability of the nocturnal boundary layer (van Loon et al., 2007). Especially TM5, as a global model,

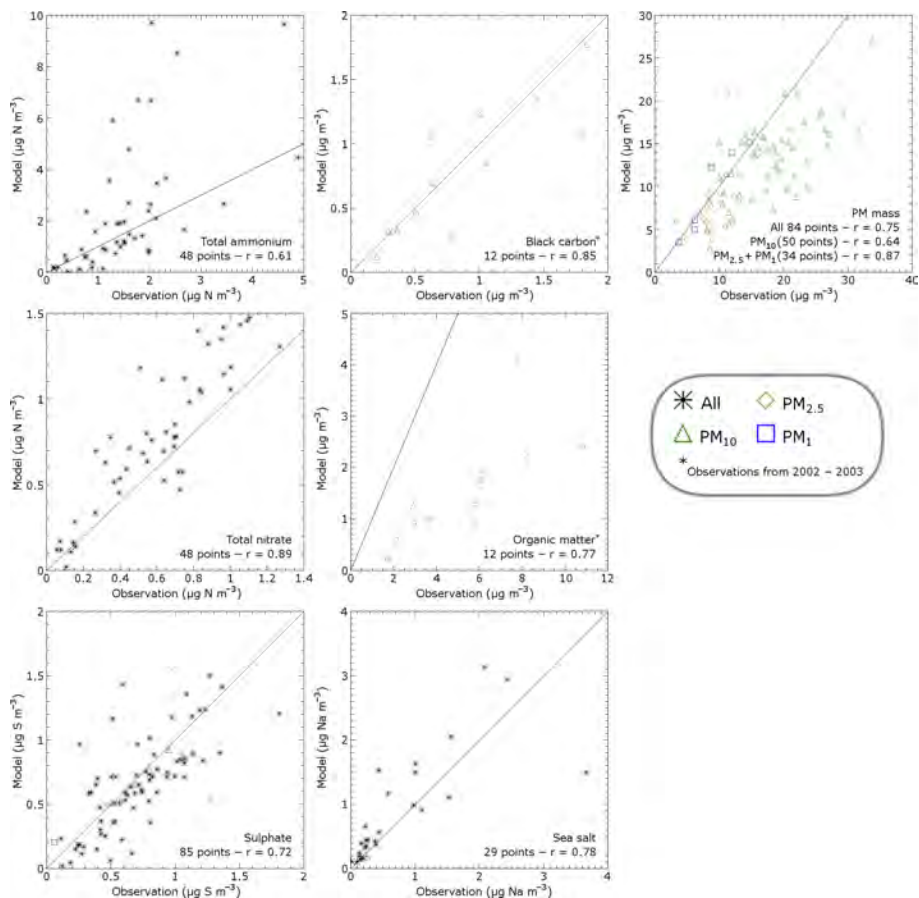


**Figure 3.3:** Comparison between modelled and observed average concentrations over 2006 for total ammonium, total nitrate, sulphate, black carbon, organic matter, sea salt and total particulate matter at EMEP ground stations. The colours and shapes indicate the aerosol size class.

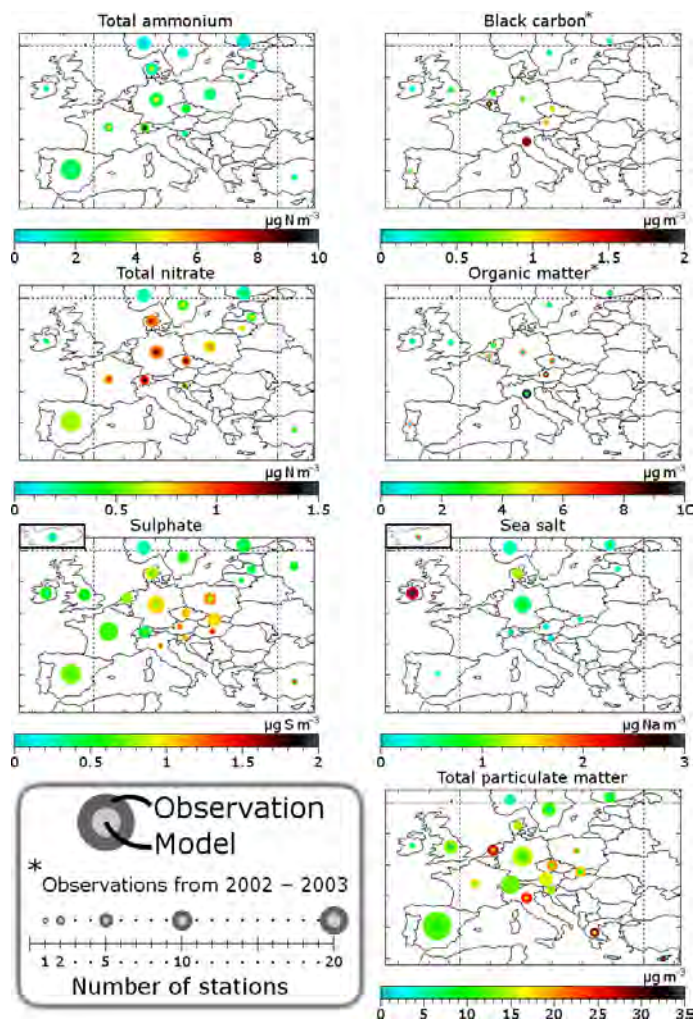


**Figure 3.4:** Graphical overview of the comparison between modelled and observed average concentrations over 2006 for total ammonium, total nitrate, sulphate, black carbon, organic matter, sea salt and total particulate matter at EMEP ground stations. Values of stations per country are averaged. The size of the circles represent the number of stations in that country. The country in the upper left box of the sulphate and sea salt maps, is Iceland.

has resolution limitation for the nocturnal boundary layer, because it is a small-scale phenomenon ( $\sim 50$  m). Therefore, the nocturnal boundary layer tends to be poorly defined in TM5. This is very important for ammonia, because the modelled emissions are assumed constant over the day (de Meij et al., 2006), which implies that ammonia is emitted into the stable boundary layer, causing night-time accumulation. In reality, ammonia emissions show a considerable diurnal variation with peak emissions during the day and even a net night-time surface uptake of ammonia (Wichink Kruit et al., 2007), which may be released during the next day.

The total oxidised nitrogen (nitric acid and aerosol nitrate) is represented better. There is some overestimation, but the spatial correlation is good ( $r = 0.89$ ). When considering aerosol nitrate, about the same conclusions could be drawn. However, the modelled concentrations of nitric acid are far off (bad correlation and overestimation by a factor of two). We already addressed that the values above sea are modelled too high because the acid displacement reaction is not taken into account (see Sect. 3.3.1 and Schaap et al., 2004a; Glasgow, 2008). This issue may affect modelled concentrations in coastal areas, where many stations are located. Though the nitric acid concentration is the difference between total nitrate and aerosol nitrate (both well represented in the model), nitric acid has higher uncertainties because of higher uncertainties in sampling for nitric acid (see Sect. 3.2.3). Also, the nitric acid concentrations are often much lower than the aerosol nitrate concentrations, which means that the relative uncertainty becomes higher.

Sulphate is represented quite well. However, there is an overestimation by a factor of two for sulphur dioxide, the precursor of sulphate (not shown). A slow oxidation of sulphur dioxide may partly explain this discrepancy, but higher oxidation would also lead to higher surface sulphate concentrations. However, increased in-cloud oxidation at higher altitudes would be more consistent. The time scale of in-cloud oxidation of sulphur dioxide is very uncertain (Langner and Rodhe, 1991). Also, the emission heights of sulphur dioxide may play an important role. For instance, the sulphur dioxide emissions from AEROCOM are higher in the lower model levels than those of EMEP, which can cause a surface concentration discrepancy of a factor of two in eastern Europe (de Meij et al., 2006). Another possibility is that the emission rate of sulphur dioxide is too high in the model or there is an unaccounted or underestimated loss of sulphur dioxide that does not lead to sulphate production, e.g. dry deposition (Chin et al., 2000).

As we mentioned in Sect. 3.2.3, we compare our modelled results with observations from the EC-OC campaign of 2002 and 2003. Black carbon is represented well, as shown also in Vignati et al. (2010b). There is a huge (factor 3 or more) underestimation of particulate organic matter, though there is a quite okay spatial correlation between observations and model results. Secondary organic aerosols (Volkamer et al., 2006) and resuspended aerosols (Sternbeck et al., 2002), which are rich in organic matter, are significantly underestimated by TM5. An earlier evaluation of organic matter (Vignati, personal communication, 2010) also shows such an underestimation.

From the comparison of modelled and observed total particulate matter, we can conclude that the aerosol spatial distribution is reproduced reasonably well.

---

There is a slight underestimation of the coarse aerosols ( $\text{PM}_{10}$ ) that is probably due to resuspension of aerosols, which is not included in the model, but may be important for local  $\text{PM}_{10}$  concentrations (Sternbeck et al., 2002). Another factor can be an underestimation of secondary organic aerosols (Volkamer et al., 2006) or the unaccounted mass (e.g. dust or water) which is frequently present in  $\text{PM}_{10}$  measurements.

The spatial variability of sea salt is represented very well. However, the absolute concentrations are significantly (50%) overestimated, probably due to uncertainties in emissions and the dry deposition parameterisation. A sea salt overestimation is also shown in Manders et al. (2010).

### 3.3.2.2 Time series January 2006

To evaluate the ability of TM5 to capture synoptic events, we compare time series of modelled and observed total  $\text{PM}_{10}$  for January 2006. Four EMEP stations provide hourly data of  $\text{PM}_{10}$  for this month. The results are shown in Fig. 3.5.

We clearly calculate less variability than observed. TM5, as a global model, is unable to simulate local effects of short durations. This is most clearly visible in Narbeth (GB) where TM5 cannot follow the rapid changes in  $\text{PM}_{10}$  that are observed. Vredepeel (NL) and Vavihill (SE) are represented quite well. The timing of the peaks is roughly correct. Only the magnitudes of two peaks are significantly underestimated, namely the Vredepeel (NL) peak around day 27 and the Vavihill (SE) peak around day 15. TM5 is clearly unable to simulate aerosol concentrations on Ayia Marina (CY). Here, resolution plays a big role, because Cyprus is an island as small as a TM5 grid box. Therefore, TM5 models dust storms at Ayia Marina (CY) that are not observed at the station. Only the broad peak at the beginning is visible in the observations, though with a much smaller magnitude.

### 3.3.3 The aerosol budget

For the analysis of the aerosol budget, we split the atmosphere over Europe into two parts: the boundary layer (surface up to 850 hPa) and the free atmosphere (850 hPa up to top of atmosphere). The budget is split into sources and sinks and the processes: emission (E), chemical reactions (C), aerosol condensation (A), dry deposition (D), wet deposition (W) and the horizontal (H) and vertical (V) transport terms. The vertical transport term denotes the transport of tracer mass between the boundary layer and the free troposphere. Nitric acid also has a stratospheric boundary condition determined by its relationship with stratospheric ozone (Santee et al., 1995). The gain or loss due to this boundary condition is counted as vertical transport (V) for the free atmosphere.

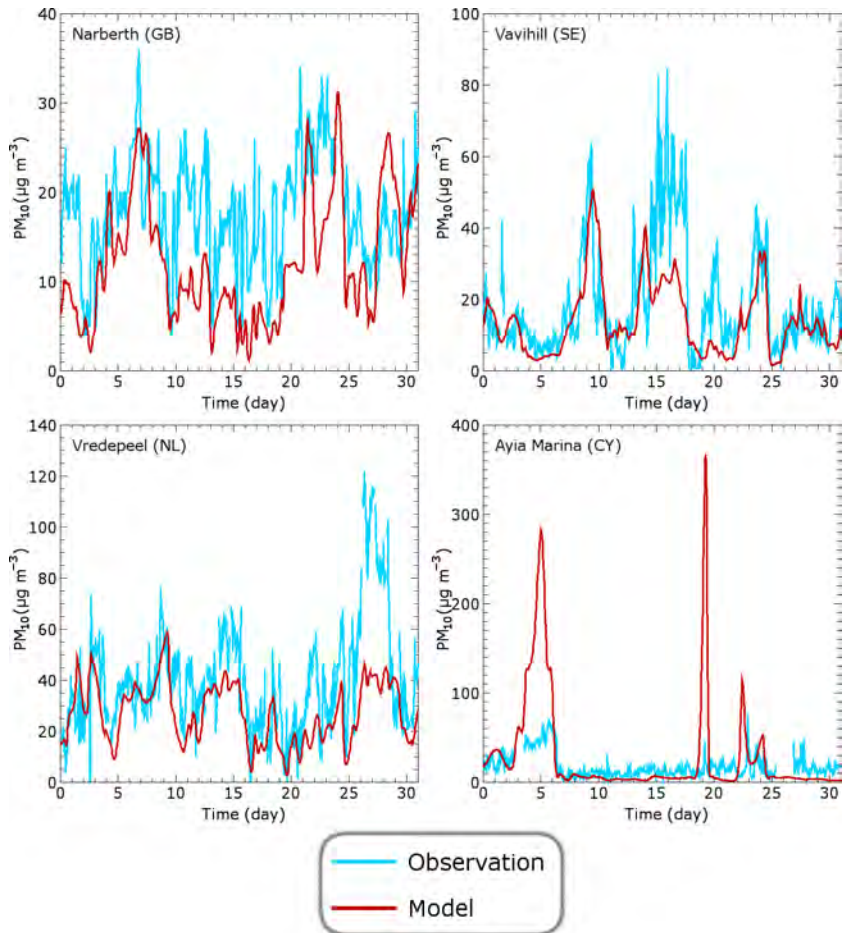


**Figure 3.5:** Comparison between modelled and observed  $PM_{10}$  concentrations in January 2006 for Narberth (GB), Vredepeel (NL), Vavihill (SE) and Ayia Marina (CY).



**Table 3.4:** European annual budget table of nine tracers for the free atmosphere (850 hPa up to top of atmosphere), with (E)burden, (L)lifetime; the sinks: (C)hemical reactions, (A)erosol condensation, (D)ry deposition, (W)et deposition, (H)orizontal transport and (V)ertical transport; and the sources: (E)mission, (C)hemical reactions, (A)erosol condensation, (H)orizontal transport and (V)ertical transport. Vertical transport includes stratospheric interchange. A value of 0 in the table means a value below 0.5 (rounded down to 0), while an empty spot means that the process does not take place at all. Burdens (Gg) are averages of monthly samples. Lifetimes (days) are burdens divided by total sinks. Fluxes ( $Ggyr^{-1}$ ) are annual totals.  $NO_y$  includes  $NO$ ,  $NO_2$ , Peroxyacetyl nitrate (PAN),  $NO_3$ ,  $HNO_4$  and  $N_2O_5$ , but no nitric acid or aerosol nitrate.  $SO_x$  includes  $SO_2$  and  $H_2SO_4$ , but no aerosol sulphate. Nitrogen compounds are expressed as masses N, sulphur compounds as masses S and sea salt as masses Na.

Tracer	Free atmosphere										
	$NO_y$	$SO_x$	$NH_3$	$HNO_3$	$NH_4^+$	$NO_3^-$	$SO_4^{2-}$	BC	POM	DU	SS
B	38.5	16.9	0.6	21.3	7.5	0.6	13.8	2.1	8.7	339.4	10.7
L	7.6	1.5	0.4	5.8	2.5	1.6	2.9	2.9	4.0	6.1	2.0
C	1384	878	6								
A		555	496	6							
D											
W		864	101	850	576	90	984	149	536	16 161	1926
H	454	1908	20	488	505	59	778	121	259		
V										4033	
E	275	2320					0	2	20		
C		102		1119			878				
A					496	6	555				
H										20 179	754
V	1567	1780	622	222	585	141	330	268	773		1176

Figure 3.6 visualises the transport terms and all budget terms are listed in Tables 3.3 and 3.4. Note that the lifetimes, especially in the boundary layer, are low because export terms, including vertical export, are regarded as sinks as well. All budgets close with an accumulation or depletion (difference between sources and sinks) of less than one percent of the budget.

Although only 15% of the air mass is in the boundary layer, the calculated burdens in the boundary layer are comparable to those in the free atmosphere. However, the horizontal fluxes in the boundary layer are much smaller than in the free atmosphere (see Fig. 3.6), indicating that the boundary layer budget is dominated by emission, deposition and vertical transport. Wet deposition is the major sink of all aerosols, except for mineral dust and sea salt, which exhibit efficient dry deposition because of their large size (see Tables 3.3 and 3.4). The numbers in these tables are raw model results, only rounded to whole gigagrams per year, while the uncertainties are much larger. Given the uncertainties, we will round percentages in the interpretations to multiples of 5%.

We model a net export of all anthropogenic aerosol compounds from Europe and a net import of natural aerosol (sea salt and mineral dust). The boundary layer over Europe exports anthropogenic aerosols in all four directions, while in the free atmosphere, Europe imports aerosols and gases from the west due to the jet stream. However, the net horizontal export in the free atmosphere is comparable to the export in the boundary layer as a large part of the tracers in the jet stream are not deposited in Europe but pass through the European domain.

Out of the emitted carbonaceous compounds (BC and POM), about 50% reaches the free atmosphere and 20% is exported in the boundary layer. The other 30% is removed, mainly by wet deposition. Dry deposition plays only a limited role (less than 5% of emission). The carbonaceous compounds that reach the free atmosphere are removed partially (65%) in clouds (wet removal). The rest is exported out of the domain. Note that biomass burning can inject non-negligible amounts of carbonaceous components into the free atmosphere (Dentener et al., 2006).

Mineral dust is the only component that has a net negative vertical flux in Europe, from the free atmosphere to the boundary layer. Figure 3.6 shows that the major transport pathway of dust lies in the free troposphere. Table 3.3 shows that the emission term for dust in the defined European domain is relatively small compared to the transport term. These features for mineral dust are in line with common understanding that during sand storms mineral dust is transported to elevated altitudes by strong convection. Outflow and transport towards Europe occurs above a marine boundary layer causing import at higher altitudes. Sea salt does not exhibit these features as a big part of its emission source (open sea) is within the budget region. Therefore, it has a net positive vertical flux, like the anthropogenic tracers.

About 25% of the emitted ammonia is absorbed by aerosols in the boundary layer. Only 10% reaches the free atmosphere, of which most (80%) gets absorbed by aerosols there. Notable is that, in contrast to aerosols, ammonia is removed much more by dry deposition (55% of emission) than by wet deposition (5% of emission). Transport of ammonia out of Europe is negligible.

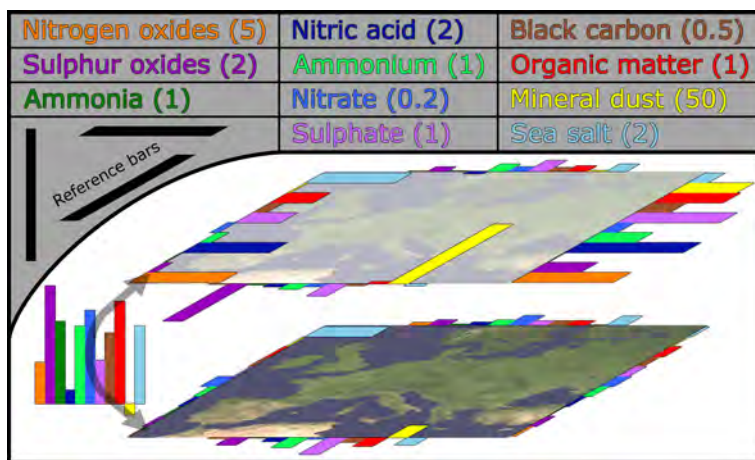


**Figure 3.6:** Transport diagram showing fluxes from north, east, south and west for the boundary layer and the free atmosphere; and the exchange between the two layers. These values are net fluxes integrated over the year 2006. The legend at the top maps the colours to the tracers and defines the value (in  $\text{Tg yr}^{-1}$ ) to which the black reference bars at the upper left corner correspond. Nitrogen oxides include  $\text{NO}$ ,  $\text{NO}_2$ , Peroxyacetyl nitrate (PAN),  $\text{NO}_3$ ,  $\text{HNO}_4$  and  $\text{N}_2\text{O}_5$ , but no nitric acid or aerosol nitrate. Sulphur oxides include  $\text{SO}_2$  and  $\text{H}_2\text{SO}_4$ , but no aerosol sulphate. Nitrogen compounds are expressed as masses N, sulphur compounds as masses S and sea salt as masses Na. For black-and-white print: the bars represent from left to right (for east/west transport from bottom to top): nitrogen oxides, sulphur oxides, ammonia, nitric acid, ammonium, nitrate, sulphate, black carbon, organic matter, mineral dust and sea salt.

About 15% of the nitric acid produced by chemistry is taken up by aerosols. Like for ammonia, dry deposition (45% of production) is a larger sink for nitric acid than wet deposition (25%). Export of nitric acid is small (10% of production). Only about 5% of the nitric acid produced in the boundary layer enters the free atmosphere, while a sizable amount of nitric acid is produced in the free atmosphere. In this atmospheric domain, there is remarkably little absorption of nitric acid by aerosols, which is due to the acidic aerosol environment. We clearly model a high sulphate burden in the free atmosphere compared to ammonium and ammonia (see Table 3.4). About 35% of the nitric acid is exported and the other 65% is removed by wet deposition.

The budget terms of the inorganic secondary aerosols (ammonium, nitrate and sulphate) are relatively similar. Almost half of the inorganic aerosol material absorbed or produced in the boundary layer is removed by wet deposition (ammonium: 40%, nitrate: 55%, sulphate: 40%). Horizontal export in the boundary layer is close to one quarter (ammonium: 25%, nitrate: 15%, sulphate: 30%). The rest, about a third, enters the free troposphere (ammonium: 40%, nitrate: 30%, sulphate: 25%). In the free troposphere, a little over half is removed by wet deposition (ammonium: 55%, nitrate: 60%, sulphate: 55%) and the rest is exported. Aerosol nitrate is more concentrated in the boundary layer, while ammonium is equally distributed between boundary layer and free atmosphere and sulphate is more abundant in the free atmosphere. This can be explained by production in the free atmosphere, which is done efficiently for sulphate in clouds (60% of production in the free atmosphere). Together with dry oxidation followed by condensation, the production of sulphate is responsible for the majority of the sulphate source in the free atmosphere (80%), so only a small part comes from the boundary layer. For ammonium, this production percentage is 45% and for nitrate only 5%. This low nitrate production in the free atmosphere is, as explained above, due to the acidic environment. Notable is that ammonium does have a significant horizontal export term (25% in boundary layer and 50% in free atmosphere), while ammonia has not. Ammonia is only abundant in the Netherlands and only a very small part will make it to the European borders without being absorbed by aerosols.

Sulphate is produced by oxidation of sulphur dioxide, partly in clouds (45% in boundary layer and 60% in free atmosphere). The sulphur dioxide oxidised in clouds directly produces sulphate in the aerosol phase ("C" as sulphate source and  $\text{SO}_x$  sink in Tables 3.3 and 3.4), while the dry oxidation of sulphur dioxide produces sulphuric acid, which quickly condenses on aerosols ("A" as sulphate source and  $\text{SO}_x$  sink in Tables 3.3 and 3.4). Out of the emitted sulphur dioxide in the boundary layer, about 10% is oxidised and another 5% is exported and 20% enters the free atmosphere. The rest is removed by dry (55% of emission) and wet (10% of emission) deposition. There is a considerable amount of sulphur dioxide that is injected directly into the free atmosphere, mainly by volcanic emissions (Andres and Kasgnoc, 1998; Halmer et al., 2002). Together with what is transported up from the boundary layer, this sulphur dioxide is oxidised to sulphate for 35%, 20% is removed by wet deposition and 45% is exported out of Europe. Sulphur dioxide production by oxidation of dimethyl sulphide ("C" as  $\text{SO}_x$  source in Tables 3.3 and 3.4) is small.

Nitric acid, and thus aerosol nitrate, originates from other nitrogen oxides in the atmosphere ( $\text{NO}_y$ ). Note that  $\text{NO}_y$  does not include nitric acid. Out of the emitted nitrogen oxides in the boundary layer, 55% is removed by chemical processes. Besides oxidation to nitric acid, nitrogen oxides are also removed by reactions with organic chemicals (not shown). Dry deposition removes 15% of the emitted nitrogen oxides in the boundary layer, 20% goes to the free atmosphere and only 5% is exported. A small amount of nitrogen oxides are directly injected into the free atmosphere by lightning (Pickering et al., 1998) and aircraft emissions. In the free atmosphere, 75% of the nitrogen oxides is removed chemically and 25% is exported.

### 3.3.4 Optical analysis

In Table 3.5, Fig. 3.7 (upper panels) and Fig. 3.8, we compare the calculated optical data with AERONET observations. We clearly underestimate AOD systematically, though the temporal variability is captured adequately by the model. Generally, the AOD in summer is much higher than in winter, and the relative underprediction by TM5 is less in summer and early autumn (factor less than two) than in other months with a factor often above two (see Fig. 3.9). Also note that more data points are available in summer than in winter.

As the AOD is severely underestimated, we can conclude that besides the small underestimation of the  $\text{PM}_{10}$  surface concentrations, the total column burden appears to be underestimated by a factor of two. Part of the underestimation may be due to emissions that are not included in the model. de Meij et al. (2006) shows that calculated AODs at low relative humidities are underestimated, indicating that the AEROCOM emissions are too low. Another reason for the underestimation of the AODs is that the vertical distribution is not well represented. The underestimated emissions include non-combustion aerosols such as emissions from agricultural activities or traffic abrasion and resuspension (Sternbeck et al., 2002). However, this will mainly affect surface  $\text{PM}_{10}$  concentrations rather than AOD. We will show in Sect. 3.3.5.2 that the severe underestimation of the AOD in eastern Europe is largely explained by inadequate biomass burning emission used by the model. The underestimation of the AOD may also be related to too high wet-deposition rates (Chin et al., 2000). Wet deposition is a dominant term in the budget (Tables 3.3 and 3.4) and we will address this further in Sect. 3.3.5.1.

At those stations that are located within or near major source regions of black carbon, part of the underestimation of AOD values may derive from biases introduced by the homogeneous sphere approximation, which is employed in Mie computations. For instance, externally mixed black carbon aggregates absorb twice as much radiation in the atmosphere as volume-equivalent homogeneous spheres (Kahnert, 2010a,b). Model computations that account for inhomogeneous mixing of BC with soluble aerosol components predict absorption cross sections that are a factor of 1.5 higher than those computed with a homogeneous mixture approximation (Bond et al., 2006). Such morphological effects are neglected in our effective medium and Mie computations and may contribute to the AOD bias.

There is a reasonable temporal correlations between observed and modelled

**Table 3.5:** Comparison between modelled and observed optical parameters. Listed are temporal correlations, averages of time series of the AOD 440 nm and the Ångström parameter 440–870 nm, and the number of points (#) in the time series at 18 European AERONET stations.

Station name	AOD 440 nm			Ångström 440–870 nm			#
	$r$	model	obs.	$r$	model	obs.	
Belsk	0.37	0.162	0.296	0.47	1.577	1.524	992
Cabauw	0.58	0.138	0.323	0.71	1.332	1.173	515
Chilbolton	0.68	0.103	0.235	0.58	1.102	1.156	746
Dunkerque	0.59	0.105	0.277	0.52	1.221	1.202	686
El Arenosillo	0.78	0.175	0.268	0.70	0.813	0.915	62
Forth Crete	0.58	0.187	0.233	0.72	1.092	1.108	1787
Granada	0.61	0.117	0.210	0.39	0.997	1.057	1733
Hamburg	0.38	0.102	0.246	0.27	1.410	1.481	843
Hornsund	0.51	0.015	0.135	0.45	0.657	1.298	265
Ispira	0.49	0.107	0.307	0.30	1.403	1.520	1280
Karlsruhe	0.60	0.149	0.334	0.57	1.435	1.394	623
La Fauga	0.61	0.117	0.205	0.55	1.222	1.403	1275
Messina	0.40	0.127	0.226	0.47	1.063	1.198	784
Minsk	0.06	0.086	0.303	0.61	1.429	1.505	669
Moldova	0.38	0.144	0.257	0.53	1.504	1.668	1302
Moscow MSU MO	0.29	0.132	0.320	0.48	1.555	1.528	772
Rome Tor Vergata	0.63	0.154	0.238	0.60	1.317	1.326	1679
SMHI	0.66	0.062	0.184	0.60	1.270	1.160	700

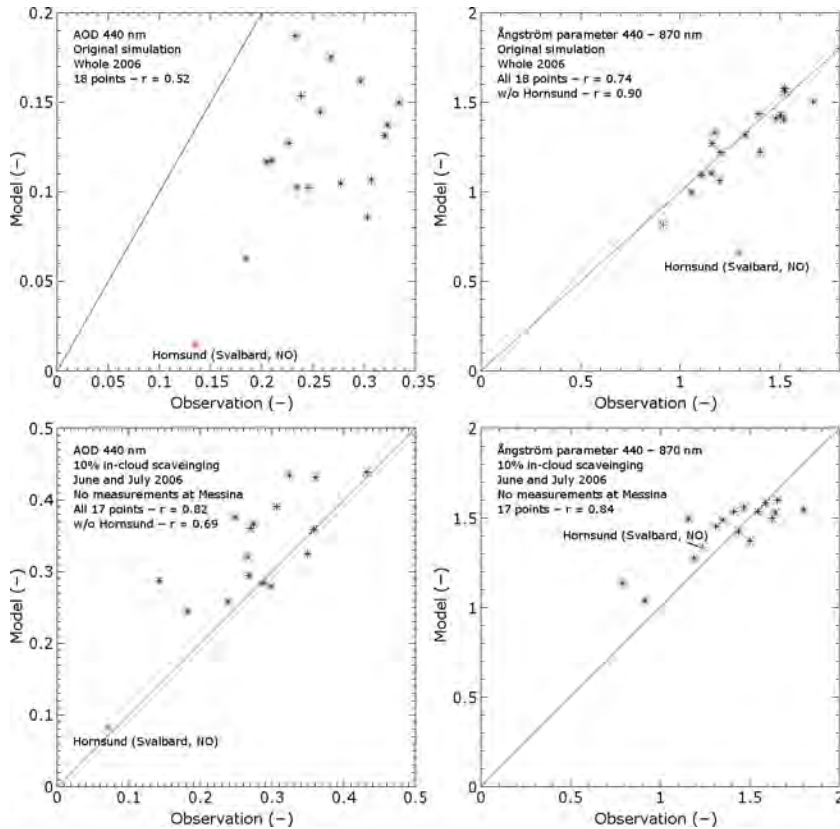


**Figure 3.7:** Comparison between modelled and observed AOD (440 nm) and Ångström parameter (440–870 nm) at AERONET stations. Above: Original results (average over whole 2006). Below: simulation with in-cloud scavenging rates scaled down by a factor of 10 (average over June and July 2006).

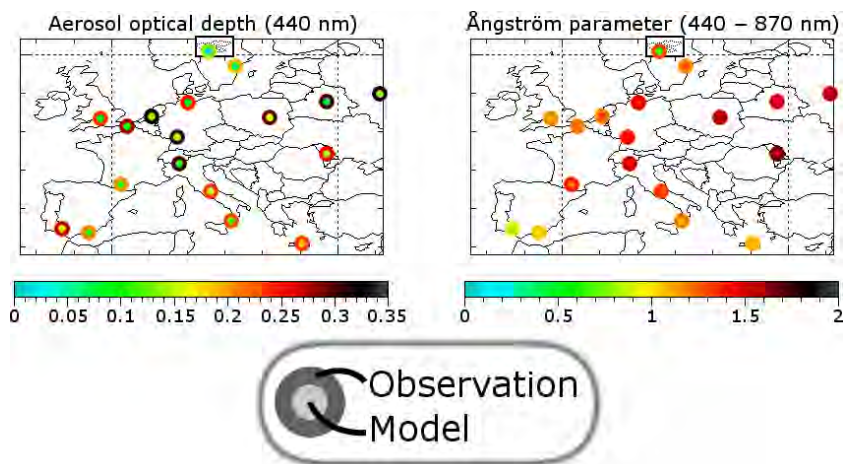


**Figure 3.8:** Graphical overview of the comparison between modelled and observed AOD (440 nm) and Ångström parameter (440 – 870 nm) at AERONET stations. The island in the upper box is Svalbard (Norway).

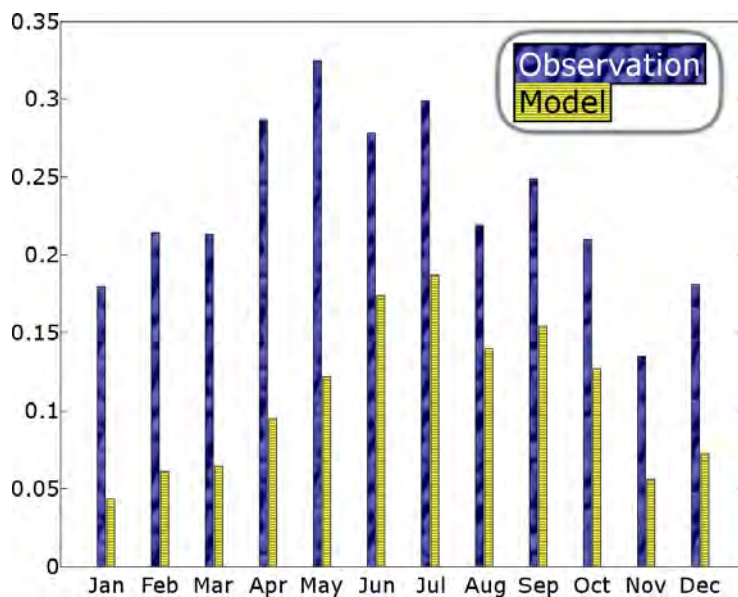


**Figure 3.9:** Comparison between modelled and observed AOD per month. Valid data of all AERONET stations are averaged.

Ångström parameter (Table 3.5). The yearly averages agree very well. Also, the spatial variability among station is represented very well. There is one exception (Hornsund, Svalbard), which is due to the low AOD values there, making the Ångström parameter very sensitive to errors.

### 3.3.5 Uncertainty analysis

In this section, we will investigate the uncertainties related to two key processes: wet removal and emission strengths. With sensitivity simulations we explore possible explanations for the underestimation of the AOD.

#### 3.3.5.1 Wet deposition

Wet deposition is an important sink, especially in the free atmosphere (see Table 3.4). A too fast wet-deposition rate may therefore explain why the AOD is underestimated while the surface concentrations look reasonable. We performed three additional simulations for May, June and July 2006 with all in-cloud scavenging rates (both for stratiform and convective precipitation) scaled down to respectively 50%, 10% and 0%. It appeared that halving (50%) the in-cloud scavenging hardly made any difference in the simulated AOD values (about 10% higher AOD after spin-up). This clearly indicates the high efficiency of wet deposition in TM5. As expected, completely ignoring it (0%) resulted in unrealistically high values for the AOD (factor 6 after three months and ever rising). We will analyse the 10% wet-removal simulation, which showed a clear improvement, for the analysis period June and July 2006.

Figure 3.7 (lower panels) shows that in the 10% simulation, the large underestimation of the AOD has been turned into a slight overestimation. The Ångström parameter is still represented quite well, which indicates that the aerosol size distribution is little affected. Although the modelled AOD and Ångström parameter now agree in Hornsund, the temporal correlation between model and observations at that station remains very poor (not shown). In general, the temporal correlations remain roughly similar (not shown).

We also investigated the changes in surface concentrations that result from a reduction of in-cloud scavenging to 10%. Sulphate and sea salt concentrations rise significantly (about 50%), while other compounds change only very little. From Fig. 3.3, it is clear that we already overestimate sea salt by 50%. Also the agreement of surface concentrations of sulphate, good in the unperturbed simulation as shown in Fig. 3.3, slightly deteriorates by reducing the wet-removal rates.

It appears that a scaling factor of 10% on the wet-deposition rates results in slightly too high surface concentrations and AOD values. For AOD, we expect a slight underestimation because of non-implemented emissions of biogenic volatile compounds and resuspension. The signal of the surface concentrations also indicates that with a 10% scaling of the in-cloud scavenging, the wet removal is underestimated. The aerosol budget changes mainly in the free troposphere. Based on an analysis of the months June and July, we estimate that the wet-deposition flux is roughly halved in favour of the net export.

We refrain from a further tuning of the wet deposition here, because a sound parameterisation should be based on the physical and numerical considerations (e.g. grid-size dependency) that are associated with both stratiform and convective wet removal. We have shown, however, that a poor representation of wet deposition may be a major cause of the general underestimation of the AOD and may have masked other model deficiencies.

### 3.3.5.2 Forest fires

Emission inventories exhibit multiple uncertainties. We already addressed the lack of resuspension in our model and the possible underestimation of secondary organic aerosols. Besides these missed sources, there is also a significant uncertainty in biomass burning emissions. Our model uses climatologic GFED fire emissions, while real biomass burning emissions tend to exhibit large variability between the years and between the seasons in a year (van der Werf et al., 2006). An extreme case occurred in spring 2006, when there were strong forest fires in western Russia (Sofiev et al., 2009; Saarikoski et al., 2007). These events take place every spring, but in 2006 they were particularly strong. Apart from that, the last week of April and the first week of May, the mean wind direction in eastern Europe (20° E–30° E) was easterly, which coincides with the fires. This transported the smoke towards Europe, so that it was recorded in the time series of the AOD in eastern European stations.

Figure 3.10 (upper two graphs) shows a comparison between modelled and observed AOD for Dunkerque and Minsk, in which we can see that Minsk exhibits a clearly separate population of points that belong to the period of the forest fires. For Dunkerque, the points of this period are more mixed with the rest of the dataset. The high observed AOD values during the event were not reproduced by the model. Because easterly circulation is associated with fair weather, the possible too high wet-deposition rates in the model is not likely to play a significant role.

To reproduce the high AOD values at the eastern European stations, we repeated the simulation with the European emission data from the Fire Assimilation System (FAS) that was used in combination with the dispersion model SILAM (Sofiev et al., 2009). The FAS-SILAM PM<sub>2.5</sub> emissions in the area specified below are 4.3 Tg for the considered monthly period, while the climatologic GFED emissions in that area were only 8.7 Gg per month (500 times less). Moreover, the GFED emissions are temporally spread over the entire months, while FAS reported them with daily resolution. As the majority of the emissions occurred during the days with easterly winds, it was evidently important to apply a daily time resolution of emissions to capture the specific transport conditions during the event.

The FAS-SILAM emission data consist of daily 2D fields of PM<sub>2.5</sub> emissions in Europe (11° W–73° E, 34° N–80° N). We assumed that 10% of this PM<sub>2.5</sub> is black carbon and 90% is organic matter, which is a rough estimation based on observations in Saarikoski et al. (2007). This assumption may influence the results as the optical properties of black carbon and organic matter are different. Also, the injection height of these emissions can be important (Chen et al., 2009). We assumed

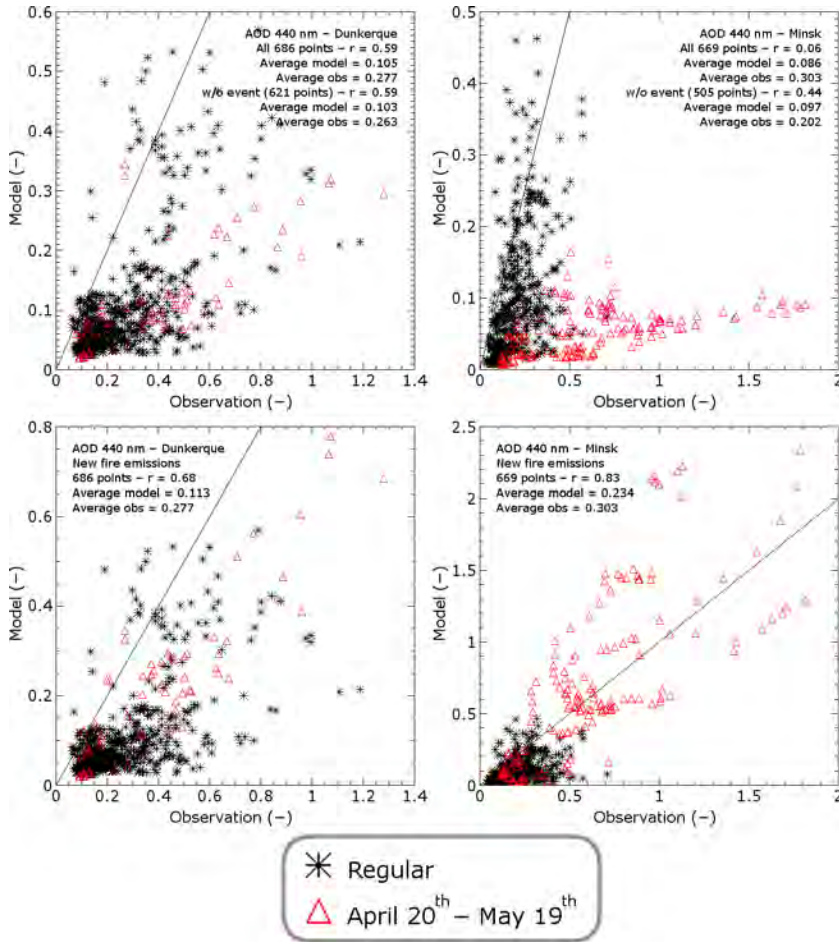


**Figure 3.10:** Time series of modelled and observed AOD (440 nm) for Dunkerque (left) and Minsk (right). Upper panels: Only climatologic GFED emissions. Lower panels: New simulation with FAS-SILAM emissions. Both simulations use the regular wet-deposition rates.

the following distribution injection heights following Dentener et al. (2006): 20% between surface and 100 m, 20% between 100 m and 500 m, 20% between 500 m and 1 km and 40% between 1 km and 2 km. We performed a simulation, replacing the original climatologic emissions from 15 April to 14 May.

Figure 3.10 (lower two graphs) show the results for the two AERONET stations. There is a drastic improvement for Minsk, which indicates that this event is caught by the model including these emissions. There is also a small improvement in the results for Dunkerque as well, which means that Dunkerque is affected by these emissions through long range transport. The improvement in the model results clearly illustrates that episodic fire events at the eastern edge of Europe in combination with certain transport patterns may have a significant impact throughout the European domain.

### 3.4 Conclusions

Size-resolved aerosol simulations with the TM5 model coupled to the M7 module have been conducted for the year 2006 with a focus on the European domain ( $34^{\circ}$  N –  $62^{\circ}$  N,  $12^{\circ}$  W –  $36^{\circ}$  E). The main conclusions can be summarised as follows:

- Comparison of the simulated aerosol distribution with surface observations over Europe shows a reasonably good agreement with spatial correlations of simulated PM mass of 0.75. As expected, spatial correlations are lowest ( $r = 0.64$ ) and biases are highest for  $\text{PM}_{10}$ , possibly due to neglected resuspension of aerosols. Total ammonium ( $r = 0.61$ ) is overestimated in the high concentration range, due to the overestimation of  $\text{NH}_3$  in emission regions.
- A three-dimensional budget analysis is carried out to enable model inter-comparison and assessment of important uncertainties. From our budget, we can conclude that Europe is a net exporter of anthropogenic aerosols, and an importer of natural aerosols (sea salt and mineral dust). For instance, it is calculated that about half of the emitted anthropogenic carbonaceous aerosols are exported from Europe. Dust is the only aerosol component that exhibits a negative vertical flux over the European domain. Notable is that the export rate of gaseous pollutants (e.g. nitrogen oxides) is considerably lower than for anthropogenic aerosols because of dry deposition.
- A comparison to AERONET AOD measurements shows a serious underestimation of the modelled AOD values. We showed that a significant down-scaling of the wet-removal rates in the model is required to bring the model closer to the observations. This, however, significantly raises the modelled surface sulphate and sea salt concentrations, while other components are little affected. The modelled Ångström parameter is little affected, which indicates that the aerosol size distribution remains roughly the same.
- We have shown that, apart from uncertainties with the wet removal, large uncertainties arise from inaccurate emission inventories. We were able to significantly improve the modelled AOD at Minsk in April and May 2006 by

replacing the GFED climatologic fire emissions by a tailored fire emission inventory that is based on daily fire counts.

Based on this study, future model developments will target at improving the aerosol wet-deposition parameterisation in the TM5 model and the aerosol emission inventories. TM5 employs multiple resolutions at the same time, which calls for a fundamental approach of resolution-dependent processes like the wet removal of aerosols. Fire emissions, but also the emissions of aerosol precursors such as  $\text{NH}_3$  exhibit day-to-day variability and diurnal emission patterns that should be taken into account to enable a sound comparison to observations. Finally, it is recommended to continue inter-model (Wilson et al., 2001; Bauer et al., 2008; de Meij et al., 2006) comparisons based on budget analysis as presented in this paper or similar techniques (Textor et al., 2006).

## Acknowledgements

This work benefited from measurements by the Programme for Monitoring and Evaluation of the Long-range Transmission of Air Pollutants in Europe (EMEP) and the Aerosol Robotic Network (AERONET). We thank the principal investigators of these networks and their staff for establishing and maintaining the sites used in this investigation. This research received financial support from the BOP (Policy supporting programme for particulate matter). We would like to thank the NCF (Foundation of national computer facilities) for providing the ability to run TM5 on the supercomputer Huygens. We would like to thank Olivier Boucher for programming Mie scattering calculations for aerosol distributions. M. Kahnert was supported by the Swedish Research Council under contract number 80438701.

Edited by: Y. Balkanski

# 4

---

## Modelling the partitioning of ammonium nitrate in the convective boundary layer

An explanatory model study is presented on semi-volatile secondary inorganic aerosols on three clear days in May 2008 during the IMPACT campaign at the Cabauw tower in the Netherlands. A single column model in combination with the equilibrium aerosol model ISORROPIA is used. This model uses surface observations from IMPACT and calculates the gas-aerosol partitioning of ammonium nitrate. The calculated gas-aerosol equilibrium overestimates the gas phase fraction during daytime, and overestimates the aerosol phase fraction during nighttime. This discrepancy can partly be solved when the approach of the gas-aerosol equilibrium is forced to proceed with a delay timescale of up to two hours. Although it is shown that the delay itself has a small effect, the most important effect is caused by the mixing of air from higher altitudes at which the equilibrium is shifted to the aerosol phase. Thus, vertical mixing is shown to have a significant influence on the calculated partitioning at the surface. On some occasions, the correspondence to the observed partitioning improves dramatically.

Even though gas-aerosol partitioning of ammonium nitrate is not instantaneous, observations show that a different equilibrium in the upper boundary layer causes aerosol ammonium nitrate concentrations to increase with altitude. Our model calculates similar vertical gradients depending on the assumed speed of gas-aerosol equilibrium. The calculated optical properties of the aerosol show a similar behaviour. The aerosol optical properties depend on the aerosol size distribution both directly, because light scattering depends on particle size, and indirectly, because the equilibration timescale depends on the aerosol sizes. Future studies should therefore focus on a fully size-resolved treatment of the gas-aerosol partitioning. Finally, coarser-resolution models may treat the gas-aerosol equilibrium of ammonium nitrate by calculating the equilibrium with a temperature and humidity sampled at a different altitude. We found that the equilibrium at an altitude of 200 m (night) up to 600 m (day) is representative for the partitioning of ammonium nitrate at the surface in the beginning of May 2008.

## 4.1 Introduction

Aerosols have a pronounced influence on the climate system, both directly by scattering and absorbing incoming solar radiation (Hess et al., 1998; Haywood and Boucher, 2000; IPCC, 2007) and indirectly by altering cloud properties (Rosenfeld et al., 2008; Kaufman et al., 2002). The combined climate effect of aerosols is poorly understood compared to the climate effect of greenhouse gases. In the Netherlands, nearly half (42%–48%) of the fine aerosol ( $\text{PM}_{2.5}$ ) mass consists of secondary inorganic aerosols (ammonium nitrate and ammonium sulphate) (Weijers et al., 2011), which are the dominant anthropogenic aerosol species in the size range with maximum light scattering (0.4–1.0  $\mu\text{m}$ ) (ten Brink et al., 1997). Also, these secondary inorganic aerosols are effective cloud condensation nuclei, because of their size and water solubility. Due to intensive agriculture, the ammonia concentrations in the Netherlands have always been sufficiently high to neutralise sulphuric and nitric acid. During the last twenty-five years, sulphur dioxide emissions have decreased much more than those of nitrogen oxides in Europe and

especially in the Netherlands (Vestreng et al., 2007, 2009). Therefore, ammonium nitrate has become increasingly important in comparison to ammonium sulphate. Ammonium nitrate and ammonium sulphate behave differently with varying temperature and relative humidity. First, ammonium sulphate resides exclusively in the aerosol phase, while ammonium nitrate resides in both the gas and the aerosol phase, where the gas-aerosol equilibrium strongly depends on the temperature and relative humidity. Furthermore, the aerosol water uptake by ammonium nitrate aerosol depends more strongly on the relative humidity than the water uptake of ammonium sulphate (Tang, 1996). Because both the aerosol dry mass (ammonium nitrate) and the aerosol water content is strongly enhanced at lower temperature and high relative humidity, the interaction of ammonium nitrate aerosol with solar radiation is also more strongly increased at these conditions than that of ammonium sulphate aerosol. With ammonium nitrate becoming increasingly important, systematic investigation of these properties seems appropriate.

Research into ammonium nitrate partitioning is hampered by insufficient data availability. Most continuous measurements at ground-based stations are made with common filter packs and are prone to artefacts due to volatilisation of ammonium nitrate or absorption of nitric acid (Yu et al., 2006; Zhang and McMurry, 1992; Cheng and Tsai, 1997). Continuous measurements of total ammonium ( $\text{NH}_3 + \text{NH}_4^+$ ) and total nitrate ( $\text{HNO}_3 + \text{NO}_3^-$ ) are more widespread and therefore often used for validating large-scale models. Correct separation between aerosol and gas phase is only possible with denuders in combination with a filter pack or a Steam Jet Aerosol Collector (Slanina et al., 2001; Schaap et al., 2002; Trebs et al., 2004). For continuous measurements, these labour intensive are rarely used. Therefore, reliable measurements of aerosol ammonium nitrate are often campaign-based like EUCAARI-LONGREX (Kulmala et al., 2009) and the IMPACT-campaign at the Cabauw tower in the Netherlands (Morgan et al., 2010).

Correct representation of the partitioning of semi-volatile species has been a challenge for modellers as well. For partitioning of ammonium nitrate, many large-scale models use equilibrium models such as EQSAM (Metzger et al., 2002a,b) or ISORROPIA (Nenes et al., 1998; Fountoukis and Nenes, 2007). Large-scale models usually assume that the gas-aerosol system is always in equilibrium, which means that the timescale of gas-aerosol partitioning is assumed much shorter than that of other processes such as turbulent mixing of the convective boundary layer ( $\sim 15$  min). Several studies, however, have pointed out that generally the gas-aerosol system is not in equilibrium (Wexler and Seinfeld, 1992; Meng and Seinfeld, 1996). Meng and Seinfeld (1996) pointed out that the timescale on which equilibrium is reached depends on the aerosol size and that the equilibrium assumption for coarse mode aerosols is generally not valid. Therefore, some studies use hybrid models, in which instant equilibrium is assumed for the fine fraction and a dynamic model is used for the coarse fractions (Capaldo et al., 2000; Feng and Penner, 2007).

Experimental evaluations of the equilibrium assumption for fine mode ammonium nitrate show contradicting results. A number of studies has shown that the predicted equilibrium is generally in accordance with observations (Zhang et al.,

2003; Takahama et al., 2004; Yu et al., 2005). Others have shown that observations show generally larger particulate phase nitrate concentrations than predicted during summer and daytime (Moya et al., 2001; Fisseha et al., 2006; Morino et al., 2006). For the Netherlands, Schaap et al. (2011) compared ISORROPIA calculations with hourly observations of the gas-aerosol partitioning obtained with a MARGA system (Thomas et al., 2009). These authors modelled too abundant aerosol nitrate during the night and at daytime in winter as well as too abundant gaseous nitric acid during the day in summer. They attributed the mismatch to either an incorrectly calculated equilibrium or a non-instantaneous equilibrium.

It has been postulated that the relative abundant nitrate during daytime in summer may partly be due to transport of nitrate richer air from the upper parts of the boundary layer to the ground (Morino et al., 2006). With flight missions in the vicinity of the Cabauw tower (the Netherlands), Morgan et al. (2010) observed that air from the upper boundary layer is indeed richer in aerosol nitrate compared to the surface. Also, they tried to explain the observed scattering coefficients in the upper boundary layer from surface observations in combination with observed humidity-dependence of aerosol light scattering, assuming a well-mixed boundary layer. The observed scattering coefficients in the upper boundary layer were higher than the predictions up to a factor two, which was attributed to enhanced partitioning of semi-volatile gas phase species to the particulate phase in the upper convective boundary layer where lower temperatures and higher relative humidities prevail. In this paper, we test the hypothesis that ammonium and nitrate gas-aerosol partitioning is in non-instantaneous equilibrium and that vertical mixing may explain the mismatch between predicted and observed partitioning.

The main part of this article is a model study on the partitioning of ammonium nitrate. The model is explained in Sect. 4.2. We will reproduce the results of Schaap et al. (2011) with an ISORROPIA box model in Sect. 4.3.1. In Sect. 4.3.2, the column model results are presented. There, we will analyse the partitioning timescale by analysing the gas-aerosol partitioning at the surface, the vertical profiles of aerosol nitrate and the optical properties. Inspired by the model results, some technical analysis is done. In Sect. 4.3.3, we test the assumptions on which our optical calculations are based (see also Sect. 4.2.2.3). In Sect. 4.3.4, we provide a solution for coarse-resolution models for the issue that one cannot assume instant equilibrium of ammonium nitrate in the convective boundary layer.

## 4.2 Materials and methods

In this section, we describe the observations and the model used in this study as well as their interaction. Our study is based on observations collected at the Cabauw tower in the Netherlands ( $51^\circ 58.223' \text{ N}$ ,  $4^\circ 55.575' \text{ E}$ ) during the EUCAARI intensive measurement campaign (IMPACT). Our analysis focuses on May 2008, as the fair-weather conditions during this month are easier to simulate and because aircraft data were available. Below, we start with an overview of the meteorological, chemical and physical measurements. Next, the Wageningen University Single Column Model (WUSCM) is introduced.

## 4.2.1 Observations

The Cabauw Experimental Site for Atmospheric Research (CESAR; <http://www.cesar-observatory.nl>; Russchenberg et al., 2005) provides a host of meteorological data. We use primarily the temperature and the dew point temperature at 2 m. From these quantities, the relative humidity is calculated. Furthermore, a CT75 Ceilometer provides aerosol backscatter profiles and therewith a qualitative indication of the boundary layer height. We will tune our model such that these observations are reproduced. Tuning parameters that influence the meteorology are initial temperature profiles, initial moisture profiles and a radiation tuning parameter that will be explained in Sect. 4.2.2.1. On clear days, this procedure leads to an excellent representation of the two-metre temperature and relative humidity (see Sect. 4.3.2.1). Furthermore, our modelled boundary layer height in the afternoon corresponds well with the ceilometer backscatter data.

We used hourly integrated data of both inorganic aerosol composition and the precursor gas concentrations as obtained with a MARGA-instrument (Schaap et al., 2011). MARGA (Monitor for AeRosols and Gases, Applikon Analytical BV) is the commercialised version of the GRAEGOR system (Thomas et al., 2009; ten Brink et al., 2009). Among other inorganic components, the gases  $\text{NH}_3$  and  $\text{HNO}_3$  as well as the PM components  $\text{NO}_3^-$ ,  $\text{SO}_4^{2-}$  and  $\text{NH}_4^+$  were measured with hourly frequency. The sampling part of MARGA comprises a wet rotating annular denuder (WAD) for the collection of the precursor gases (Keuken et al., 1988) and subsequently a steam jet aerosol collector (SJAC) for the collection of the particulate matter (Khlystov et al., 1995; Slanina et al., 2001). The MARGA was located indoor while a Teflon coated  $\text{PM}_{10}$  (URG) inlet was mounted on the edge of the roof. For a more detailed description of the campaign and the instrument, we refer above-mentioned references (Schaap et al., 2011; Thomas et al., 2009; ten Brink et al., 2009; Keuken et al., 1988; Khlystov et al., 1995; Slanina et al., 2001). The concentrations of sulphate, total ammonium ( $\text{NH}_3 + \text{NH}_4^+$ ) and total nitrate ( $\text{HNO}_3 + \text{NO}_3^-$ ) are used to prescribe the model. The observed partitioning of ammonium nitrate is used to evaluate the model.

The aerosol size distribution is measured with a Scanning Mobility Particle Sizer (SMPS; Zieger et al., 2011; ten Brink et al., 1983; Wang and Flagan, 1990). The mobility size spectrometer consists of a sequential set-up of an impactor, neutraliser, differential mobility analyser (DMA) and a condensation particle counter (CPC). In the DMA, aerosol particles are classified according to their electrical mobility. The analyser consists of a cylinder with a negatively charged rod at the centre. Only aerosols in a narrow range of mobility exit through the output slit, where they enter the CPC, which determines the particle concentration of that size. The size of the particles reaching the output slit is being determined by the control rod voltage and the flow within the DMA. Before entering the DMA, aerosols are brought to a bipolar charge equilibrium using a  $^{85}\text{Kr}$  bipolar charger (neutraliser). In charge equilibrium, the fraction of particles with a single elementary charge is known for all sizes (Wiedensohler, 1988). Particles with diameter larger than about 800 nm are removed by a 0.0457 centimetre-diameter-orifice aerosol inlet in order to facilitate multiple charge correction. Because the aerosols are in charge

equilibrium, the total number of particles can be calculated. The output data of the SMPS is a particles number size distribution as  $(\frac{dN}{d\log D})$ , where  $N$  is the number of aerosols and  $D$  is the aerodynamic diameter. The SMPS at Cabauw measures 70 logarithmically equidistant size bins ranging from 10 nm to 520 nm. The aerosol size distribution is only used for the optical module (see Sect. 4.2.2.3).

Morgan et al. (2010) present aircraft observations of 8 May and 21 May in the vicinity of Cabauw. Particulate sulphate, nitrate, ammonium and organics were observed during the flights at different altitudes with an on-board Aerodyne compact time-of-flight aerosol mass spectrometer (cToF-AMS) (Drewnick et al., 2005; Canagaratna et al., 2007). The AMS measures the fine fraction of the aerosol, with 100% transmission for aerodynamic diameters of 40–700 nm (DeCarlo et al., 2004). The scattering coefficient is measured with a TSI 3563 nephelometer (Anderson et al., 1996) at wavelengths of 450 nm, 550 nm and 700 nm, of which the value at 550 nm wavelength is used in our analysis. The humidity dependence of the light scattering by the aerosols was obtained by measuring the scattering coefficient of a sample of aerosols at varying relative humidity (RH) values, while keeping all other parameters fixed. The measured RH-dependency was fit with the following formula which is referred to as  $f(\text{RH})$  (Morgan et al., 2010).

$$\sigma = \sigma_{\text{dry}}(1 + a\text{RH}^b) \quad (4.1)$$

Here, RH is the relative humidity (0–1),  $\sigma$  is the scattering cross section and  $\sigma_{\text{dry}}$  is the scattering cross section at dehydrated conditions (RH < 40%). The parameters  $a$  and  $b$  were determined to fit the observations. The values of  $a$  and  $b$  may depend on aerosol composition and aerosol size distribution, but they should not directly depend on temperature. The  $f(\text{RH})$  is measured multiple times during a flight. As a result, the values for  $a$  and  $b$  represent the average situation during the whole flight.

## 4.2.2 The model

The Wageningen University Single Column Model (WUSCM) simulates boundary layer meteorology (radiation, land-atmosphere interaction and mixing) and can support chemistry schemes. For this study, we adopted a simple chemistry scheme that only involves gas-aerosol partitioning. Only seven tracers are taken into account: ammonia ( $\text{NH}_3$ ), ammonium ( $\text{NH}_4^+$ ), nitric acid ( $\text{HNO}_3$ ), nitrate ( $\text{NO}_3^-$ ), sulphate ( $\text{SO}_4^{2-}$ ), bisulphate ( $\text{HSO}_4^-$ ) and aerosol water ( $\text{H}_2\text{O}$ ). The optical module is not coupled directly to the WUSCM model. This module calculates the scattering coefficient from the model output, without feeding back to the model.

For simplicity, this study does not employ a size-resolved aerosols scheme. Sizes of aerosols are only used for optical calculations, for which we use the observed aerosol size distribution (see Sects. 4.2.1 and 4.2.2.3). Furthermore, the interaction between sulphate, ammonium and nitrate with other components is neglected. It should be noted that sea salt (sodium chloride) may displace nitric acid, becoming sodium nitrate and outgassing hydrochlorid acid (Schaap et al., 2004a; Glasgow, 2008), shifting the partitioning of nitrate towards the aerosol phase. However,

the simulated days were dominated by easterly winds and therefore low sea salt concentrations. Additionally, soluble organic matter may also influence the activity of inorganic components by uptake of additional water. These effects are difficult to represent in our model and are considered beyond the scope of this study.

The model has a resolution of 200 levels with equal pressure intervals of 150 Pa, ranging from the surface to about three kilometres altitude and the soil is represented with four layers. No upper boundary condition is applied. In all our cases, the top of the domain ( $\sim 3$  km) is far above the boundary layer, so the upper boundary condition does not directly influence our study area (the boundary layer) on the timescale of one day. The surface boundary condition is determined by observations as explained in Sect. 4.2.1. We use a model spin-up of one day. The model integrates with a third order Runge-Kutta system (Wicker and Skamarock, 2002), which means that tendencies for the individual processes (e.g. diffusion and chemistry) are evaluated and added. The overall time step is 20 s.

#### 4.2.2.1 Meteorological module

The radiation scheme is based on the Tropospheric Ultraviolet and Visible radiation model (TUV; Madronich, 1987). With TUV, we calculated the incoming short-wave radiation as function of zenith angle. We apply this radiation with a tuning parameter that accounts for the optical depth of the atmosphere (e.g. clouds). The calculated aerosol light scattering does not feed back on the incoming short-wave radiation.

Evapotranspiration is parameterised by calculating the canopy resistance, which depends on e.g. leaf area index. This resistance is corrected for short-wave radiation (Jarvis, 1976). The soil temperature, which is important for the long-wave radiation budget, is also calculated by the model's surface scheme.

Boundary layer diffusion is simulated with the Medium-Range Forecast (MRF) scheme following Troen and Mahrt (1986) and Hong and Pan (1996). Diffusion tendencies are implicitly determined. It includes non-local momentum fluxes according to Noh et al. (2003). The local diffusivities are calculated with the local Richardson numbers and the counter-gradient fluxes are calculated with a constant for excess temperature.

#### 4.2.2.2 Chemical module

Our model employs ISORROPIA version 2 (Fountoukis and Nenes, 2007) to calculate the gas-aerosol equilibrium. ISORROPIA calculates the fraction of aerosol phase ammonium and nitrate at equilibrium given the total ammonium ( $\text{NH}_3 + \text{NH}_4^+$ ) concentration, the total nitrate ( $\text{HNO}_3 + \text{NO}_3^-$ ) concentration, the sulphate concentration, the temperature and the relative humidity. ISORROPIA also calculates the water content of the aerosols at equilibrium. ISORROPIA uses a bulk aerosol approach, so no aerosol size distribution is taken into account to calculate the gas-aerosol equilibrium. To mimic the fact that equilibrium is not reached instantaneously, we introduce a parameter,  $\tau_p$  to set the speed at which the equi-

librium is reached. The tendency given by ISORROPIA to the model is

$$\frac{d\mathbf{C}}{dt} = \frac{\mathbf{C}_{\text{eq}} - \mathbf{C}}{\tau_p} \quad (4.2)$$

Here,  $\mathbf{C}$  is the concentration vector of all tracers, and  $\mathbf{C}_{\text{eq}}$  is the equilibrium calculated by ISORROPIA. The parameter  $\tau_p$  will be used as a tuning parameter that we will vary to improve the correspondence to observations. If we want to assume instant equilibrium, we use  $\tau_p = 20$  s, equal to the general time step to keep the model numerically stable.

In reality, aerosols may exhibit a phase hysteresis (Wang et al., 2008). Depending on the history of the relative humidity, aerosols may be in a metastable (supersaturated) state or in a solid state coated with saturated liquid material. In our study area (the Netherlands), the humidity is generally high enough (40% and higher), so we assume that our aerosols remain at the humid, metastable side of the hysteresis.

The concentrations of the inert tracers: sulphate, total nitrate ( $\text{NO}_3^- + \text{HNO}_3$ ) and total ammonium ( $\text{NH}_4^+ + \text{NH}_3$ ) at the surface were prescribed equal to the time-interpolated observations at Cabauw. This allows us to represent the correct concentrations of these tracers without implementation of processes like advection, emission and deposition. When updating a concentration, the partitioning between gas and aerosol phase is set equal to that of the previous time step in the model. Although this prescription works well, it should be realised that advection, emission or deposition of ammonium or nitrate with a different partitioning can cause biases, because the prescription leaves the partitioning the same. This can influence the results when the timescale of partitioning is large. Finally, prescription of the total-concentrations at the surface may result in slight biases when advection occurs in the upper convective boundary layer. Due to the strong vertical mixing during daytime, we think that these biases are generally small. In general, the above-described procedure works adequately for a well-mixed boundary layer. Our analysis will therefore focus on the daytime, which is also the most relevant for the radiative effect of aerosols.

#### 4.2.2.3 Optical module

We model the light scattering by the aerosols with a Mie-scattering module (O. Boucher, personal communication, 2004). This code calculates the scattering cross section of aerosols with a certain size ( $x = \frac{2\pi r}{\lambda}$ ) and complex refractive index ( $m$ ). We apply the Mie-calculation for 70 size bins with SMPS measurements as input.

The SMPS instrument measures the aerosol size distribution as a differential aerosol count in an aerodynamic diameter range ( $\frac{dN}{d \log D_a}$ ). The optical calculations require the number concentrations ( $\frac{N}{V}$ ) per size bin. For the optical calculations, it is very important that the aerosol number concentration and size distribution are consistent with the total aerosol mass. Without calibration, the observed aerosol number concentration is not consistent with the modelled aerosol mass. For example, the model neglects organic aerosol mass, while organic aerosols are

counted by the SMPS. Also, the model assumes spherical aerosols with volume equal to  $\frac{\pi}{6}D_a^3$ . In reality, the mass of an aerosol with aerodynamic diameter  $D_a$  may be different. Therefore, the SMPS output has to be calibrated to match with the model assumptions. Thus a normalisation constant is required for the conversion.

$$\frac{N}{V} \equiv S \frac{dN}{d \log D} \quad (4.3)$$

This normalisation constant  $S$  scales the measured  $\frac{dN}{d \log D}$  to reproduce  $\frac{N}{V}$  for all size bins in such a way that it fits with the modelled aerosol material. It is obtained by setting up an equation for the total aerosol volume per cubic metre air. On the left hand side, we calculate the total aerosol volume by adding up the volume (mass divided by density) of the aerosol components. On the right hand side, we add up the aerosol numbers and calculate their volumes assuming a spherical shape.

$$\sum_j \frac{C_{j,\text{surf}}}{\rho_j} = \frac{\pi}{6} S \sum_i \left( \frac{dN}{d \log D} \right)_i D_{i,\text{SMPS}}^3 \quad (4.4)$$

On the left hand side,  $j$  is an aerosol component (ammonium nitrate and ammonium sulphate),  $\rho_j$  is the density of component  $j$  and  $C_{j,\text{surf}}$  is the modelled mass concentration of component  $j$  at the surface. On the right hand side,  $i$  is a size bin,  $\left( \frac{dN}{d \log D} \right)_i$  is the measured quantity by the SMPS for bin  $i$ , and  $D_{i,\text{SMPS}}$  is the size (diameter) of the size bin  $i$ . The label ‘‘SMPS’’ is added to indicate that this is the size of the aerosols when they are measured by the SMPS. The normalisation constant  $S$  is then obtained as:

$$S = \frac{6}{\pi} \frac{\sum_j \frac{C_{j,\text{surf}}}{\rho_j}}{\sum_i \left( \frac{dN}{d \log D} \right)_i D_{i,\text{SMPS}}^3} \quad (4.5)$$

Note that we do not include water in the aerosol components  $j$ , because the SMPS measures the size of the aerosols after drying. However, we include ammonium nitrate, although it may have evaporated from the aerosols on drying.

The aerosol number concentration is required over the entire vertical model domain, while the above-mentioned algorithm only calculates the aerosol number concentration at the surface. We assume that aerosol numbers are inert, which means that we assume that no nucleation or coagulation of particles takes place on vertical transport. Therefore, the vertical profile of the aerosol number concentrations should be similar to that of an inert tracer (e.g. total nitrate). To apply this vertical profile, we introduced an inert vertical normalisation tracer ( $Z$ ) that is fixed at unity at the surface and subject to vertical mixing. In general,  $Z$  will be well-mixed ( $Z = 1$ ) in the convective boundary layer and will have a sharp descending gradient in the transition to the free troposphere. Applying this vertical profile completes our definition of the number concentration per size bin.

$$\frac{N_i}{V}(z) = Z(z) S \left( \frac{dN}{d \log D} \right)_i \quad (4.6)$$

We calculate the refractive index of the aerosol with the modelled volume fractions of the aerosol tracers (including water) and the refractive indices of the materials.

We assume a mixture of water, ammonium nitrate and ammonium sulphate with no clear dominant component (The modelled concentrations of ammonium bisulphate or not-neutralised ammonium or nitrate are negligible). The formula for the effective refractive index is as follows (Aspnes et al., 1979; Bruggeman, 1935).

$$\sum_j p_j \frac{m_j^2 - m_{\text{eff}}^2}{m_j^2 + 2m_{\text{eff}}^2} = 0 \quad (4.7)$$

Here,  $m_{\text{eff}}$  is the effective refractive index,  $p_j$  is the volume fraction of component  $j$ , and  $m_j$  is the refractive index of component  $j$ . The effective refractive index is solved numerically.

Our model only includes ammonium nitrate ( $m = 1.6$ ; Weast, 1985), ammonium sulphate ( $m = 1.53$ ; Toon et al., 1976) and water ( $m = 1.33$ ; Hecht, 2003). Therefore,  $m_{\text{eff}}$  is not expected to vary considerably. Moreover, the effect of the refractive index is much smaller than the effect of an increase in geometrical cross section of the aerosols by hygroscopic growth. Therefore, we think that variations in the refractive indices only play a minor role.

The last thing required for the optical calculation is the actual size of the aerosols per bin (at any altitude). The actual size is generally larger than the dry size measured at the SMPS because of condensation of water and eventually additional ammonium nitrate. Our assumption of inert aerosol numbers (see above) implies that the number concentration does not change because of condensation of water and additional ammonium nitrate. The new size of the aerosols should be sufficient to fit all material (ammonium sulphate, ammonium nitrate and water):

$$\sum_j \frac{C_j(z)}{\rho_j} = \frac{\pi}{6} Z(z) S \sum_i \left( \frac{dN}{d \log D} \right)_i D_{i,\text{actual}}^3(z) \quad (4.8)$$

This equation differs from Eq. 4.4 in three aspects. First, the concentration of aerosol components and numbers are now at altitude  $z$  instead of at the surface. Second, the diameter of the aerosols is now the actual (wet) diameter instead of the dry diameter and therefore water is also included in the components  $j$ . Third, the normalisation constant  $S$  is now known (from Eqs. 4.4 and 4.5) while the diameters ( $D_{i,\text{actual}}(z)$ ) are unknown and should be solved. This single equation has 70 unknowns (one  $D_{i,\text{actual}}(z)$  for size bin), so there is by far no unique solution. By choosing which solution of Eq. 4.8 to take, we will choose the way in which additional material is distributed over the size bins. We will introduce two possibilities to distribute the condensed material over the size bins.

One way is to assume mutual equilibrium between the aerosols. That is achieved by enforcing the same composition for each aerosol size class, which means that the volume of condensed matter should be proportional to the aerosol volume.

$$\begin{aligned}
dV &\equiv XV = \frac{\pi}{6}XD^3 \\
dV &= \frac{\pi}{2}D^2dD \\
\frac{\pi}{2}D^2dD &= \frac{\pi}{6}XD^3 \\
dD &= \frac{1}{3}XD
\end{aligned} \tag{4.9}$$

Here,  $X$  is defined as the constant of proportionality between the volume of the condensed matter ( $dV$ ) and the aerosol volume ( $V$ ). In this case, all aerosol diameters grow with a constant *factor* ( $\frac{1}{3}X$ ). This factor can be calculated with the following formula.

$$\frac{D_{i,\text{actual}}}{D_{i,\text{SMPS}}} = \sqrt[3]{\frac{\sum_j \frac{C_j(z)}{\rho_j}}{\sum_j \frac{C_{j,\text{surf}}}{\rho_j}}} \tag{4.10}$$

Note that aerosol water is not counted in the term  $C_{j,\text{surf}}$ , like in Eq. 4.5.

A second possibility that we will explore is the distribution of the condensable material proportional to aerosol surface, the area where condensation takes place.

$$\begin{aligned}
dV &\equiv XA = \pi XD^2 \\
dV &= \frac{\pi}{2}D^2dD \\
\frac{\pi}{2}D^2dD &= \pi XD^2 \\
dD &= 2X
\end{aligned} \tag{4.11}$$

Here,  $X$  is defined as the constant of proportionality between the volume of the condensed matter ( $dV$ ) and the aerosol surface area ( $A$ ). In this case, all diameters grow with a constant *amount* ( $2X$ ). The value of  $dD$  can be solved by substituting  $D_{i,\text{actual}}$  with  $D_{i,\text{SMPS}} + dD$  in Eq. 4.8 and solve  $dD$  numerically.

$$\sum_j \frac{C_j(z)}{\rho_j} = \frac{\pi}{6}Z(z)S \sum_i \left(\frac{dN}{d \log D}\right)_i (D_{i,\text{SMPS}} + dD)^3 \tag{4.12}$$

On short timescales, aerosols will tend to grow proportional to surface area ( $\sim D^2$ ). If the ambient conditions remain constant for a longer time period, the different aerosol size classes have time to equilibrate. In such cases, the aerosols have grown proportional to volume ( $\sim D^3$ ). This change from ( $\sim D^2$ ) to ( $\sim D^3$ ) has been shown by Meng and Seinfeld (1996). They present a box-model simulation with two different aerosol size classes in disequilibrium with gas. Initially the fine aerosols equilibrate with the gas by quick condensation ( $\sim D^2$ ). Later on, the coarse aerosols equilibrate with the gas, depleting the gas phase concentrations. Then, the fine aerosols are no longer in equilibrium with the gas and the semi-volatile components evaporate out again ( $\sim D^3$ ). An illustrative example is given in Fig. 2 of Meng and Seinfeld (1996). It is hard to determine which of the two possibilities is best and the actual distribution is probably somewhere in between,

depending on the rate of change of the ambient conditions. Since conditions of an air mass change fast in a convective boundary layer, our main result will be calculated with the ( $\sim D^2$ )-distribution. Sensitivity studies will show the difference when using the ( $\sim D^3$ )-distribution (Sect. 4.3.3).

With the number concentrations for each bin, the refractive index of the aerosols and the actual size of each bin, we can calculate the scattering coefficient with the Mie module.

## 4.3 Results and discussion

First, we will calculate the equilibria of the gas-aerosol system with ISORROPIA and compare these to surface observations for a long measurement period. Next, we will present the calculated surface partitioning, aerosol nitrate profiles and scattering profiles, using the model as explained in Sect. 4.2 for three clear days in May 2008. We will compare these with surface and aircraft observations.

### 4.3.1 ISORROPIA only

In contrast to other countries, the ammonia concentration in the Netherlands is in most cases sufficiently high to neutralise all sulphate and all nitrate (Schaap et al., 2004a). Excess ammonia remains in the gas phase regardless of the meteorological situation, resulting in a minimum gas phase fraction greater than 0% for ammonium (not shown). The nitrate partitioning, however, varies between 100% gas and 100% aerosol, making it a good indicator for the gas-aerosol equilibrium. Therefore, we will focus on the nitrate partitioning.

Schaap et al. (2011) already showed that ISORROPIA calculates a too large aerosol nitrate fraction during winter and during summer nights and a too large gas phase fraction during summer days. We reproduced these results. In Fig. 4.1, the results of just May 2008 are shown, which can be considered a summer month. The observed nitrate partitioning sometimes exhibits a clear diurnal cycle, for example in the period from 6 to 13 May (see Fig. 4.1). During this period with fair weather conditions with weak wind, the diurnal cycles in the calculated equilibria are too large and have a small phase shift, with the calculations an hour or two ahead of the observations. Because these periods are easier to represent in a simplified model, the focus of our study will be on three clear days. On some days, for instance 17 to 31 May, the diurnal cycle in the observations is disturbed. ISORROPIA sometimes calculates no diurnal cycle at all (e.g. 17 or 27 May), overestimating the aerosol phase fraction like in the winter. On many days, however, ISORROPIA exhibits a diurnal cycle, which is smaller than during the fair-weather period. There is no clear relationship between total nitrate concentration and the partitioning.

The three days selected for our study are displayed in Fig. 4.2. We recognise a diurnal cycle in the observed partitioning on 6 May. On 8 May, the observations start similar to 6 May, but the gas phase fraction suddenly decreases in the evening hours. On 21 May, both ISORROPIA and the observations show a large aerosol fraction, which is due to the relatively low temperature on that day. However, the observed partitioning lacks a clear diurnal cycle, while ISORROPIA still

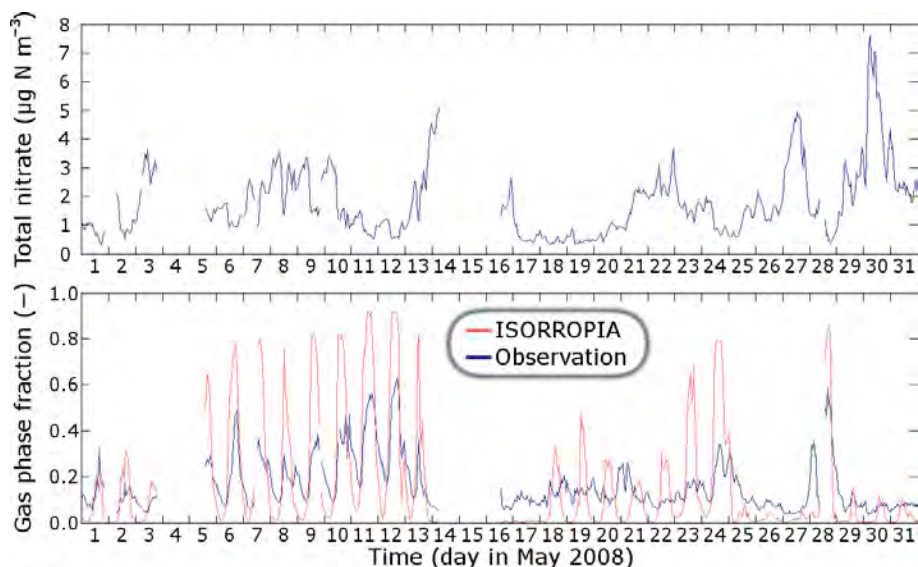


**Figure 4.1:** Upper panel: observed total nitrate (nitric acid plus aerosol nitrate) concentration at Cabauw for May 2008. Lower panel: observed partitioning of nitrate and equilibrium by ISORROPIA for May 2008. Gaps in the graphs are caused by missing data.

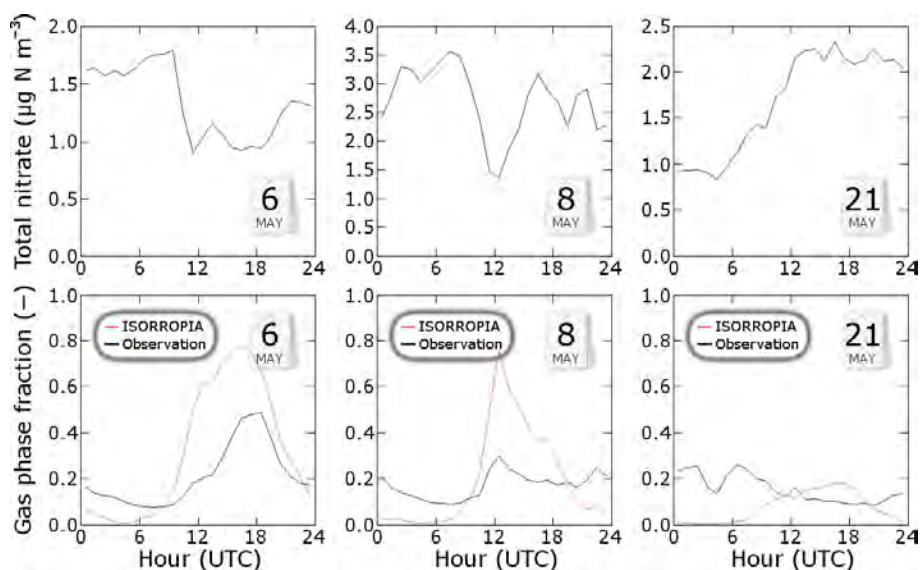


**Figure 4.2:** Upper panels: observed total nitrate (nitric acid plus aerosol nitrate) concentration at Cabauw for 6 May (left), 8 May (middle) and 21 May (right). Lower panels: observed partitioning of nitrate and equilibrium by ISORROPIA for these days.

shows a diurnal cycle like the other days. Our hypothesis is that the gas-aerosol system does never reach equilibrium. This may explain differences between the ISORROPIA calculations and the observations, even if the equilibrium calculated by ISORROPIA is correct. With a non-instantaneous equilibrium, turbulent mixing of air from higher altitudes influences the partitioning at the surface.

### 4.3.2 Column model results

We performed three simulations for each of the three selected days, in which we set the partitioning timescale parameter ( $\tau_p$ ) to 20 s, 1800 s and 7200 s (see Eq. 4.2). The 20-s timescale mimics instant equilibrium. With these simulations, we test the hypothesis that a non-instantaneous equilibrium bridges the gap between the calculated equilibrium by ISORROPIA and the observed partitioning (see Figs. 4.1 and 4.2).

#### 4.3.2.1 Tuning the meteorology

As we explained in Sect. 4.2.1, we tune meteorological input data to reproduce the CESAR data. In Fig. 4.3 is shown that the temperature is represented very well and the relative humidity is represented reasonably. The root of the mean square error in the temperature is 0.44, 0.77 and 0.54°C for 6, 8 and 21 May respectively and during the afternoon hours (the period of interest, 12:00–18:00 UTC) only 0.18, 0.21 and 0.34°C. The root of the mean square error in the relative humidity is 7.5, 7.8 and 6.2 percent (3.4, 4.7 and 2.6 percent during afternoon) for 6, 8 and 21 May, respectively.

We underestimate the humidity in the morning by 10–14% and we overestimate the humidity in the evening by an equal amount. This is probably caused by a too sharp increase and decrease of the boundary layer height during the morning and evening transitions in the model. This means that we model too much dry air entrainment in the morning, reducing the humidity. In the evening, we model a too shallow boundary layer ( $\sim 30$  m), where moist air is trapped, increasing the humidity. The nocturnal boundary layer height at Cabauw usually ranges from 60 m to 540 m and is often underestimated by models (Steenefeld et al., 2007). The boundary layer height reaches its maximum close to 2 km for 8 and 21 May and about 1.5 km for 6 May. With the aid of the provided backscatter data, we estimate that the mismatch with the real boundary layer heights is in the order of a hundred metres.

#### 4.3.2.2 Partitioning at the surface

To illustrate the effect of a delayed equilibrium, we first show ISORROPIA calculations with a partitioning timescale taken into account and applying Eq. 4.2, but not taking into account boundary layer mixing. For these calculations, we used time-interpolated meteorological data from the CESAR observations and time-interpolated observations of total ammonium, total nitrate and sulphate from the MARGA. This results in a very small weakening and delay of the diurnal cycle

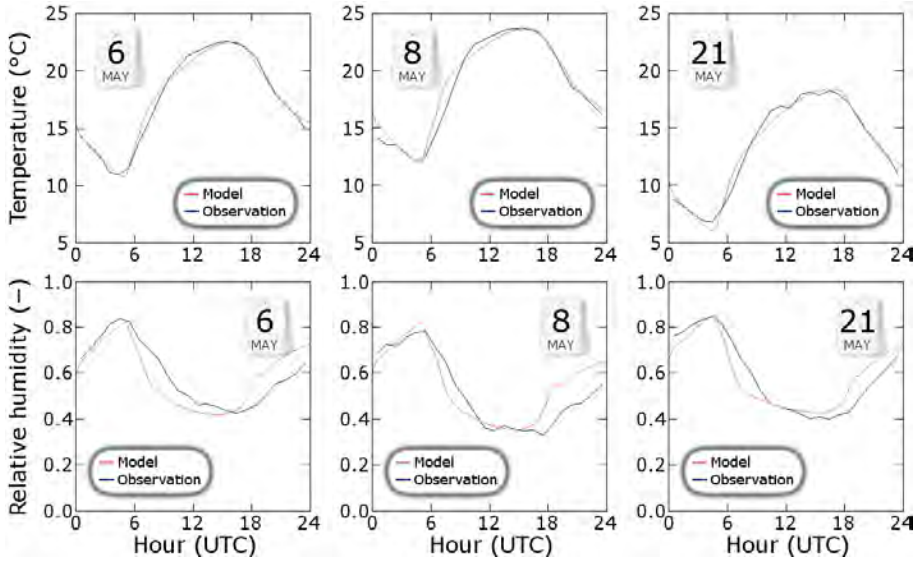


**Figure 4.3:** Upper panels: observed and modelled surface temperature for 6 May (left), 8 May (middle) and 21 May (right). Lower panel: observed and modelled relative humidity for these days.

on increasing  $\tau_p$  (see Fig. 4.4). Secondly, we show modelled surface partitioning of nitrate in our column model with the meteorological situation tuned as in Sect. 4.3.2.1. This results in a much greater weakening and delay of the diurnal cycle as well as an average shift towards the aerosol phase (see Fig. 4.5). Additionally, small differences occur because the column model uses tuned meteorology (Sect. 4.3.2.1), while the (nudged) ISORROPIA equilibrium use direct CESAR data. These latter differences are the only differences visible in the simulation with quasi-instantaneous equilibrium ( $\tau_p = 20$  s).

The greater weakening and delay of the diurnal cycle as well as the shift towards the aerosols phase in the column model (Fig. 4.5) are caused by vertical mixing. In the convective boundary layer, air from the upper boundary layer is mixed towards the surface. That air experienced a lower absolute temperature and a higher relative humidity and thus contains more aerosol nitrate and less nitric acid compared to the equilibrium at the surface. If the equilibrium is restored only slowly (high  $\tau_p$ ), the nitrate remains longer in the aerosol phase, resulting in a higher aerosol fraction of nitrate at the surface. This effect causes a further weakening of the diurnal cycle. Moreover, because there is no counterbalancing effect during the night (mixing through the nocturnal boundary layer is inefficient), this effect also displaces the average towards the aerosol phase. Furthermore, the enhancement of aerosol nitrate in the convective boundary layer causes the maximum gas phase fraction to occur after the convective boundary layer has collapsed (18:00 UTC or later, see Fig. 4.5), indicating that convective mixing has

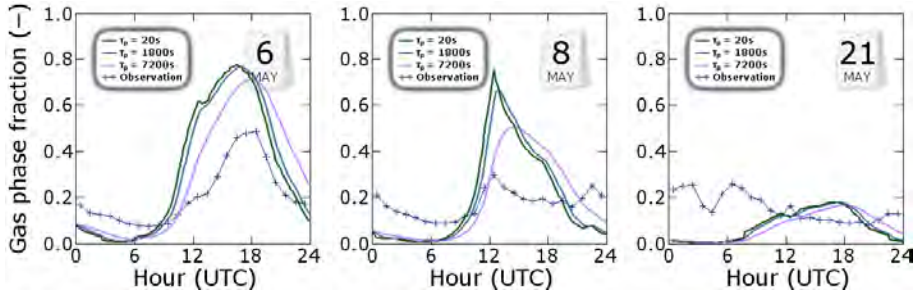


**Figure 4.4:** Partitioning of nitrate, modelled by nudging the equilibrium calculated by ISORROPIA with different timescales, and observation, for 6, 8 and 21 May.

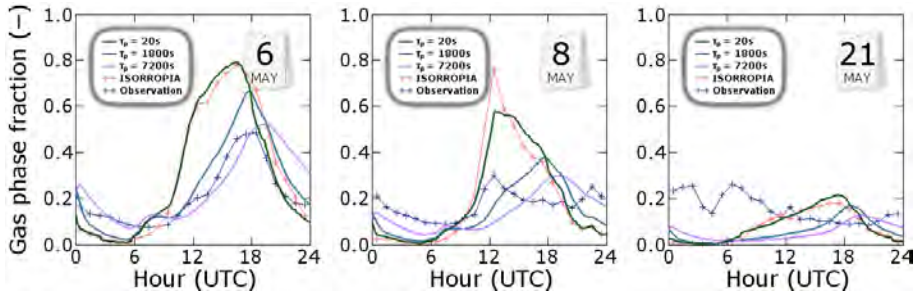


**Figure 4.5:** Partitioning of nitrate modelled by the column model with different timescales of partitioning ( $\tau_p$ ), the ISORROPIA-only simulation and the observation for 6 May (left), 8 May (middle) and 21 May (right).

a significant effect on the nitrate partitioning at the surface.

Increasing the timescale of partitioning improves the correspondence of the modelled nitrate partitioning at the surface to the observations, especially on days where advection plays no significant role, which is indicated by a smooth diurnal cycle in the observed surface nitrate partitioning (e.g. 6 and 11 May). The improvement on 6 May with  $\tau_p = 7200$  s is impressive (compared to ISRRROPIA-only, the root mean square error is reduced by factor 2.1 over the entire day and by 5.9 over the afternoon hours: 12:00–18:00 UTC, see Fig. 4.5). On 8 and 21 May, we model too low gas phase fractions during the night. Our model, specialised in the convective boundary layer, evidently has more difficulties during the night. Also, the diurnal cycles in the observed partitioning on 8 May and 21 May are disturbed, very likely by advection. Our model, not able to simulate advection, will always result in a smooth diurnal cycle. On 8 May, we model the correct maximum gas phase fraction (30%) with  $\tau_p = 7200$  s, which is an improvement over the instant-equilibrium simulation. However, the timing of the peak is better with shorter  $\tau_p$ . On 21 May, we model approximately the correct gas phase fraction in the afternoon (10%), with a smaller  $\tau_p$ -sensitivity. This low gas phase fraction is caused by the low temperature on that day.

It should be considered that there may be a systematic overestimation of the nitrate gas phase fraction in our model, because the model does not take the interaction with sea salt into account (where chloride is displaced by nitrate, see Sect. 4.2.2). Though it is difficult to quantify this effect, this might suggest that a timescale of 1800 s produces good results on 6 May with a well-timed maximum gas phase fraction around 18:00 UTC that is overestimated by 17%.

#### 4.3.2.3 Aerosol nitrate profiles

The diurnal variation of the modelled aerosol nitrate profiles are displayed in Fig. 4.6. Several afternoon profiles show enhanced aerosol nitrate concentrations with altitude within the well-mixed boundary layer due to different gas-aerosol equilibria in the lower and upper boundary layer. The longer the partitioning timescale, the weaker the vertical nitrate gradients, because vertical mixing plays a more prominent role at high  $\tau_p$ . The strength of the vertical gradient is positively correlated with the gas phase fraction of nitrate at the surface, which is largest on 6 May and smallest on 21 May. This is logical, because the conditions favour the aerosol phase at higher altitude. Therefore, it is the gas phase nitric acid at the surface that may undergo a phase transition when moving to the upper boundary layer.

In Fig. 4.7, the modelled aerosol nitrate profiles are compared to aircraft observations presented in Morgan et al. (2010) (shown in Fig. 6 therein for 8 May). For the comparison, the aircraft data were converted in two aspects. First, the masses  $\text{NO}_3^-$  were converted to masses N (scales down a factor 4.4). Second, the scaling to standard temperature and pressure, which is done in Morgan et al. (2010), was undone. The latter conversion reduces the concentrations in the upper boundary layer. To visualise this effect, the dashed reference line is shown. This line corresponds to a fixed scaled concentration of  $2.0 \mu\text{g N sm}^{-3}$ . The modelled profiles in

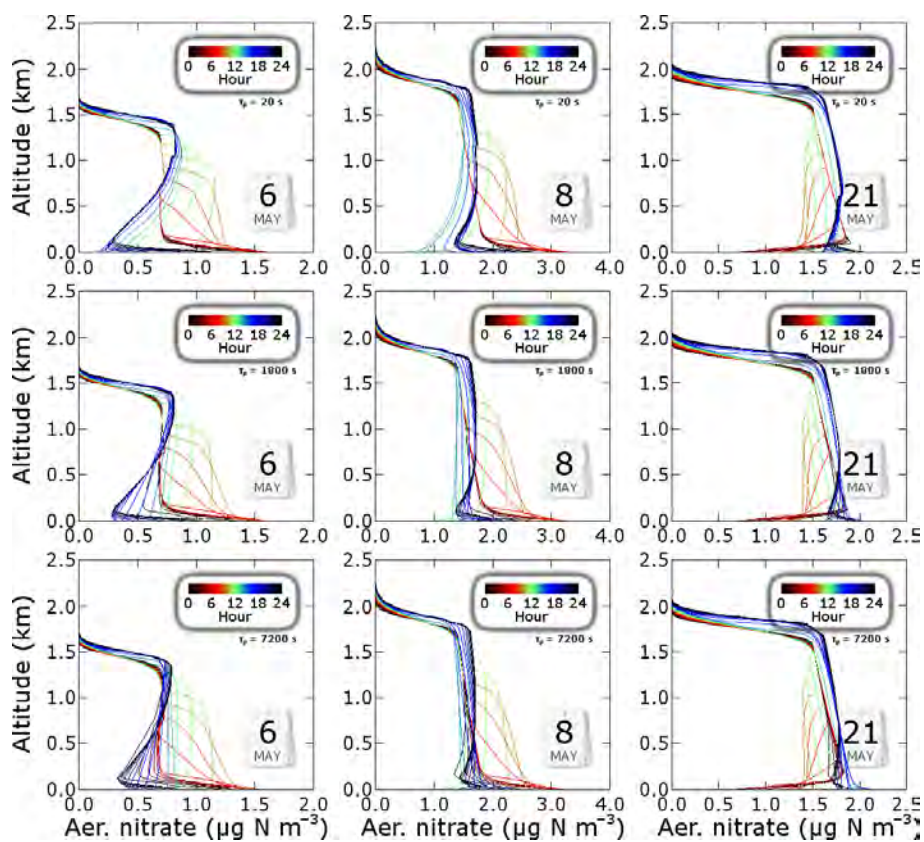


**Figure 4.6:** Modelled aerosol nitrate profiles with partitioning timescales of 20 s (top panels), 1800 s (middle panels) and 7200 s (bottom panels), for 6 May (left), 8 May (middle) and 21 May (right). Each panel contains twenty-four profiles, one per hour, and the colour indicates the time.

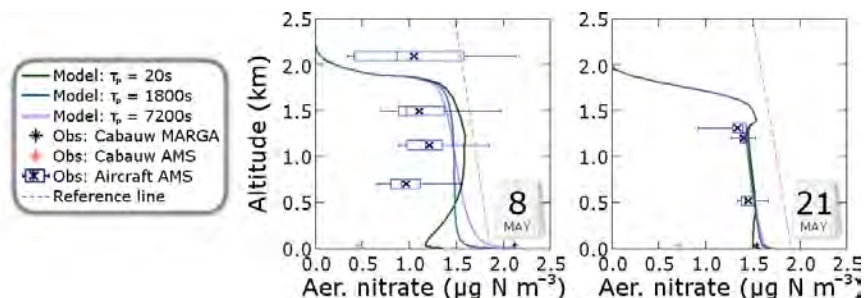


**Figure 4.7:** Modelled aerosol nitrate profiles with partitioning timescales of 20 s, 1800 s and 7200 s, at 15:30 UTC for 8 May and at 11:30 UTC for 21 May. Airborne aerosol nitrate concentrations measured with the aerosol mass spectrometer, surface aerosol nitrate concentration measured with the aerosol mass spectrometer at Cabauw, and  $PM_{10}$  observations by the MARGA instrument at Cabauw. The reference line shows a scaled concentration of  $2.0 \mu\text{g N sm}^{-3}$  (scaled to standard temperature and pressure).

Fig. 4.7 are from 15:30 UTC for 8 May and from 11:30 UTC for 21 May, the times when the aircraft was close to the Cabauw tower.

For 8 May, we clearly model higher nitrate concentrations than observed. This discrepancy can be explained by the fact that the model is based on  $PM_{10}$  observations (MARGA), while the aircraft observations (AMS) are  $PM_{0.7}$ . Apart from this expected overestimation, we can conclude that the simulation with short (20 s) partitioning timescale represents the vertical profile best, with highest concentrations around 1200 m altitude. The fact that this short-timescale simulation performs best can partly be explained by the fact that the aircraft AMS measures the finest particles, which are equilibrated quickly. The spread of the observations is quite large, which may partly be explained by different aerosol nitrate concentrations in updrafts and downdrafts due to the vertical gradient. This explanation requires further investigation, e.g. with large-eddy simulation.

For 21 May, both the model and the observations show similar nitrate concentrations at 500 m altitude and at 1200 or 1300 m altitude. Still, the observed aerosol nitrate concentration at the surface (AMS) is remarkably low, almost  $1 \mu\text{g N m}^{-3}$  lower than expected from the aircraft observations. If total nitrate was well-mixed through the boundary layer, at least that amount of nitrate should be present in the gas phase at the surface. The MARGA-observations, however, show much lower nitric acid concentrations ( $< 0.2 \mu\text{g N m}^{-3}$ ), so just the transition from gas phase to aerosol phase can not explain the entire difference between the surface AMS and the airborne AMS. Coarse-mode aerosols, which are not measured by the AMS, or surface processes affecting the fine mode aerosol (see also Nemitz et al., 2009), are possible explanations. See also Mensah et al. (2012) for a comparison between MARGA and AMS data.

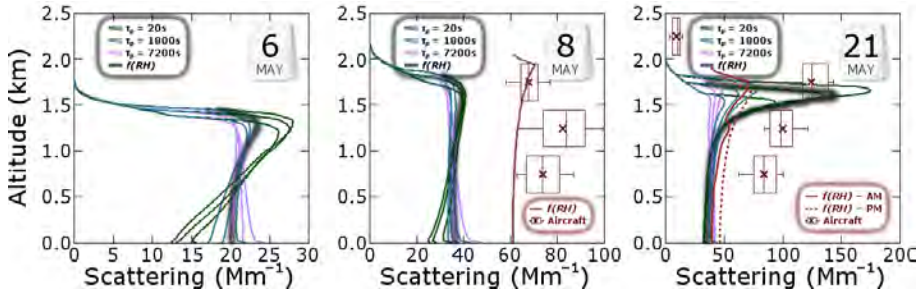


**Figure 4.8:** Modelled scattering profiles for 6 May (left), 8 May (middle) and 21 May (right) at 550 nm wavelength. Simulations with different partitioning timescales are shown in different colours. For each simulation the profiles of 13:30 UTC, 14:30 UTC and 15:30 UTC are shown. The  $f(\text{RH})$  line shows the profile without repartitioning of ammonium nitrate (constant mixing ratios), with instant equilibrium for aerosol water, at 14:30 UTC. For 8 and 21 May, data from Morgan et al. (2010) is shown in red (550 nm wavelength), consisting of aircraft observations and  $f(\text{RH})$ , which is based on observed scattering coefficient at the surface and observed relative humidity with an assumed power-law relationship between relative humidity and scattering coefficient.

#### 4.3.2.4 Optical analysis

We calculated the scattering coefficients according to Sect. 4.2.2.3 and compared them with the scattering coefficients measured by Morgan et al. (2010). The SMPS data required for the optical calculations were only available for the second half of May 2008, so for 6 and 8 May, we used the SMPS data from 21 May. We will analyse the sensitivity of the optical properties to the aerosol size distribution in Sect. 4.3.3. Figure 4.8 shows the modelled scattering profiles for the three selected days. Of each simulation, a plume of three profiles from afternoon hours is shown. The thick  $f(\text{RH})$  line is obtained by taking a fixed mixing ratio of aerosol components representative for the lower boundary layer and assuming instant equilibrium for aerosol water. Repartitioning of ammonium nitrate is not taken into account in this latter calculation. Generally,  $f(\text{RH})$  rises with altitude. Thus, the effect of additional moisture by rising relative humidity with altitude outweighs the effect of lower aerosol volume concentrations due to lower air density (note that in a well-mixed boundary layer, the mixing ratio is constant with height, not the concentrations).

The observations presented in Fig. 9 of Morgan et al. (2010) are projected on the graphs of 8 and 21 May. The  $f(\text{RH})$  profiles of Morgan et al. (2010) are obtained in a similar way as the modelled one. It is based on the measured scattering coefficient at the surface at Cabauw and the observed relative humidity. The effect of additional moisture on aerosols is parameterised as Eq. 4.1 (see Sect. 4.2.1). This equation is solved as follows.

$$\sigma_z = \sigma_0 \frac{1 + a\text{RH}_z^b}{1 + a\text{RH}_0^b} \quad (4.13)$$

Here,  $\sigma_z$  is the scattering coefficient at altitude  $z$ ,  $\sigma_0$  is the measured scattering coefficient at the surface,  $\text{RH}_z$  and  $\text{RH}_0$  are the relative humidities at altitude  $z$  and surface. Coefficients  $a$  and  $b$  are obtained by measurements in the aircraft (see Sect. 4.2.1). As with the modelled  $f(\text{RH})$ , the effect of additional moisture on aerosols is also partially compensated by the lower aerosol concentrations due to lower air density.

Like for aerosol nitrate concentrations, our model calculates increasing scattering coefficients with altitude when the partitioning timescale is assumed short. These gradients are stronger on 6 May (almost a doubling of the scattering coefficient over the boundary layer) and weaker on 21 May (no gradient). On 8 May, the situation is in between, with a scattering coefficient increment of 50% over the boundary layer for short (20 s) partitioning timescale. Longer partitioning timescales result in small gradients in the scattering coefficient (at most 20% increase on 6 May with  $\tau_p = 1800$  s).

On 6 and 8 May we model a stronger gradient in the scattering coefficient than  $f(\text{RH})$  when the timescale of partitioning is not too long. For 21 May, we model a strongly rising  $f(\text{RH})$  due to the high relative humidity in the upper boundary layer. The differences between  $f(\text{RH})$  and the modelled scattering profiles is mostly due to disequilibrium of aerosol water, as repartitioning of nitrate plays only a small role on this day (see Sect. 4.3.2.3).

For both 8 and 21 May, our model underestimates the scattering coefficient by about a factor of two. An important issue is that the model only takes secondary inorganic aerosols into account. The lack of organic aerosols in the model can cause quite an underestimation of the scattering coefficient, because organic aerosols are a major component of particulate matter in Europe (Putaud et al., 2004). For 8 May, increasing scattering coefficients with altitude have been observed. Such a gradient is only reproduced by the simulation in which the partitioning timescale is set to 20 s. Like the observed aerosol nitrate concentrations, the observed scattering coefficients on 8 May exhibit large variability, which can be due to differences between convective updrafts and downdrafts as discussed in Sect. 4.3.2.3. For 21 May, Morgan et al. (2010) do observe a clear gradient in the scattering coefficient, much stronger than  $f(\text{RH})$  (red in Fig. 4.8). The observed aerosol nitrate profile from the AMS, however, does not show such a gradient (see Fig. 4.7). This suggests that the gradient in the scattering profiles is not due to additional aerosol ammonium nitrate. Possibly, the gradient in the observed scattering coefficient is due to organic aerosol components that are more volatile than ammonium nitrate. Our model, lacking these organic components, evidently does not calculate a gradient in the scattering coefficient.

At high relative humidities, the aerosol water uptake becomes extra sensitive to small changes in the relative humidity. This causes the aerosol water uptake and therefore the calculated scattering coefficient to reach very high values at relative humidities above 90%. This is the case in our simulation of 21 May, above 1.5 km altitude. For  $\tau_p = 20$  s and for  $f(\text{RH})$ , we calculate a very sudden increase in the scattering coefficients to a value more than three times as high as at the surface. The simulations with higher  $\tau_p$  do not reach those high values yet in the afternoon because the model also slows down aerosol water uptake with that time constant.

However, the high- $\tau_p$  simulations also show high scattering coefficients later in the day when the convective boundary layer collapses (not shown). The observations also do not show such a sudden increase in the scattering coefficients, indicating that that the very sensitive regime was not reached at the time of the observations.

### 4.3.3 Sensitivity of optical properties

In this section, we present a more technical analysis on how the optical properties of the aerosol vary with the aerosol size distribution, the aerosol composition, and the assumption on how condensed matter is distributed ( $\sim D^2$  or  $\sim D^3$ ). We calculate the optical properties with fixed concentrations of aerosol components in equilibrium with air with varying relative humidity ( $f(\text{RH})$ ). Like in the  $f(\text{RH})$  case in Sect. 4.3.2.4, we do not allow for repartitioning of ammonium nitrate, only the equilibrium for water is calculated. We will compare the calculated  $f(\text{RH})$  with observed function fits. First, we rewrite Eq. 4.1 (see Sect. 4.2.1).

$$\frac{\sigma}{\sigma_{\text{dry}}} - 1 = a\text{RH}^b \quad (4.14)$$

The left hand side of Eq. 4.14 is the relative gain in scattering coefficient. The right hand side of Eq. 4.14 is the function fit with parameters  $a$  and  $b$ . Note that these  $a$  and  $b$  values depend on the type of aerosol measured. The function fit is a straight line on a log-log plot with slope  $b$  and value  $a$  at 100% relative humidity ( $\text{RH} = 1$ ). By plotting the relative gain in scattering coefficient (left hand side) on a log-log scale, we can evaluate if our optical calculations result in a similar relationship between scattering coefficient and relative humidity.

Out of the three selected days, valid data of the aerosol size distribution is only available for 21 May. We will therefore evaluate the modelled  $f(\text{RH})$  during this day. Measurements of  $f(\text{RH})$  are available for several flights in May 2008, including 21 May. Figure 4.9 displays the comparison between modelled and observed  $f(\text{RH})$ . The highlighted lines in Fig. 4.9 correspond to the same time, 21 May around 11:30 UTC. For the majority of the RH-domain, we calculate a power-law relationship between the scattering gain and the relative humidity, indicated by the straight lines. If we analyse these straight parts, we can assign an  $a$  and  $b$ -value to each of the calculations. At high relative humidities, however, the calculations give higher scattering gains. This issue was also discussed in Sect. 4.3.2.4 (see also Fig. 4.8). The value  $a$  is a multiplication factor of the RH-dependent part of  $f(\text{RH})$ . Thus, a high (low) value for  $a$  indicates that the optical properties of the aerosol are more (less) sensitive to the relative humidity. The value  $b$  is the power of the relative humidity, which reduces the scattering gain especially at moderate relative humidities. Thus, a high (low) value for  $b$  indicates a reduced (increased) scattering coefficient at moderate humidities compared to low or high humidities.

Remarkable is that the aircraft measurements show very little variability in their  $a$ -values ( $a = 1.033 \pm 0.085$ ), while the  $b$ -values vary considerably ( $b = 4.812 \pm 1.049$ ). The calculations assuming condensation ( $\sim D^2$ ) also give  $a$ -values

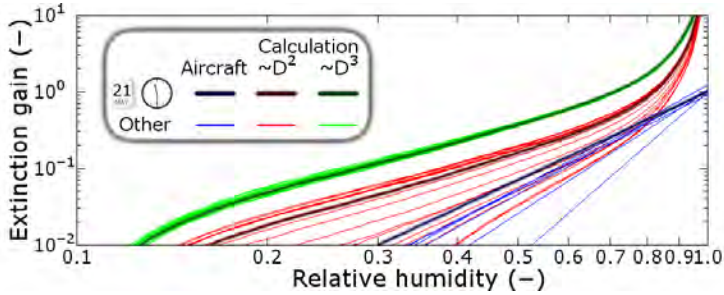


**Figure 4.9:** Relative gain in scattering coefficient of aerosols as a function of relative humidity, without repartitioning of ammonium nitrate, with instant equilibrium for aerosol water. The calculations use observed (MARGA) surface concentrations of ammonium nitrate and ammonium sulphate and SMPS-observations at Cabauw of the aerosol size distribution, both for 21 May. One plume assumes condensation ( $\sim D^2$ ) and the other assumes condensation ( $\sim D^3$ ). Both plumes consist of twenty-four calculations, one per hour. The aircraft plots are power-law fits of measurements during several flights. Highlighted are the calculations for 11:30 UTC and the function fit during the flight of 21 May, which was around the same time.

very close to 1.0 ( $a = 1.046 \pm 0.087$ ) and strong variations in  $b$ -values, although the calculated  $b$ -values are significantly lower on average ( $b = 3.167 \pm 0.928$ ). The calculations assuming condensation ( $\sim D^3$ ) differ more from the observations. The  $a$ -values are too high ( $a = 1.979 \pm 0.058$ ). The  $b$ -values of the ( $\sim D^3$ ) simulation are all similar to the lowest (i.e. worst)  $b$ -values of the ( $\sim D^2$ ) simulation, resulting in a low average and a very small spread ( $b = 2.318 \pm 0.048$ ). To compare, the lowest  $b$ -value for the  $\sim D^2$ -simulation is 2.356. This analysis suggests that the ( $\sim D^2$ ) assumption performs better than the ( $\sim D^3$ ) assumption, which is an indication that the gas-aerosol system is generally in disequilibrium (see discussion in Sect. 4.2.2.3).

High values of  $b$  are associated with a higher ammonium nitrate content with respect to ammonium sulphate, which is in line with Tang (1996). On 21 May, however, the ratio between ammonium nitrate and ammonium sulphate did not vary much. High values of  $b$  are also associated with an aerosol size distribution dominated by fine particles. Differences in the aerosol size distribution are responsible for the variations in  $b$  for the ( $\sim D^2$ ) calculations. In the ( $\sim D^3$ ) calculations, where condensation on coarse aerosols is favoured, the  $b$ -values are small. The observations show higher  $b$ -values than the calculations, which can mean two things. One possibility is that the real aerosols take up more water than the modelled aerosols. As discussed in Morgan et al. (2010) and in this work, aircraft observations show elevated nitrate to sulphate ratios compared to the surface, on which the calculations of Fig. 4.9 are based. This is associated with higher  $b$ -values. Moreover, semi-volatile organic aerosols might also result in higher  $b$ -values. Organic compounds have strongly varying hygroscopic properties (Varutbangkul et al., 2006), so organic compounds could in theory also be respon-

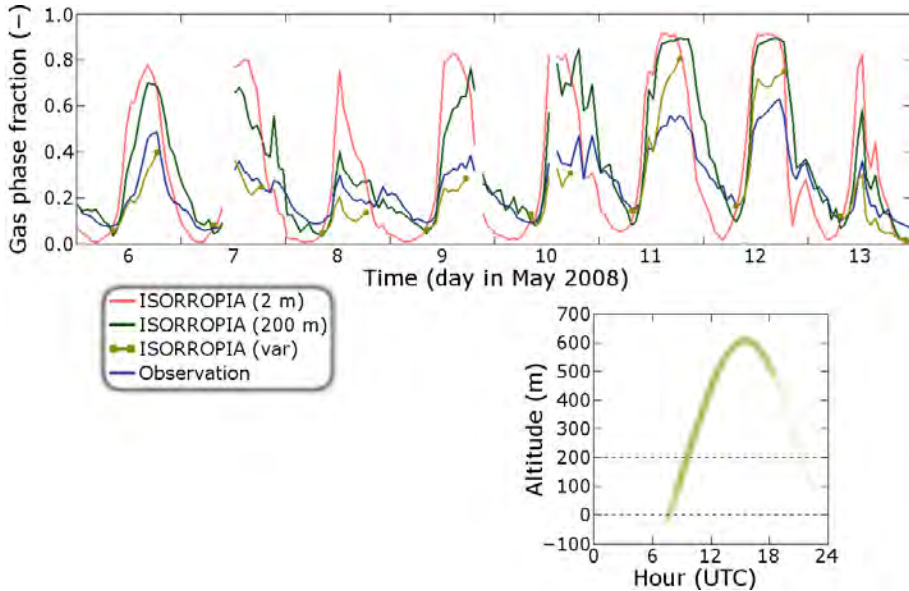


**Figure 4.10:** Upper panel: calculated equilibrium gas phase fraction of nitrate using observations of total ammonium, total nitrate and sulphate, using temperature and relative humidity at 2 m, at 200 m, and at varying altitude (only for unstable conditions), and observed gas phase fraction of nitrate, in the period 6–13 May 2008. Lower panel: altitude as function of time of the day used for the varying-altitude calculation. The thickness of the line represents the number of days at which the conditions were unstable at that time.

sible for the high observed  $b$ -values. The second possibility is that the assumption of homogeneous spherical aerosols causes a bias, an issue that will not be explored here.

#### 4.3.4 Correcting the instant equilibrium

In Sects. 4.3.1 and 4.3.2.2 we showed that assuming instant gas-aerosol equilibrium may result in biases in the surface nitrate partitioning (already shown in Schaap et al., 2011). Most coarse-resolution models, however, do not benefit from a delay time as used in this study, because it is required that turbulent mixing is resolved by the model. We will therefore present a practical modification of the instant-equilibrium assumption by using ISORROPIA with the temperature and relative humidity at a higher altitude rather than at the surface.

We repeated the instant-equilibrium calculations for the fair-weather period (6–13 May) with observations of temperature and relative humidity at 200 m altitude (highest observation in the Cabauw tower). As shown in Fig. 4.10 (upper panel, green line), we see that the results improve significantly during the nights. In daytime, the difference between the 200-m meteo and the 2-m meteo is very small, indicating that the altitude of 200 m is still too low during daytime.

Because no observations are available at altitudes above 200 m, we obtained the temperature and humidity at higher altitudes by transforming the observations at 200 m assuming constant specific humidity and potential temperature. These assumptions are only valid in a well-mixed boundary layer. We will therefore only use this transformation at unstable conditions ( $T_{2\text{ m}} > T_{200\text{ m}}$ ). We prescribed an altitude as function of the time in the day with three fit parameters. We calculated the equilibrium of the gas-aerosol system using the meteorological data at that altitude (using the transformation from the 200-m observation), only at unstable conditions in the period from 6–13 May. We determine the fit parameters such that the error in the calculated gas-aerosol equilibrium is smallest. The fit function that is used looks like:

$$h = a + b \cdot \sin\left(2\pi\left(\frac{t}{24\text{h}} - c\right)\right) \quad (4.15)$$

Here,  $t$  is the time,  $h$  is the altitude and  $\{a, b, c\}$  are fit parameters that are tuned to  $a = 190.1\text{ m}$ ,  $b = 418.5\text{ m}$  and  $c = 0.398$ . The height function is displayed in the lower panel of Fig. 4.10 and the gas-aerosol equilibrium with this height function is shown in upper panel of Fig. 4.10 in dark yellow. Note again that periods with stable conditions are skipped.

This analysis shows that, at least for clear days in May, biases in the surface nitrate partitioning can be substantially decreased by calculating the equilibrium using temperature and humidity at a higher altitude rather than at the surface. The altitude at which the temperature and humidity should be sampled can be described with a simple function with only three parameters (Eq. 4.15).

## 4.4 Conclusions

An explanatory model study has been carried out to investigate the partitioning of ammonium nitrate aerosols in the convective boundary layer on clear days in May 2008. On clear summer days, the equilibrium model ISORROPIA show a clear diurnal cycle in the equilibrium of ammonium nitrate, with a maximum gas phase fraction during daytime and a maximum aerosol phase fraction during night-time. This diurnal cycle in the calculated equilibrium, however, is stronger than the diurnal cycle in the partitioning observed with the MARGA-instrument at Cabauw. Our hypothesis is that the gas-aerosol equilibrium is never fully established in reality.

When introducing a finite speed at which gas-aerosol equilibrium is established, the modelled partitioning is closer to the observations than when assuming instant equilibrium. The diurnal cycle in the gas-aerosol partitioning at the surface is delayed, weakened and on average shifted towards the aerosol phase due to mixing with air from the upper boundary layer. The observed gas-aerosol partitioning at the surface is best reproduced with a long partitioning timescale (two hours). Coarse-resolution models can account for the delayed gas-aerosol equilibrium by calculating the surface gas-aerosol partitioning using the temperature and relative humidity at a higher altitude. For clear days in May 2008, this altitude is close to 200 m in the night and up to 600 m on daytime.

In the upper boundary layer, ammonium nitrate shifts to the aerosol phase because of lower temperatures and higher relative humidities. This creates a gradient of aerosol nitrate concentration in the convective boundary layer even though the layer is well-mixed. When the timescale of gas-aerosol equilibrium is long, the gradient is small. Our model shows aerosol nitrate gradients comparable to Morgan et al. (2010) when partitioning is assumed quick (less than a half an hour). Quantitative comparison is difficult because the measurements of Morgan et al. (2010) consist of the fine fraction ( $\text{PM}_{0.7}$ ), while our model models  $\text{PM}_{10}$ .

The calculated scattering coefficient shows gradients with altitude similar to those of aerosol nitrate. Our model underestimates the scattering coefficient by about a factor of two due to the lack of organic aerosols in our model. Morgan et al. (2010) measured organic aerosol with the AMS and concluded that its contribution to the total aerosol mass is large in line with Putaud et al. (2004). Sensitivity studies point out that the optical properties depend on the aerosol size distribution, the aerosol composition and on how the model assumes the distribution of condensed matter. As explained in Tang (1996), the hygroscopic growth on ammonium nitrate aerosols is more sensitive to the relative humidity than that of ammonium sulphate aerosols. With our optical analysis, we also found indirect evidence that for situations similar to the days simulated in this article, assuming condensation proportional to aerosol surface ( $\sim D^2$ ) is more realistic than assuming condensation proportional to aerosol volume ( $\sim D^3$ ).

The situation at the surface ( $\text{PM}_{10}$ ) is simulated best with a long partitioning timescale while the vertical profiles ( $\text{PM}_{0.7}$ ) are modelled best with a short partitioning timescale. This issue should be investigated with a size-resolved aerosol approach (e.g. M7; Vignati et al., 2004). The size-dependence of the equilibration time (Meng and Seinfeld, 1996) can be implemented in more detail than in the bulk approach described here.

## Acknowledgements

Airborne data was obtained using the BAe-146-310 large Atmospheric Research Aircraft (ARA) flown by Directflight Ltd and managed by the Facility for Airborne Atmospheric Measurements (FAAM), which is a joint facility of the Natural Environment Research Council (NERC) and the Met Office. We acknowledge Astrid Kiendler-Scharr and Amewu Mensah for providing ground-based AMS data. We would like to thank Geert-Jan Roelofs for sharing his knowledge about aerosol microphysics. This work is supported by the EU FP7 IP PEGASOS (FP7-ENV-2010/265148).

Edited by: N. Riemer

# 5

---

## A large-eddy simulation of the phase transition of ammonium nitrate in a convective boundary layer

Under warm and dry conditions, ammonium nitrate aerosol outgasses to form ammonia and nitric acid in the lower atmospheric boundary layer. In the upper boundary layer, where the temperature is lower and the relative humidity is higher, nitric acid and ammonia condense back to the aerosol phase. Measurements show that aerosol nitrate mixing ratios increase with altitude, confirming this phase transition. Since phase equilibrium is not reached instantaneously, updrafts transport aerosol-poor air from the surface to high altitudes and aerosol-rich air subsides from high altitudes to the surface under turbulent conditions. As a result, the partitioning deviates from equilibrium, so the horizontal and temporal variabilities of the aerosol nitrate mixing ratio are enhanced and a continuous downward aerosol-nitrate flux emerges. We postulate that observations of this variability and flux should not be interpreted as instrument noise and deposition of nitrate. In an idealised Large-Eddy Simulation (LES) experiment of a convective boundary layer, we find that the larger variability and flux occurred at about one third of the boundary layer height. Both are largest when the gas-aerosol partitioning timescale is assumed to be about half the timescale of turbulence. Our LES result show negatively-skewed nitrate mixing ratios. Under colder conditions, a smaller fraction of ammonium nitrate aerosol outgasses at the surface, so the absolute effect of nitrate repartitioning becomes smaller. However, dimensionless statistical properties do not change as long as the turbulent properties of the boundary layer remain similar. This indicates that the identified processes are also present under colder conditions.

## 5.1 Introduction

Aerosols have a pronounced influence on the climate system, both directly by scattering and absorbing incoming solar radiation (Hess et al., 1998; Haywood and Boucher, 2000; IPCC, 2007) and indirectly by altering cloud properties (Rosenfeld et al., 2008; Kaufman et al., 2002). Knowledge about the combined climate effect of aerosols is poor compared to that of the climate effect of greenhouse gases. In the Netherlands, nearly half (42%–48%) of the fine aerosol ( $\text{PM}_{2.5}$ ) mass consists of secondary inorganic aerosols (ammonium nitrate and ammonium sulphate) (Weijers et al., 2011), which are the dominant anthropogenic aerosol species in the size range of maximum light scattering (0.4–1.0  $\mu\text{m}$ ) (ten Brink et al., 1997). Furthermore, secondary inorganic aerosols are effective cloud condensation nuclei, because of their size and water solubility. During the last twenty-five years, nitrogen oxide emissions have been reduced to a smaller extent than sulphur dioxide emissions (Vestreng et al., 2007, 2009). Ammonia emissions in the Netherlands are very high due to intensive livestock (Buijsman et al., 1987). This emission stoichiometry implies that ammonium nitrate aerosol is particularly important in the Netherlands.

Under warm and dry conditions, ammonium nitrate aerosol dissociates and outgasses to form ammonia and nitric acid gas (Stelson and Seinfeld, 1982). As the temperature is highest at low altitudes, ammonium nitrate will outgas near the surface and condense back onto aerosols in the upper boundary layer. In a

convective boundary layer, ammonium nitrate is being mixed continuously between low and high altitudes, where different phases prevail. In theory, this interaction between turbulence and gas-aerosol partitioning induces spatial variability on the aerosol nitrate mixing-ratio field. Here, we use a Large-Eddy Simulation (LES) to study the main controlling processes driving this variability and to quantify the vertical profiles of the aerosol nitrate mixing ratio, flux, variance and skewness.

Large-eddy simulations have been used to investigate the effect of small-scale turbulence on processes such as chemical reactions. For instance, Ouwersloot et al. (2011) studied the effect of mesoscale circulations, induced by surface heterogeneity, on the reaction between isoprene and the hydroxyl radical. The advantage of large-eddy simulations is that the segregation of chemical species is explicitly resolved (Ouwersloot et al., 2011). Segregation between the hydroxyl radical and volatile organic compounds has also been investigated without LES (Dlugi et al., 2010; Ugh et al., 2011). Krol et al. (2000) studied the effect of heterogeneous emissions of hydrocarbons on their oxidation rates. For both the studies of Ouwersloot et al. (2011) and Krol et al. (2000), the chemical reaction is slowed down because the concentrations of the reacting chemicals anticorrelate in space. This segregation has been studied in idealised cases by Schumann (1989); Sykes et al. (1992); Vilà-Guerau de Arellano et al. (1993b). LES studies have also been performed on physical processes such as cloud formation (van Heerwaarden and Vilà-Guerau de Arellano, 2008). Like partitioning of ammonium nitrate, cloud formation is a reversible phase transition induced by temperature and moisture.

Wolff et al. (2010) pointed out that the phase transition of nitrate may induce a flux divergence. Without correcting for these effects, dry deposition of aerosol nitrate may be substantially overestimated. For nitric acid, these fluxes are reversed and could falsely be interpreted as emission of nitric acid (Huebert et al., 1988; Neftel et al., 1996; Nemitz et al., 2004a; Zhang et al., 1995). Phase transitions and chemical reactions at timescales comparable to that of turbulence make the flux-gradient relationship more complex as demonstrated by Vilà-Guerau de Arellano et al. (1993a). The timescale of turbulence is the typical time for air parcels within the boundary layer to be transported and mixed and has typical values of 15–20 minutes during daytime. The timescale of gas-aerosol partitioning is the characteristic time in which the gas-aerosol system restores to equilibrium. Theoretical studies pointed out that the timescale of partitioning depends strongly on the aerosol size and composition (Meng and Seinfeld, 1996; Wexler and Seinfeld, 1992; Shiraiwa et al., 2011). Fine liquid aerosols equilibrate well within one eddy-turnover time (15–20 minutes), while coarse solid aerosol equilibrate much slower. Several experimental studies investigated whether or not a gas-aerosol system remains in equilibrium or not, which is related to the ratio between the timescales of partitioning and turbulence. Whereas several studies (Zhang et al., 2003; Takahama et al., 2004; Yu et al., 2005) conclude that the equilibrium corresponds well to the observations, other studies (Moya et al., 2001; Fisseha et al., 2006; Morino et al., 2006; Schaap et al., 2011) show that during summer and daytime, observations show a larger particulate phase than the equilibrium, which can be explained by a non-instantaneous equilibrium.

Partitioning of ammonium nitrate in the convective boundary layer has been

investigated in a study with airborne measurements (Morgan et al., 2010). They observed increasing aerosol nitrate mixing ratio with altitude throughout the entire boundary layer on 8 May 2008 in the Netherlands. In contrast, observations on 21 May showed no further increase in the nitrate mixing ratio from 500 metres altitude onwards (not shown in Morgan et al. (2010)). Interestingly, the horizontal variability of nitrate mixing ratios at any altitude was much greater on 8 May than on 21 May. None of these features were present in the observations of sulphate, which is not subject to phase transition. Inspired by these observations, a one-dimensional model study on the partitioning of ammonium nitrate with a single-column model was performed in chapter 4. They discussed how a delayed gas-aerosol equilibrium in the model can improve the match between the model and the observations. Regarding the results from experimental and theoretical studies, it seems likely that a gas-aerosol partitioning timescale close to the turbulent timescale is representative for a clear day in May at Cabauw.

Phase transition of ammonium nitrate has been investigated in many other model studies as well, for instance by Brost et al. (1988); Kramm and Dlugi (1994); Nemitz and Sutton (2004); Ryder (2010); van Oss et al. (1998). However, none of these studies used large-eddy simulations. Our large-eddy simulation complements these studies by adding an explicit representation of the segregations of concentrations of different species, temperature and humidity. Moreover, our simulation focuses on the middle boundary layer (around 500 metres altitude) rather than the surface layer. In contrast to the abovementioned studies, surface-layer processes, such as dry deposition, will not be analysed in this article. The goal of this article is to unravel the interaction between boundary-layer turbulence and gas-aerosol partitioning of nitrate. To maintain focus on this interaction, other processes have not been included in the model. Our specific research questions are:

- What features (e.g. variability and flux) of aerosol nitrate are explicitly reproduced in an LES of an ammonium-nitrate-sulphate system under diurnal convective conditions?
- What is the dependence of these features on the assumed timescale of gas-aerosol partitioning and on temperature?

Additionally, we discuss what observational evidence could be obtained to acquire information about gas-aerosol partitioning.

## 5.2 Numerical simulation

Our simulation of the ammonium-nitrate-sulphate system will focus on the daytime situation for two reasons: First, turbulent mixing, which is active during daytime, is the main driver in transport and mixing. Secondly, the radiative impact of aerosols is relevant during daytime. All the numerical experiments start at 7:00 UTC and we obtain model output every minute between 13:00 and 16:00 UTC, referred to as the analysis period. We will analyse the phase state of the semi-volatile aerosols and use the aerosol nitrate mixing ratio as indicator. Throughout

this article, when nitrate is mentioned, it refers to just the nitrate in the aerosol phase ( $\text{NO}_3^-$ ) unless “total nitrate” ( $\text{NO}_3^- + \text{HNO}_3$ ) is explicitly mentioned.

We use the Dutch Atmospheric Large-Eddy Simulation (DALES) (Heus et al., 2010), version 3.2. This model originates from Nieuwstadt and Brost (1986) and has been further developed and improved (Cuijpers and Duynkerke, 1993; Dosio, 2005). DALES explicitly resolves processes on a relatively large scale using the filtered Navier-Stokes equations in combination with the Boussinesq approximation (Heus et al., 2010). In general, the filter size is set equal to the grid size of the simulations. Subfilter-scale processes are parameterised using one-and-a-half-order closure.

The vertical grid is a non-equidistant grid of 200 cells from the surface up to about 3 km, with a fine resolution close to the surface and a coarser resolution aloft. This grid approximates pressure levels with 150 Pa per cell, which is inspired by the column model study of chapter 4. In our cases, the boundary layer does not grow larger than two kilometres, which implies that the vertical domain size is sufficiently large for a boundary-layer study. The horizontal grid consists of  $64 \times 64$  cells of  $50 \times 50$  metres each leading to a simulation of a domain of  $3200 \times 3200$  metres. As usual, periodic boundary conditions are employed to mimic an infinite homogeneous convective boundary layer (Heus et al., 2010). The maximum time step is 1 s. Non-resolved fluxes, which are negligible except at the surface, are parameterised.

DALES is extended with a chemistry module, allowing for simultaneous simulation of both boundary-layer dynamics and chemistry (Vilà-Guerau de Arellano et al., 2005). Our chemistry scheme only involves gas-aerosol partitioning of ammonium nitrate, using six scalars for the mixing ratios of the aerosol species: sulphate ( $\text{SO}_4^{2-}$ ), bisulphate ( $\text{HSO}_4^-$ ), nitrate ( $\text{NO}_3^-$ ), ammonium ( $\text{NH}_4^+$ ) and the gas species: nitric acid ( $\text{HNO}_3$ ) and ammonia ( $\text{NH}_3$ ). The equilibrium between the gas and the aerosol phase is calculated with ISORROPIA version 2 (Fountoukis and Nenes, 2007), an extension of the original version as described in Nenes et al. (1998). This equilibrium depends on the absolute temperature and the relative humidity. We apply the tendency by first-order nudging.

$$\frac{d\mathbf{C}}{dt} = \frac{\mathbf{C}_{\text{eq}} - \mathbf{C}}{\tau_p} \quad (5.1)$$

Here,  $\frac{d\mathbf{C}}{dt}$ , is the tendency of the mixing ratios,  $\mathbf{C}_{\text{eq}}$  are the equilibrium mixing ratios calculated by ISORROPIA,  $\mathbf{C}$  are the actual mixing ratios and  $\tau_p$  is the partitioning timescale.

Because chemical processes of aerosols are limited by bulk diffusion (Shiraiwa et al., 2011), the timescale of gas-aerosol partitioning depends strongly on microphysical properties of the aerosols such as size and viscosity. Because these microphysical aerosol properties have not been measured during IMPACT, there is a large uncertainty around the  $\tau_p$  value. The ratio between  $\tau_p$  and the timescale of turbulence ( $\tau_t$ ) is particularly important in this study, because partitioning and turbulent mixing are the two processes that are modelled explicitly. The timescale

**Table 5.1:** *Uniformly initialised mixing ratios in this study*

Species	Mixing ratio (ppb)
Total ammonium	23.0
Total nitrate	3.6
Total sulphate	1.3

of turbulence is obtained from the DALES results as:

$$\tau_t \equiv \frac{z_i}{w_*} \quad (5.2)$$

where  $\tau_i$  is the timescale of turbulence,  $w_*$  is the convective velocity scale and  $z_i$  is the boundary layer height.

We perform simulations in which we vary  $\tau_p$ . We present the results with  $\tau_p = 1800$  s as the main results and show how the results change with a different partitioning timescale. Note that 1800 s is close to typical timescales of turbulent mixing in a convective boundary layer, and that therefore the interaction between mixing and gas-aerosol partitioning is explicitly simulated.

This research employs an idealised model setup, in which just the interaction between turbulence and gas-aerosol partitioning is simulated. To mimic typical fair-weather conditions, we imitate the meteorological conditions of 8 May 2008 at Cabauw, a clear day during the IMPACT campaign. This is done by setting initial conditions and boundary conditions such that the temperature and relative humidity at the surface correspond well to the observations at Cabauw. To acquire satisfactory meteorological boundary conditions, the meteorological situation has been simulated with the Wageningen University single Column Model (WUSCM; chapter 4). Thereby we checked with which boundary conditions the results of WUSCM correspond well to observations from the CESAR website (<http://www.cesar-observatory.nl> (Russchenberg et al., 2005)). These boundary conditions were adopted for the LES.

The mixing ratios of total sulphate ( $\text{SO}_4^{2-} + \text{HSO}_4^-$ ), total nitrate ( $\text{HNO}_3 + \text{NO}_3^-$ ) and total ammonium ( $\text{NH}_3 + \text{NH}_4^+$ ) are initialised uniformly over the entire domain (including the free troposphere) to mixing ratios that are observed with the MARGA instrument (Thomas et al., 2009; ten Brink et al., 2009) at Cabauw on 8 May 2008 at the time of the flight mission on that day. These mixing ratios are 1.3 ppb total sulphate, 3.6 ppb total nitrate and 23 ppb total ammonium (Table 5.1). Note that ammonia is sufficiently abundant to neutralise both sulphuric and nitric acid, a situation typical for the Netherlands. Exchange processes at the surface are not imposed. By doing so, this model setup allows us to avoid complex boundary conditions and to simulate a homogeneous convective boundary layer close to the observed situation on 8 May shown in Morgan et al. (2010).

## 5.3 Results

We first highlight the meteorological conditions of our main simulation: 8 May 2008. Then, we analyse the interaction between turbulence and nitrate repartitioning assuming a timescale of partitioning equal to 1800 s. Subsequently, we analyse how the interaction between turbulence and repartitioning changes with different partitioning timescales. Finally, we investigate the sensitivity to colder conditions.

Figure 5.1 shows the modelled and observed temperature and relative humidity at the surface, and the modelled timescale of turbulence, starting at 8:00 UTC. As stated in Sect. 5.2, the initial conditions and boundary conditions are set such that the observations are reproduced. Both the modelled temperature and relative humidity at the surface remain very close to the observations, especially during the analysis period (13:00–16:00 UTC), with root mean square errors of 0.16 °C for the temperature and 1.1 % for the relative humidity. Moreover, with standard deviations of 0.16 °C for the modelled temperature and 0.6 % for the modelled relative humidity during the analysis period, it can be stated that the meteorological conditions remain relatively constant during these three hours, so the diurnal evolution plays only a minor role. During the analysis period, the timescale of turbulence (Eq. 5.2) reaches typical values of 15 to 20 minutes. The boundary layer grows to about 1900 metres in the afternoon.

To show the 2D vertical structure, we present snapshots of potential temperature, specific humidity, actual nitrate mixing ratio and nitrate equilibrium at 14:30 UTC (middle of analysis period) are shown in Fig. 5.2. In all four panels, the wind is shown as vector field. Close to the surface, updrafts are characterised by higher potential temperatures and higher specific humidities that indicates the transport of heat and moisture from the surface into the atmospheric boundary layer. In the upper boundary layer, warmer and drier air is transported by the subsidence motions because of entrainment. The nitrate equilibrium (lower right panel) depends strongly on the altitude due to decreasing absolute temperature and increasing relative humidity at higher altitudes. The horizontal variability in the nitrate equilibrium due to horizontal variability of potential temperature and specific humidity is small ( $\sigma < 0.1$  ppb at surface, decreasing rapidly with altitude).

Due to the assumed non-instantaneous equilibrium ( $\tau_p = 1800$  s), the actual nitrate mixing ratio differs substantially from the equilibrium. At the surface, the average mixing ratio of nitrate (2.6 ppb; 72 % of total nitrate) is significantly higher than the equilibrium (1.4 ppb; 39 % of total nitrate) due to mixing of aerosol-rich air from higher altitudes. At higher altitudes, the reverse is the case. From 1200 metres onwards, the equilibrium is shifted virtually completely (> 98 %) towards the aerosol phase. The actual nitrate mixing ratio, on the other hand, is only 3.1 ppb (86 % of total nitrate) at 1200 metres. Only in the free troposphere, where the influence of mixing is small, the simulated nitrate mixing ratio equals the equilibrium mixing ratio. The simulated nitrate mixing ratio displays more horizontal variability than the equilibrium, because updrafts transport aerosol-poor air and downdrafts transport aerosol-rich air.

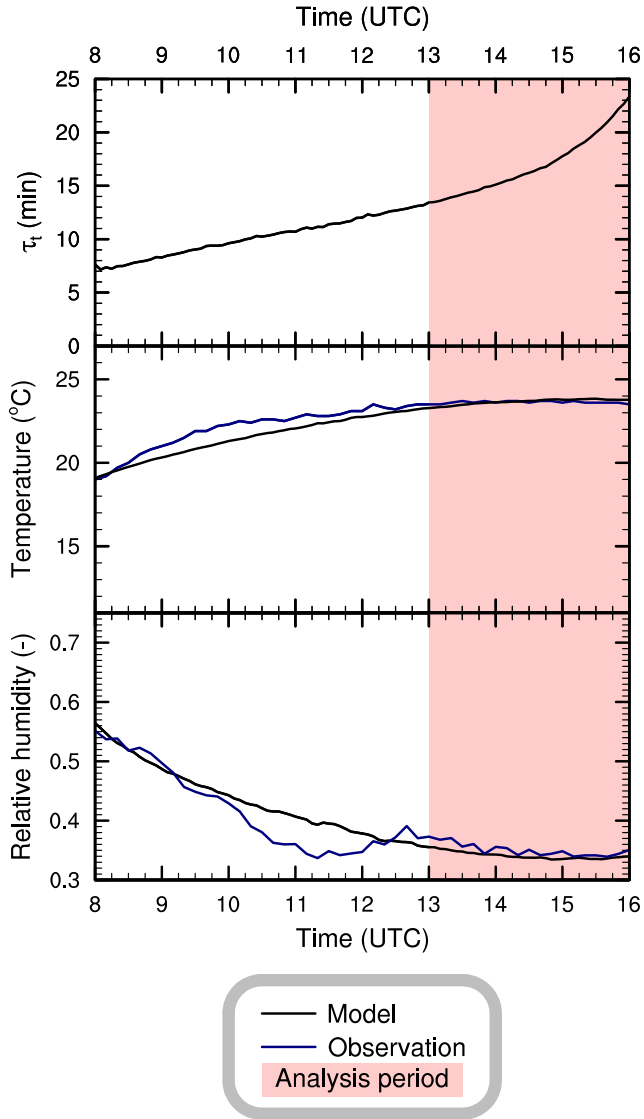


**Figure 5.1:** Modelled and observed surface temperature and relative humidity, and modelled timescale of turbulence ( $\tau_t$ ) at Cabauw on 8 May 2008. The analysis period is shaded.

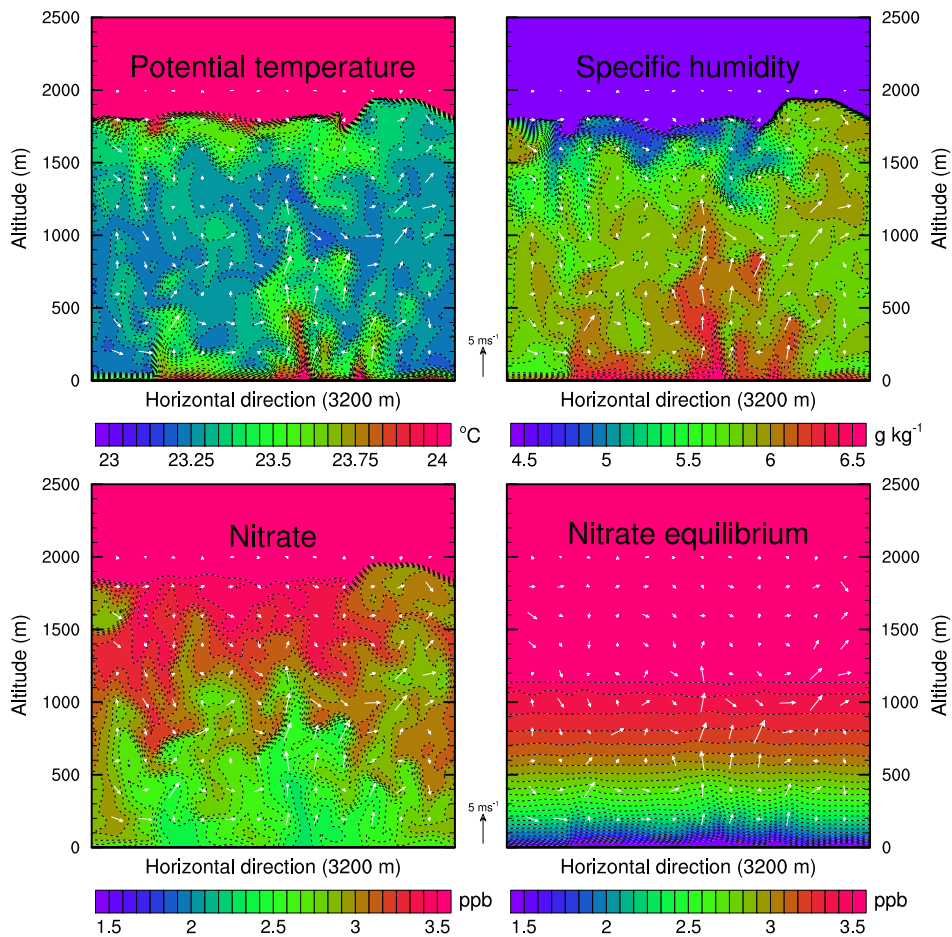


**Figure 5.2:** Vertical 2D snapshots on 14:30 UTC of modelled potential temperature, specific humidity, actual nitrate mixing ratio and equilibrium nitrate mixing ratio, along with a vector field for the wind in the two displayed directions. The timescale of partitioning is set to 1800 s.

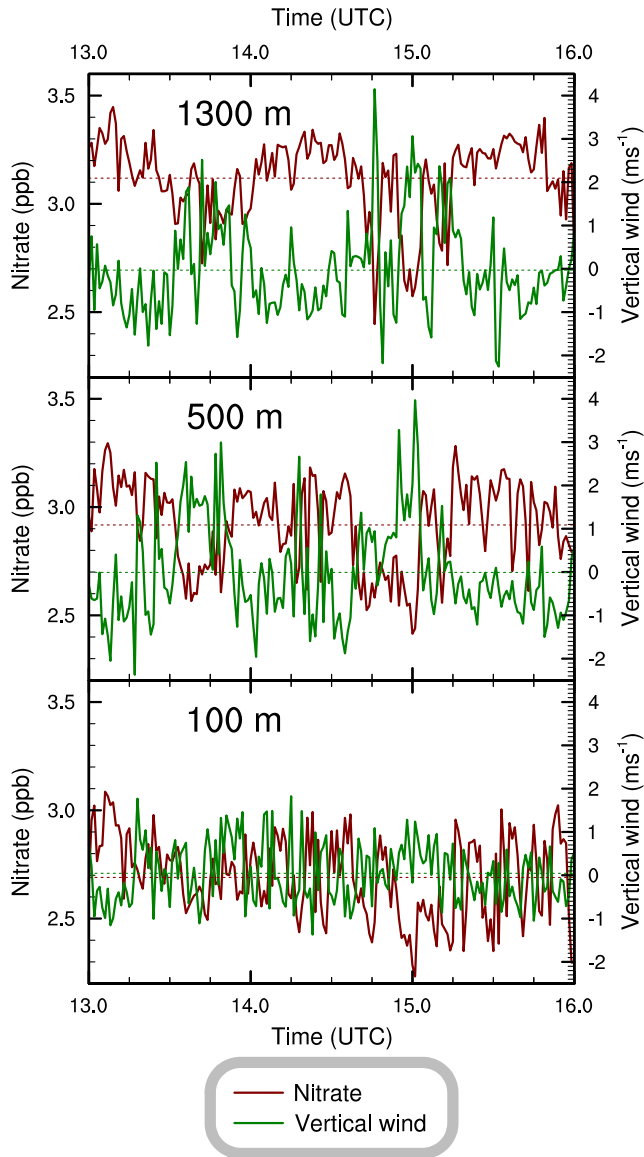


**Figure 5.3:** Modelled nitrate mixing ratio and vertical wind at a fixed point at three different altitudes. The time-averaged values are marked with dotted lines. The timescale of partitioning is set to 1800 s.

Variability in the nitrate mixing ratio is also visible in the temporal domain even though there is no significant temporal evolution in the meteorological conditions during the analysis period (see Fig. 5.1). Figure 5.3 shows virtual measurements of the nitrate mixing ratio and the vertical wind in a stationary virtual balloon at 100 metres, 500 metres and 1300 metres altitude. On any altitude, the simulated nitrate mixing ratio and the vertical wind show rapid oscillations. Striking is the strong anticorrelation between nitrate and vertical wind, especially at 500 metres altitude ( $r = -0.53$  at 100 m,  $r = -0.78$  at 500 m and  $r = -0.68$  at 1300 m). Except for the lowest altitude, which is located in the surface layer, specific updrafts can be identified around 13:45 UTC and 15:00 UTC, in which the nitrate mixing ratio is significantly (up to 0.5 ppb) lower.

### 5.3.1 Vertical profiles

The vertical nitrate flux is one of the main contributions in the 1D budget equation of the horizontally averaged nitrate mixing ratio. In order to analyse it, we first introduce the 1D budget equation for the potential temperature (Stull, 1988).

$$\frac{\partial \bar{\theta}}{\partial t} = -\frac{\partial \overline{w'\theta'}}{\partial z} \quad (5.3)$$

Here,  $\overline{w'\theta'}$  is the potential-temperature flux. Except for the surface, there is no additional production or loss term, so the potential temperature is inert. If we differentiate Eq. 5.3 with respect to  $z$ , we obtain

$$\frac{\partial^2 \bar{\theta}}{\partial t \partial z} = -\frac{\partial^2 \overline{w'\theta'}}{\partial z^2} \quad (5.4)$$

In the quasi steady state approximation, the change of the potential-temperature gradient in time (left hand side of Eq. 5.4), approximates zero due to intense mixing of the convective boundary layer. This means that the right hand side approximates zero as well. Therefore, the flux varies linearly with altitude as derived in the mixed-layer approach by Tennekes and Driedonks (1981) (see for instance Fig. 1 therein).

For chemical tracers with a production or loss term throughout the boundary layer, like for nitrate, a chemical term enters the 1D budget equation.

$$\frac{\partial \bar{C}}{\partial t} = -\frac{\partial \overline{w'C'}}{\partial z} + f \quad (5.5)$$

$$\frac{\partial^2 \bar{C}}{\partial t \partial z} = -\frac{\partial^2 \overline{w'C'}}{\partial z^2} + \frac{\partial f}{\partial z} \quad (5.6)$$

Here,  $C$  is the mixing ratio of the chemical and  $f$  is a production (or loss) function. Nitrate outgasses at low altitudes and nitric acid condenses onto aerosols at high altitudes. Consequently, nitrate has a sink (negative  $f$ ) close to the surface and a source (positive  $f$ ) aloft. This implies that  $\frac{\partial f}{\partial z}$  is positive for the majority of the boundary layer. We apply the quasi steady state approximation to Eq. 5.6 as well, so the left hand side approximates zero. To satisfy the equation, the second

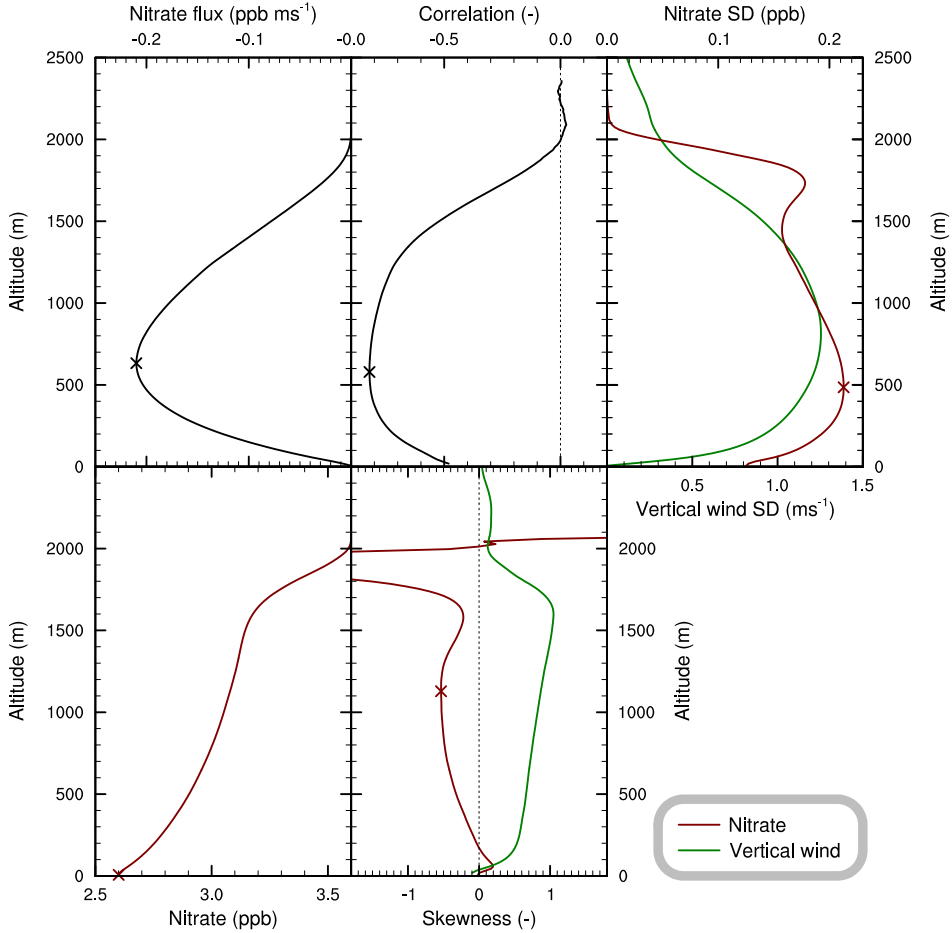


**Figure 5.4:** Modelled vertical profiles of the nitrate flux, the correlation coefficient between nitrate and vertical wind fluctuations, the standard deviation of nitrate and vertical wind, the average nitrate mixing ratio and the skewness of nitrate and vertical wind. All profiles are time-averaged over the period from 13:00 to 16:00 UTC. The timescale of partitioning is set to 1800 s. Characteristic points of the profiles are marked.

derivative of the nitrate flux must be a positive number. Therefore, we expect a convex flux profile for nitrate rather than a linear one.

Figure 5.4 shows the modelled vertical profiles of five statistical quantities. As predicted, the flux profile (upper left panel) is convex with a maximum downward flux of  $-0.21 \text{ ppb ms}^{-1}$  at about 600 metres altitude and it approaches zero at the surface and at the top of the boundary layer. The correlation coefficient between nitrate mixing ratio and vertical wind reaches its maximum negative value of  $-0.82$  also at about 600 metres altitude, although this value stays relatively constant between 400 and 900 metres altitude. This means that for these altitudes and an assumed partitioning timescale of 1800 s, updrafts can reliably be associated with lower nitrate mixing ratios. Worth noting is that the correlation coefficient between the nitrate mixing ratio and the specific humidity (not shown) is around  $-0.8$  throughout the entire boundary layer, indicating that the current specific humidity is an even better indicator of an air parcel's half-hour history than the current vertical wind. However, whether the specific humidity or the vertical wind is more strongly anticorrelated with the nitrate mixing ratio highly depends on the assumed partitioning timescale.

The flux is related to the correlation coefficient with the following formula:

$$r_{wC} \equiv \frac{\overline{w'C'}}{\sigma_w \sigma_C} \quad (5.7)$$

Here,  $\overline{w'C'}$  is the nitrate flux,  $r_{wC}$  is the correlation coefficient between nitrate mixing ratio and vertical wind,  $\sigma_C$  is the standard deviation of the nitrate mixing ratio and  $\sigma_w$  is the standard deviation of the vertical wind. The standard deviation of the nitrate mixing ratio (upper right panel of Fig. 5.4) peaks at a lower altitude than that of vertical wind, though both depend on turbulence. At lower altitudes, the gradient in the nitrate mixing ratio is stronger, so turbulence enhances  $\sigma_C$  to a greater extent than at higher altitudes. The additional peak in the nitrate standard deviation at 1800 m is caused by entrainment of air from the free troposphere of which the nitrate is completely ( $> 99\%$ ) in the aerosol phase.

The skewness (lower middle panel of Fig. 5.4), is a dimensionless measure of the asymmetry of the probability distribution. Due to strong updrafts and large-scale areas with slow sinking motions, the vertical wind is positively skewed in a convective boundary layer (Moeng and Rotunno, 1990). Because the nitrate mixing ratio anticorrelates with the vertical wind, a negative skewness is expected for nitrate. This is the case for the majority of the boundary layer, though above one kilometre altitude, the weaker correlation causes the nitrate skewness to be less in magnitude than the vertical velocity skewness (see lower middle panel of Fig. 5.4). The skewness of nitrate in the free troposphere is undefined as fluctuations are suppressed.

### 5.3.2 Sensitivity to the partitioning timescale

To assess the sensitivity to the assumed partitioning timescale, the simulation has been repeated with different assumptions for the partitioning timescales (see Eq. 5.1). The profiles as shown in Fig. 5.4 change only little in shape, but vary

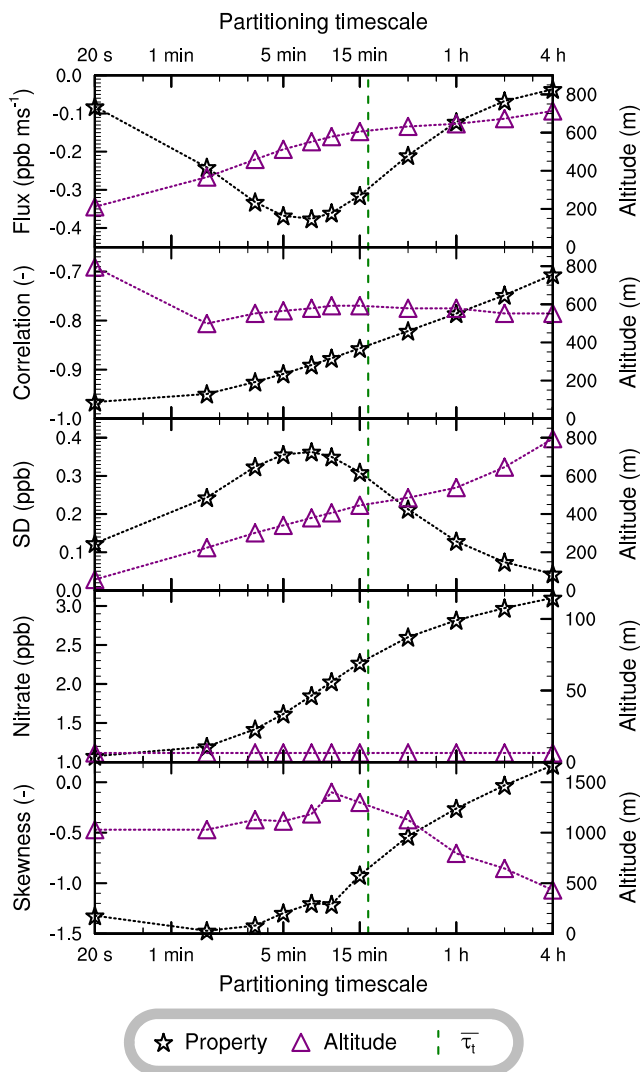
significantly in magnitude. To compare these profiles for the different partitioning timescales, we summarise each profile with the most extreme value in the boundary layer, disregarding features in the entrainment zone. These points are marked with crosses in Fig. 5.4.

Figure 5.5 presents how the profiles change with assumed partitioning timescale. The largest flux and standard deviation in nitrate are modelled when the partitioning timescale is assumed to be 450 s (around half the timescale of an eddy turnover in the convective boundary layer) at approximately 500 metres (550 m for the flux and 380 m for the standard deviation). For both short and long partitioning timescales, the flux and standard deviation are suppressed. For short partitioning timescales, the nitrate mixing ratio approaches the equilibrium (lower right panel of Fig. 5.2). As discussed there, the horizontal standard deviation of this nitrate equilibrium is low ( $< 0.1$  ppb at the surface, decreasing with altitude). Figure 5.5 (third panel) shows that for short partitioning timescales, the largest standard deviation of the nitrate mixing ratio is indeed located near the surface and reaches a value around 0.1 ppb. For long partitioning timescales, the nitrate mixing ratio approaches a well-mixed profile throughout the entire boundary layer, so variability is suppressed. With small horizontal variability, the flux is small as well. The correlation between vertical wind and nitrate mixing ratio is a large negative number ( $-0.89$  at  $\tau_p = 450$  s slightly increasing to more moderate values with increasing  $\tau_p$ ). Because of the low sensitivity of  $r_{wC}$  to the partitioning timescale, the nitrate flux and the nitrate standard deviation behave similarly (Eq. 5.7). The nitrate skewness remains rather constant ( $-1.2$  to  $-1.5$ ) until  $\tau_p$  exceeds ten minutes, after which large negative skewnesses disappear.

### 5.3.3 Probability density functions

The relationship between the nitrate mixing ratio and the vertical wind can be visualised with two-dimensional probability density functions (2D-PDF). Such a 2D-PDF is constructed with all data points (nitrate and vertical wind) at one altitude for the entire analysis period. As reference case, representative for the convective boundary layer, we take  $z = 500$  m and  $\tau_p = 1800$  s.

The probability density function generally shows that nitrate and vertical wind are strongly anticorrelated and significantly skewed, with more extreme values with upward wind and low nitrate mixing ratio. At different altitudes, the shapes of the 2D-PDFs are slightly different. At 1300 m altitude, moderate downdrafts ( $w \sim -0.5 \text{ ms}^{-1}$ ) contain more frequently very high nitrate mixing ratios ( $> 3.3$  ppb) than strong downdrafts ( $w < -1 \text{ ms}^{-1}$ ). The reason for this feature is that slowly moving air has resided a longer period in the upper boundary layer, where the aerosol phase prevails. At 100 m altitude, the vertical velocity is much lower (closer to zero) because the eddies close to the surface are smaller. Also, the correlation between nitrate and vertical wind is weaker ( $r_{wC} = -0.6$ ), indicating that, because of the less coherent eddies close to the surface, the actual vertical wind is a less good indicator for the history of the air parcel than at higher altitudes. Finally, the 2D-PDF shows sharper and straighter edges at shorter (300 s) partitioning timescales. In such case, the nitrate mixing ratio becomes more predictable, because only a



**Figure 5.5:** Sensitivity of the vertical profiles of the nitrate flux, the nitrate standard deviation, the correlation between nitrate and vertical wind fluctuations, the average nitrate mixing ratio, and the nitrate skewness, to the assumed partitioning timescale. Profiles are characterised by the most extreme value in the boundary layer, disregarding features in the entrainment zone. The timescale of turbulence averaged over the analysis period is marked. The displayed altitudes are the altitudes where the extreme values are found.

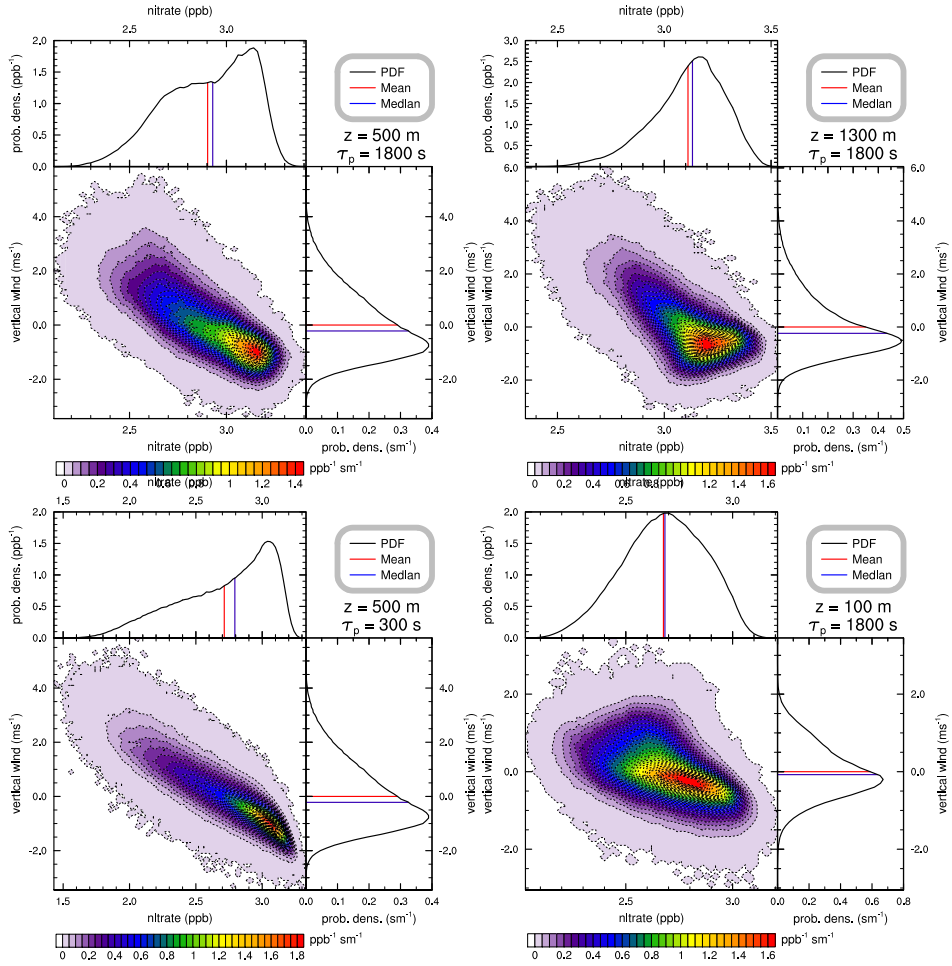


**Figure 5.6:** Probability density functions for nitrate mixing ratio and vertical wind at one altitude.

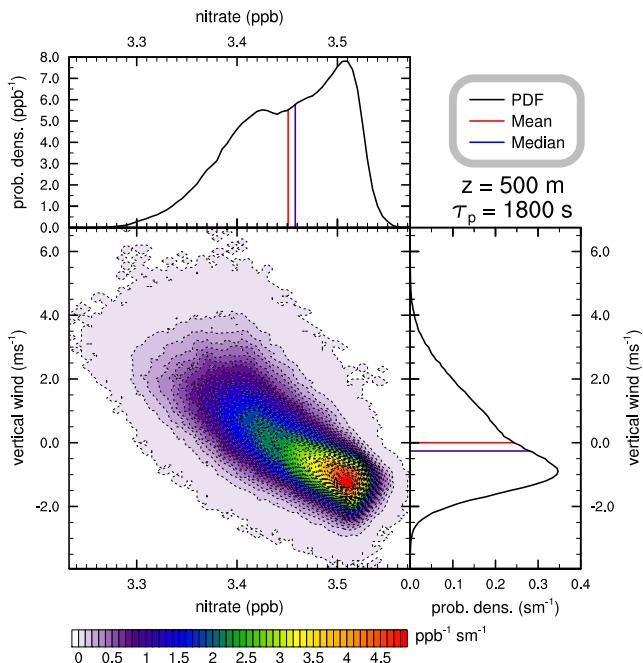


**Figure 5.7:** Probability density functions for nitrate mixing ratio and vertical wind at 500 metres altitude for the cold-case simulation. The partitioning timescale is set to 1800 s.

shorter history of the air parcel is relevant.

### 5.3.4 Effects of a colder boundary layer on the partitioning

To investigate the effect of colder conditions, the simulation ( $\tau_p = 1800$  s) has been repeated for a colder day, 21 May 2008. During the analysis period on 21 May, the surface temperature is much ( $5.6^\circ\text{C}$ ) lower and the relative humidity at the surface is slightly (8.3%) higher than on 8 May. However, the turbulent properties of the boundary layer were similar to 8 May. Under these colder conditions, a smaller fraction of nitrate outgasses at the surface, reducing the difference in the nitrate mixing ratio between the surface and higher altitudes by a factor of four to five. Because of this, the nitrate flux and the nitrate standard deviation are reduced by a similar factor. However, the dimensionless properties, correlation and nitrate skewness, are rather insensitive to these conditions.

The probability density function of the colder day (Fig. 5.7) summarises the sensitivity of the system to the meteorological conditions adequately. The only significant difference is that the nitrate mixing ratios are shifted to higher values and compressed to a smaller range. Consequently, the probability densities in the compressed nitrate domain are scaled up with the same factor.

## 5.4 Discussion

The gas-aerosol transition of nitrate has a wide range of timescales, depending on the size and the viscosity of the aerosols (Shiraiwa et al., 2011). This timescale is very difficult to derive from in situ measurements. Our LES shows that statistical information from measurements in the convective boundary layer of the vertical wind and nitrate mixing ratios can potentially help to obtain information about the partitioning timescale. We have also shown under colder conditions, the statistical indicators of the partitioning timescale remain the same, but with much smaller fluctuations in the nitrate mixing ratio.

We expect that the statistics of the nitrate mixing ratio fluctuations are more strongly influenced by large-scale subsidence, a different Bowen ratio or a different initial stratification of the free troposphere. In the cold case, the equilibrium nitrate mixing ratio profile became more constant with height (lower  $\frac{dC_{eq}}{dz}$ ), resulting in less pronounced nitrate mixing ratio fluctuations. In addition to turbulence, other chemical factors influence only the profile of  $\frac{dC_{eq}}{dz}$ . Examples are the concentrations of total nitrate and other species involved (e.g. total ammonium, total sulphate, sodium and total chloride). For such perturbations, we expect that the nitrate mixing ratio fluctuations can be predicted from the  $\frac{dC_{eq}}{dz}$  profile.

Unfortunately, non-modelled surface interactions (e.g. emission and deposition) also influence these statistical properties. Especially deposition of nitric acid is an important process, since it is not only influenced by the phase transition of nitrate, but it also influences the statistical properties of the nitrate mixing ratio by reducing the total-nitrate concentration near the surface. Moreover, our simulation assumes horizontally homogeneous conditions, while in reality, heterogeneous land-use and non-uniform emissions also cause variability. Because of these processes, one can expect enhanced nitrate standard deviations and reduced correlations between nitrate and vertical wind in real observations. Heterogeneous concentrations of total-nitrate may affect the nitrate skewness as well. As concentrations of pollutants usually show a positive skewness (Lee, 2002), a positive skewness for total-nitrate is expected as well, compensating the negative skewness for nitrate that we infer for short partitioning timescales as discussed in Sects. 5.3.1 and 5.3.2. Entrainment of free-tropospheric air with lower total-nitrate mixing ratios can influence the observed nitrate mixing ratios as well. Intrusion of pristine air is expected to enhance the nitrate standard deviation and to reduce the nitrate skewness in the entrainment zone (Mahrt, 1991). This effect is minimised in the model, because the total-nitrate mixing ratio in the free troposphere is set equal to that of the boundary layer.

Experimental determination of the partitioning timescale through sampling of fluctuations of the nitrate mixing ratio and the vertical wind will be better determined under homogeneous conditions. Observations should preferably be performed when the wind is weak and steady. Furthermore, airborne measurements with a low-speed vessel, such as a balloon or a zeppelin, minimise the spatial range of the observations and thereby the influence of heterogeneity. Note that it is important to perform measurements at high altitudes (e.g.  $z > 300$  m), since the model results show that the effects are strongest at sufficiently high altitudes (see

Fig. 5.4). By measuring additional species besides nitrate, one could indicate to what extent spatial surface heterogeneity plays a role. It is particularly important to sample the nitric acid mixing ratio to obtain the total-nitrate mixing ratio as well, so that it can be determined whether changes in nitrate mixing ratios are induced by repartitioning or by changes in total-nitrate mixing ratios. More research is required to understand the effects of heterogeneous conditions on the nitrate partitioning.

The aircraft observations on 8 May by Morgan et al. (2010) indicate that the nitrate mixing ratios are enhanced at higher altitudes and that they have a large spatial variability. Sulphate, an aerosol component that is not subject to repartitioning, does not show these features. These findings are in agreement with the model results presented in this article (see Fig. 5.4). However, the spatial variability of nitrate in the observations is larger than what would be expected from the homogeneous model results. Furthermore, the skewness of the observed nitrate mixing ratios is positive at all altitudes, which cannot be explained with our homogeneous model results. We hypothesise that a significant fraction of the spatial variability of the nitrate mixing ratios is induced by heterogeneous concentrations of total nitrate (see above and Lee (2002)) or by heterogeneities in other driving factors, such as temperature, humidity, total-ammonium concentrations and large-scale air motions. The aircraft observations have been collected over quite a large area around Cabauw (see Fig. 5 of Morgan et al. (2010)), so that significant spatial heterogeneity could indeed be expected. Note that the spatial variability of the sulphate mixing ratio is not a good proxy for the spatial variability of the total-nitrate mixing ratio, because sulphate and nitrate have different sources.

On 21 May, when the conditions are colder, the difference between the phase equilibria at the surface and aloft is smaller. This implies that the features caused by repartitioning are smaller than on 8 May. The observations show that there is no significant enhancement of nitrate mixing ratios from 500 m altitude onwards (see Sect. 5.1) and that the spatial variability of the nitrate mixing ratios is much smaller than on 8 May.

Our model simulations predict that local measurements of nitrate mixing ratios in a convective boundary layer show a fluctuating signal. One might be inclined to ascribe the signal to instrument noise. However, as pointed out above, the temporal correlation between nitrate and vertical wind contains valuable information about gas-aerosol partitioning. Unfortunately, experimental confirmation needs fast measurements (more than 1 Hz) of the nitrate mixing ratio, which is technically challenging (Crosier et al., 2007). Such fast measurements are normally only performed for specific flux studies at the surface (Farmer et al., 2011; Fowler et al., 2009; Gordon et al., 2011; Nemitz et al., 2008). Our simulations further predict that gas-aerosol partitioning induces a downward flux of nitrate in the convective boundary layer. This is in agreement with Wolff et al. (2010), who pointed out that this downward flux can lead to overestimations of the dry-deposition velocity of nitrate. Several other studies also measured large apparent deposition fluxes of aerosol nitrate and ammonium with an aerosol mass spectrometer eddy-covariance flux system and by measuring concentration gradients (Fowler et al., 2009; Gordon et al., 2011; Nemitz et al., 2004b; Wolff et al., 2011; Wyers and Duyzer, 1997).

We have confirmed that flux measurements of total nitrate are more suitable for estimating deposition velocities.

## 5.5 Conclusion

This article presents a study based on an LES of gas-aerosol partitioning of nitrate in a convective boundary layer. We have shown that when gas-aerosol partitioning occurs at a timescale comparable to the convective timescale, a structure of updrafts with reduced nitrate mixing ratios and downdrafts with enhanced nitrate mixing ratios arises. These features may appear in observations as rapid fluctuations in nitrate mixing ratios. Also, apparent deposition fluxes of aerosol nitrate, which have been observed by measurement studies, have been reproduced by our model.

Our model results show that the horizontal variance of the nitrate mixing ratio and the nitrate flux are maximum when  $\tau_p \approx \frac{1}{2} \cdot \tau_t$  and decline for both short and long partitioning timescales. This variance and flux peak at around one third of the boundary layer height, slightly depending on  $\tau_p$ . For short partitioning timescales, the skewness of the nitrate spatial distribution is predicted to be negative due to the strong negative correlation with the vertical velocity. For longer partitioning timescales, the nitrate skewness increases towards zero. Future observations of these statistical properties of the nitrate mixing ratio may provide information about the partitioning timescale, a quantity that is difficult to measure directly.

At colder conditions, the interaction between turbulence and nitrate repartitioning remains qualitatively similar as long as the turbulent properties of the boundary layer remain similar. However, the magnitudes of the nitrate variability and flux are lower at colder conditions, because the phase equilibria at the surface and in the upper boundary layer differ to a smaller extent than at warmer conditions.

## Acknowledgments

We would like to thank the NCF (Foundation of national computer facilities) for providing the ability to run DALES on the supercomputer Huygens (project SH-060-12). This work is supported by the EU FP7 IP PEGASOS (FP7-ENV-2010/265148).

# 6

---

## **The Generic Aerosol Optics Toolbox: an aerosol optics module for any atmospheric model**

This paper presents the Generic Aerosol Optics Toolbox (GAOT), a software package for the calculation of the optical properties of homogeneous spherical aerosols. GAOT includes a lookup table generator that calculates optical properties of predefined aerosol modes and stores the results in lookup tables. Usage of such lookup table saves a lot of computational time compared to online calculations. These lookup tables can be used in any atmospheric model that represents the aerosol composition and the aerosol size distribution. The toolbox also contains coupling code, which takes care of the communication between the model and the lookup table. This code can easily be adapted for any kind of atmospheric model. The calculations have been evaluated and reproduce the observed characteristic size-dependence of the optical activity of aerosols. Furthermore, the formulas of Rayleigh scattering are reproduced by the calculations of this toolbox. The toolbox has been used in a study with the regional climate model RACMO2 coupled to the regional transport model LOTOS-EUROS. This study concluded that the reduction of aerosol emissions compared to the 1990s is responsible for a temperature increment up to  $0.4^{\circ}\text{C}$  in Europe at ground level for the simulated year from May 2008 to May 2009.

## 6.1 Introduction

Aerosols influence the climate by altering the radiation budget of the earth through scattering and absorption of solar radiation (Hess et al., 1998; Haywood and Boucher, 2000; IPCC, 2007). Over polluted continental regions, the direct forcing of sulphate alone can be as large as that of the combined greenhouse gases, but opposite in sign (e.g. Charlson et al., 1992; Kiehl and Briegleb, 1993). In the last decade, the influence of a number of other aerosol components, like organic carbon, black carbon and mineral dust, on the radiation budget has also been shown (IPCC, 2007). The aerosol effect has masked the real climate sensitivity towards an increase in greenhouse gases to an unknown extent (Anderson et al., 2003). Aerosols are involved in many climate feedback loops, both positive and negative, of which many are related to the interaction between aerosols and radiation (Carslaw et al., 2010). Indirect aerosol-climate feedback loops usually involve clouds. However, increased diffuse radiation due to scattering aerosols may also influence photosynthesis and thereby indirectly the climate system (Mercado et al., 2009). In short, to understand the climate impact of aerosols, it is necessary to understand and adequately parameterise the aerosol optical properties in climate models.

The interaction between aerosols and radiation is also explored to obtain information on aerosols through remote sensing. Aerosol optical properties are measured through ground-based networks (e.g. AERONET; Holben et al., 2001) and satellite-based sensors (e.g. MODIS; Justice et al., 1998). The obtained remote-sensing data provide information for the entire atmospheric column. Information on the entire column is of great importance to evaluate chemistry transport and climate models as they complement traditional ground-based monitoring networks such as EMEP (Lazaridis et al., 2002; EMEP, 2008). Moreover, assimilation of

---

satellite products into models may be a cost-effective method to better monitor aerosol distributions across large regions (Sekiyama et al., 2010). For improved use of remote-sensing data, it is also important to understand the relationship between the aerosol physical and chemical characteristics on the one side, and their optical properties on the other side.

The relationship between the chemical composition and the scattering coefficient of aerosols has been investigated with simultaneous measurements of these two aspects. White and Roberts (1977) indicated that sulphate and nitrate are the most optically active aerosol species. The relationship between the aerosol optical activity and the aerosol size was not yet mentioned in that study. In ten Brink et al. (1997), it was stated that in the Netherlands, nitrate and sulphate are the dominant (anthropogenic) aerosol species in the size range of maximum light-scattering (0.4–1.0  $\mu\text{m}$  diameter). This statement confirmed the findings of White and Roberts (1977), adding the relationship to the aerosol size.

Because of the sensitivity of the aerosol optical properties to the aerosol size distribution, the aerosol optical properties can only be modelled adequately if the aerosol size distribution is properly represented. This implies that the size range of aerosol emissions should be specified in emission inventories. Furthermore, the size-dependence of aerosol processes (e.g. sedimentation) should be taken into account in model parameterisations. Such a size-resolved representation of aerosols (e.g. M7; Vignati et al., 2004) is already commonly used in models, so implementation of a proper calculation of the aerosol optical properties is possible in many models.

Modelling teams developing CTMs or GCMs are largely oriented at other process descriptions than the aerosol optical properties and therefore high-level expertise on this issue is often lacking. Many models include parameterisations for aerosol optical properties, but to a different degree of complexity. For instance, a very simple implementation is a fixed extinction coefficient per bulk mass per aerosol component. Parameterisations of complicated aerosol processes are often tuned to match observations. Arbitrary tuning of processes remains often poorly documented and may include compensations for discrepancies in other processes. A poor agreement among models with respect to aerosol parameters was shown in a model intercomparison study (Textor et al., 2006), indicating that models are difficult to compare. Parameterisations for aerosol optical properties are particularly hard to compare due to the strong non-linear character of aerosol optics. To derive aerosol optical properties from modelled aerosol concentrations, a common toolbox has been developed. This toolbox facilitates many models and improves their description, enhances model comparability and quality.

This article presents the Generic Aerosol Optics Toolbox (GAOT). The theory governing the aerosol optical properties is described in Sect. 6.2. Section 6.3 is a brief description of the toolbox. For a more detailed description, we refer to the supplemented documentation. A few applications in large-scale model are highlighted in Sect. 6.4. We will finalise the article with a summary in Sect. 6.5.

## 6.2 Theory

The optical calculations are based on Mie-theory (Mie, 1908; Debye, 1909; Stratton and Houghton, 1931). Mie-theory calculates the interaction between a spherical medium and incoming electromagnetic radiation. To apply this theory on aerosols, the aerosols have to be approximated as spheres composed of a homogeneous and isotropic medium. Thereby, the aerosol is fully described with the radius ( $r$ ) and the complex refractive index ( $m$ ). Our toolbox uses this homogeneous sphere approximation, so for accounting for the effects of non-homogeneous or non-spherical aerosols, the toolbox should be expanded. Though this approximation is generally quite accurate, it was pointed out that this could lead to an underestimation in the aerosol radiative forcing close to black-carbon sources (Kahnert, 2010a).

### 6.2.1 Effective-medium theory

Aerosols are generally composed of several materials (e.g. sulphate, black carbon and water). To approximate these aerosols as single-medium particles, the effective medium has to be calculated. The effective medium is an imaginary material that represents the optical properties of the mixture of which the aerosol is composed. The refractive index of the effective medium can be calculated from the refractive indices and volume fractions of the components of the real aerosol. It is known that a volume-weighted average refractive index gives inaccurate results. Rather, we use a more proper effective-medium theory based on electrodynamics (Maxwell-Garnett, 1904; Bruggeman, 1935; Jarnik et al., 2006; Saarinen et al., 2003; Aspnes et al., 1979). The generalised formula for effective medium theory is given in Aspnes et al. (1979):

$$\frac{m_{\text{eff}}^2 - m_h^2}{m_{\text{eff}}^2 + 2m_h^2} = \sum_i \nu_i \frac{m_i^2 - m_h^2}{m_i^2 + 2m_h^2} \quad (6.1)$$

In this equation,  $i$  is an aerosol component,  $\nu_i$  is the volume fraction of component  $i$  and each  $m$  is a complex refractive index:  $m_{\text{eff}}$  is the one of the effective medium,  $m_i$  is the one of component  $i$  and  $m_h$  is the one of the host. The definition of the host is a point of discussion. Where Bruggeman (1935) defines the host equal to the effective medium, Maxwell-Garnett (1904) defines the host as the most abundant component. The different definitions of the host result in different refractive indices for the effective medium. The rule of thumb is that the Maxwell-Garnett assumption is valid when minor components form small inclusions in one dominant component and the Bruggeman assumption is valid for equivalent mixtures. This is visualised in Fig. 1 of Saarinen et al. (2003).

We assume that water-soluble materials form Bruggeman mixtures, while insoluble components form Maxwell-Garnett inclusions. These two perspectives can be combined for aerosols with both soluble and insoluble components, by defining the host as a Bruggeman mixture of the soluble components. Equation 6.1 can be solved in two steps. First, the refractive index of the host is calculated (Eq. 6.2)

and subsequently, the refractive index can be calculated with Eq. 6.3.

$$0 = \sum_{i \in H} \nu_i \frac{m_i^2 - m_h^2}{m_i^2 + 2m_h^2} \quad (6.2)$$

$$\frac{m_{\text{eff}}^2 - m_h^2}{m_{\text{eff}}^2 + 2m_h^2} = \sum_{i \notin H} \nu_i \frac{m_i^2 - m_h^2}{m_i^2 + 2m_h^2} \quad (6.3)$$

In these equations  $H$  is the collection of host species, which is formed by all water soluble components.

## 6.2.2 Optical properties of aerosols

The optical properties of a single aerosol at a particular wavelength are defined with three quantities:

- The extinction cross section  $\sigma_{\text{ext}}$  (unit  $\text{m}^2$ ): the amount of radiation scattered or absorbed by the aerosol divided by the incoming radiation flux
- The single-scattering albedo  $a$  (unit  $-$ ): fraction of radiation interacting with the aerosol that is scattered rather than absorbed
- The asymmetry parameter  $g$  (unit  $-$ ): parameter indicating the preference for forward scattering over backward scattering

The optical properties of the atmosphere at a wavelength are determined by the optical properties of all aerosols together and are also defined with three quantities:

- The extinction coefficient  $k$  (unit  $\text{m}^{-1}$ ): the loss rate of direct radiation
- The average single-scattering albedo  $\bar{a}$  (unit  $-$ ): the fraction of the total radiation that interacted with an aerosol that is scattered rather than absorbed
- The average asymmetry parameter  $\bar{g}$  (unit  $-$ ): parameter indicating the average preference for forward scattering over backward scattering

The extinction coefficient  $k$  (unit  $\text{m}^{-1}$ ) is obtained by multiplying the extinction cross section  $\sigma_{\text{ext}}$  (unit  $\text{m}^2$ ) with the aerosol number concentration  $N$  (unit  $\text{m}^{-3}$ ) for each aerosol population (mode or bin). These quantities can be measured, for instance with a nephelometer (Anderson et al., 1996). Also, these quantities can be used by radiation models (e.g. TUV; Madronich, 1987) to calculate the radiation intensities throughout the atmospheric column.

$$k = \sum_m N_j \sigma_{\text{ext},j} \quad (6.4)$$

Here,  $j$  is a mode or a bin. The aerosol optical depth  $\tau$  (unit  $-$ ) is obtained by integrating the extinction coefficient from the surface to the top of the atmosphere.

$$\tau = \int_0^{\text{TOA}} k dz \quad (6.5)$$

Analysis of the aerosol optical depth at different wavelengths indicates whether fine or coarse aerosols dominate. When fine aerosols dominate, the aerosol optical depth decreases with wavelength to a greater extent than when coarse aerosols dominate (Russell et al., 2010). The wavelength-dependence of the aerosol optical depth is expressed as the Ångström parameter (Ångström, 1929).

$$\tau(\lambda) = \beta \lambda^{-\alpha} \quad (6.6)$$

Here,  $\tau(\lambda)$  is the aerosol optical depth as function of the wavelength,  $\beta$  is a prefactor,  $\lambda$  is the wavelength and  $\alpha$  is the Ångström parameter. A large Ångström parameter indicates that fine aerosols dominate.

The average single-scattering albedo should be defined in such a way that it is equal to the total amount of scattered radiation divided by the total amount of radiation that interacted with any aerosol.

$$\bar{a} = \frac{\sum_j a_j N_j \sigma_{\text{ext},j}}{\sum_j N_j \sigma_{\text{ext},j}} = \frac{\sum_j a_j N_j \sigma_{\text{ext},j}}{k} \quad (6.7)$$

The asymmetry parameter of one aerosol is defined as the average cosine of the scattering angle of radiation scattered by that aerosol (zero angle is forward). The average asymmetry parameter should therefore be defined as the average cosine of the scattering angles of all scattered radiation.

$$\bar{g} = \frac{\sum_j g_j a_j N_j \sigma_{\text{ext},j}}{\sum_j a_j N_j \sigma_{\text{ext},j}} = \frac{\sum_j g_j a_j N_j \sigma_{\text{ext},j}}{\bar{a} k} \quad (6.8)$$

Note that the asymmetry parameter does not define a unique angular distribution for the scattered light. As we will discuss in Sect. 6.2.3, particles may scatter more efficiently forward or backward and less efficiently sideward. This aspect is not represented in the asymmetry parameter, which only describes the preference of forward scattering over backward scattering.

### 6.2.3 The Mie-curve

In this section, we will analyse the aerosol optical properties as function of the aerosol size. The aerosol size is expressed as the size parameter ( $x$ ), a dimensionless number that expresses the aerosol size with respect to the wavelength. The extinction cross section is also expressed as a dimensionless number, the extinction efficiency ( $\varepsilon_G$ ). The extinction efficiency is the extinction cross section divided by the geometric cross section.

$$x \equiv \frac{2\pi r}{\lambda} \quad (6.9)$$

$$\varepsilon_G \equiv \frac{\sigma_{\text{ext}}}{\pi r^2} \quad (6.10)$$

The aerosol optical properties also depend on the refractive index of the aerosol. The refractive index is a dimensionless complex number, which, in the convention we choose, has a negative imaginary part.

$$m \equiv n - i\kappa \quad (6.11)$$

The aerosol optical properties as function of the size parameter (with constant refractive index) is a complicated function referred to as the Mie-curve. Three size regimes are distinguished in the Mie-curve, for low (Rayleigh), moderate (Mie) and high (wavelength-independent) size parameters (Barnett, 1942). The Mie-curve is displayed for three complex refractive indices in Fig. 6.1. Below, we will discuss some analytical expressions for limit cases. These are better visualised in a double-logarithmic plot of the extinction efficiency (Fig. 6.2).

Rayleigh scattering is caused by the interaction between electromagnetic radiation and oscillating dipoles. The efficiency of Rayleigh scattering is sensitive to the aerosol size because oscillating dipoles in the same aerosol interfere constructively. Both the electric and the magnetic field generated by the aerosol are proportional to the aerosol volume ( $V$ ) and the inverse square of the oscillation frequency ( $\sim \lambda^{-2}$ ). The power of the scattered radiation is proportional to the product of the electric and the magnetic field for a total proportionality to  $V^2 \lambda^{-4}$  (Lord Rayleigh, 1871; Moosmüller and Arnott, 2009).

$$\sigma_{\text{ext,RS}} = \frac{24\pi^3 V^2}{\lambda^4} \left| \frac{m^2 - 1}{m^2 + 2} \right|^2 \quad (6.12)$$

The shape and orientation of the aerosol does not influence the efficiency of Rayleigh scattering (Savéry and Cloutier, 2002). When assuming spherical aerosols,  $r$  is defined as  $\sqrt[3]{\frac{3V}{4\pi}}$ , revealing the well-known proportionality to  $x^4$  of the scattering efficiency (using Eqs. 6.9 and 6.10).

$$\varepsilon_{G,\text{RS}} = \frac{8}{3} x^4 \left| \frac{m^2 - 1}{m^2 + 2} \right|^2 \quad (6.13)$$

Absorption in the Rayleigh-regime is caused by the existence of absorbing matter in the atmosphere. It depends on the amount (volume) and on the refractive index of the material, but not on the size and shape of the aerosols. Because the extinction efficiency is defined as the extinction per unit of geometric cross section (not per unit of volume), the extinction efficiency is proportional to  $x$  (Lord Rayleigh, 1871; Moosmüller and Arnott, 2009). The Rayleigh absorption coefficient can be calculated by applying effective medium theory on the entire atmosphere, representing the atmosphere as a Maxwell-Garnett mixture of air with aerosol inclusions. The wave-propagation equation through the effective medium gives the correct absorption coefficient.

$$\sigma_{\text{ext,RA}} = \frac{6\pi V}{\lambda} \Im \left( \frac{1 - m^2}{m^2 + 2} \right) \quad (6.14)$$

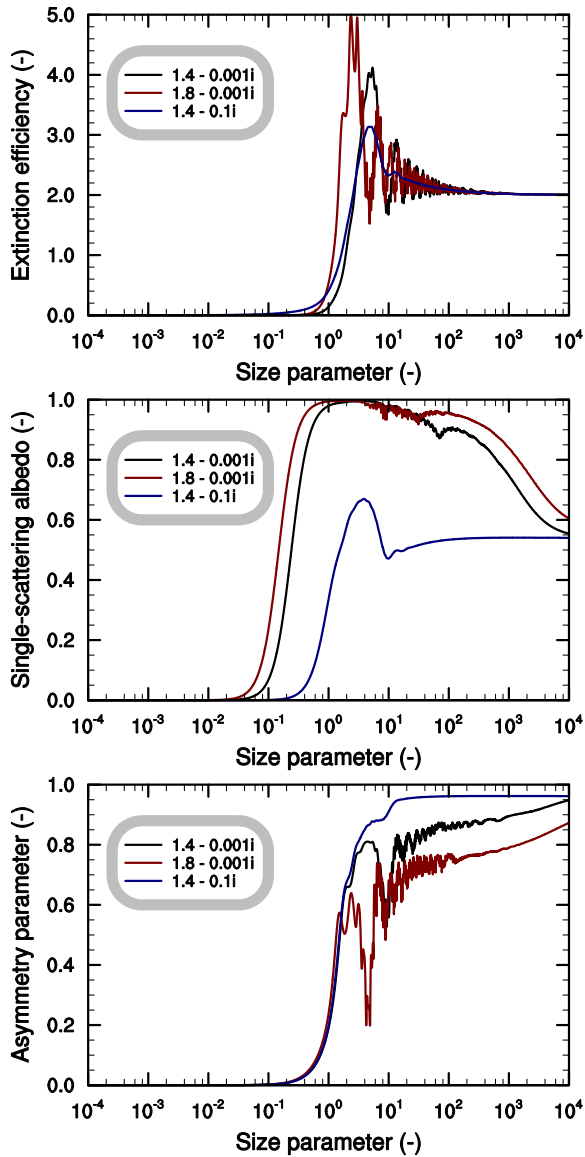


**Figure 6.1:** Extinction efficiency, single-scattering albedo and asymmetry parameter as function of the size parameter for single aerosols of three different complex refractive indices. The x-axes are logarithmic.

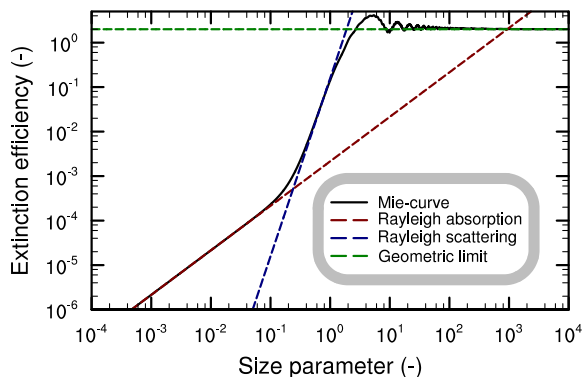


**Figure 6.2:** Extinction efficiency as function of the size parameter for  $m = 1.4 - 0.001i$ . Both axes are logarithmic. Analytical limits are highlighted.

Like for Eq. 6.13, we convert the equation to the absorption efficiency as function of the size parameter assuming spherical aerosols.

$$\varepsilon_{G,RA} = 4x\Im\left(\frac{1 - m^2}{m^2 + 2}\right) \quad (6.15)$$

When filling in Eq. 6.11, the extinction efficiency becomes

$$\varepsilon_{G,RA} = \frac{24xn\kappa}{|m^2 + 2|^2} \quad (6.16)$$

Because Rayleigh absorption is proportional to  $x$  and Rayleigh scattering is proportional to  $x^4$ , the single-scattering albedo for the limit of small  $x$  is zero as long as  $\kappa$  is nonzero. Rayleigh scattering prefers forward and backward scattering to sideward scattering because of preservation of polarisation. The asymmetry parameter, which determines the preference for forward scattering over backward scattering, is zero.

For particles in a size range comparable to the wavelength of the incoming radiation (Mie-regime), the theories of Rayleigh scattering and absorption are no longer valid. The dipoles of a single aerosol only interfere constructively if the aerosol is much smaller than the wavelength of the light. Without constructive dipole interference, the formula for Rayleigh scattering is not valid. Rayleigh absorption is based on the Maxwell-Garnett mixing rule for an effective medium of the atmosphere with aerosols. The Maxwell-Garnett formula is only valid for inclusions that are much smaller than the wavelength (Saarinen et al., 2003).

The start of the Mie-regime can be identified with the behaviour of the asymmetry parameter. This parameter is zero in the Rayleigh-regime and increases to a positive value in the Mie-regime. In the Mie-regime, there is no longer a straightforward solution or approximation for the extinction efficiency, the single-scattering albedo or the asymmetry parameter. The theory for this regime has

been worked out by Mie (1908) and Debeye (1909) and illustrated by Stratton and Houghton (1931). The extinction efficiency reaches its maximum value in the Mie-regime and oscillates on changing  $x$ , indicating features of constructive and destructive interference of light. The frequency of this oscillation depends on the real part of the refractive index, while a large imaginary part of the refractive index suppresses the oscillation. The asymmetry parameter oscillates in phase with the extinction efficiency, indicating that it is the forward scattered light that is subject to interference.

When the aerosols are much larger than the light's wavelength, the geometric limit applies and the optical properties of the aerosols no longer depend on the wavelength. Intuitively one would expect that the extinction efficiency converges to a value of unity for large size parameters. Mie-scattering calculations in this limit, however, show that the extinction efficiency converges to a value of 2 instead. Where the total extinction cross section is  $2\pi r^2$ , at least  $\pi r^2$  of this is a contribution of perfectly forward scattering. Perfectly forward scattering is physically the same as no scattering at all, though the former is counted as extinction and the latter is not. This large contribution of forward scattering is indicated by high values for the asymmetry parameter and a single-scattering albedo that does not drop below one half.

From an environmental perspective, it is more interesting to calculate the extinction efficiency per unit of aerosol mass than per unit of geometric cross section, because it is the aerosol mass, not the geometric cross section, that is emitted or produced in the atmosphere. Therefore, we define a new dimensionless extinction efficiency ( $\varepsilon_M$ ) that indicates how efficiently the aerosol mass extincts light. Such number can only be made dimensionless by adding a multiplication with the density of the aerosol and the light's wavelength.

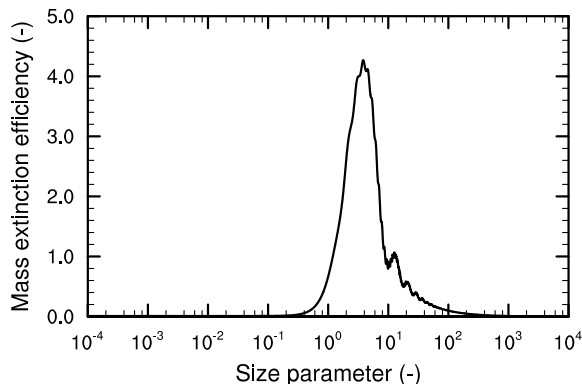
$$\varepsilon_M \equiv \frac{\sigma_{\text{ext}}}{m_a} \cdot \rho_a \lambda = \frac{3\pi}{2x} \varepsilon_G \quad (6.17)$$

Figure 6.3 shows the extinction efficiency per unit of aerosol mass as defined in Eq. 6.17 as function of the size parameter. Remarkable is that aerosols are optically most active in a small window from  $x = 1$  to  $x = 10$ . This confirms the statement in ten Brink et al. (1997) that aerosols in the diameter range of 0.4–1.0  $\mu\text{m}$  scatter visible light the most efficiently.

## 6.3 Implementation

The Generic Aerosol Optics Toolbox consists of the following utilities:

- A wavelength-independent lookup table generator for optical properties of lognormally distributed aerosols or single aerosols
- Coupling code for using the lookup table in a model, consisting of
  - A template of an optics module in a global circulation model using a lookup table generated by this toolbox



**Figure 6.3:** *Nondimensionalised extinction efficiency per unit of aerosol mass as function of the size parameter for  $m = 1.4 - 0.001i$ . The x-axis is logarithmic.*

- A multi-component effective-medium approximator for refractive indices using mixing rules of Bruggeman and Maxwell-Garnett
- A database of wavelength-dependent refractive indices for aerosol components
- An interface for a single Mie-calculation of a lognormal aerosol distribution or a single aerosol

### 6.3.1 Lookup table generator

Aerosols exist in a size range close to the wavelength of incoming solar radiation, a size range where the relationship between the aerosol optical properties and the size is highly nonlinear. For a correct calculation of the aerosol optical properties, the aerosols have to be distributed in many size bins. For each of these size bins, computationally heavy optical calculations have to be performed. Performing these calculation online will slow down global circulation models. A practical solution for these models is to pre-calculate optical properties of assumed size distributions of aerosols and store these results in lookup tables so that time-consuming calculations need not to be done online.

The lookup table generator generates a file containing the optical properties of aerosols as function of the refractive index and the size parameter. The specifications of the lookup table can be defined by the user in a block-oriented script (see documentation). The structure of the lookup table generator is displayed in Figure 6.4 and further explained in the documentation. As discussed in Sect. 6.2.3, a dimensionless extinction efficiency (not the extinction cross section) can be determined from just the size parameter and the refractive index. The lookup table generator supports both dimensionless extinction efficiencies along with a third one, where the extinction cross section is divided by the square of the wavelength. As this third nondimensionalisation does not involve any division by the aerosol

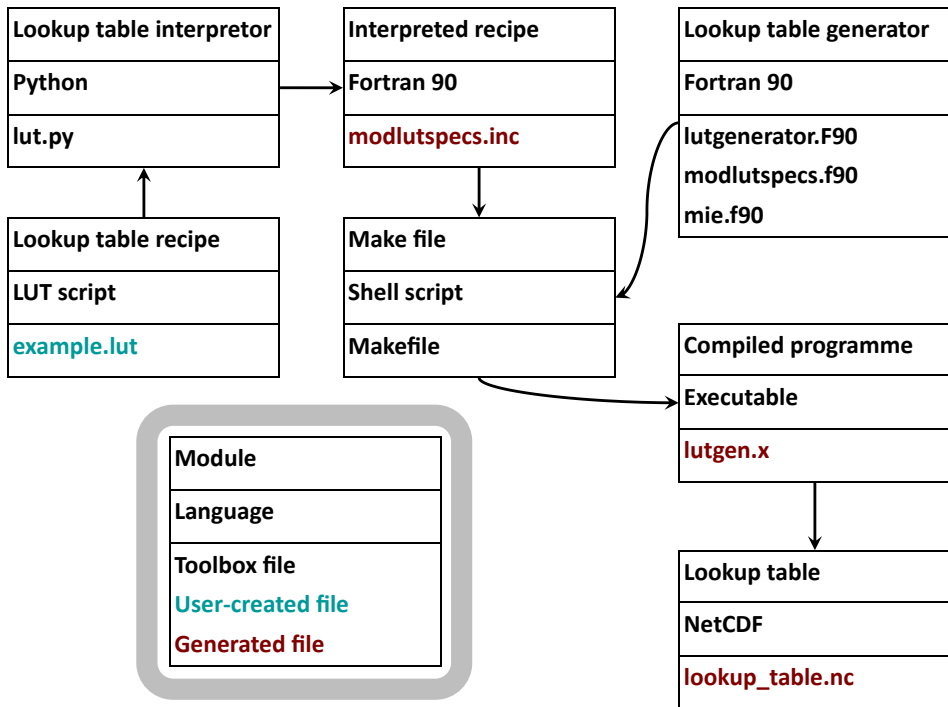


**Figure 6.4:** Diagram displaying the communication between different modules of the lookup table generator.

radius, we refer to this as the nondimensionalised extinction cross section per aerosol number ( $\varepsilon_N$ ). Though the extinction efficiently per aerosol number has less physical meaning than the extinction efficiencies discussed in Sect. 6.2.3, it is the most practical one for implementation in models.

$$\varepsilon_N \equiv \frac{\sigma_{\text{ext}}}{\lambda^2} = \frac{x^2}{4\pi} \varepsilon_G \quad (6.18)$$

The lookup table generator can pre-integrate optical properties of lognormal distributions with an assumed standard deviation. A lognormal distribution in radius ( $r$ ) is also a lognormal distribution in size parameter ( $x$ ) with the same standard deviation and a straightforward formula for the median size parameter:

$$\bar{x}_g = \frac{2\pi\bar{r}_g}{\lambda} \quad (6.19)$$

And the lognormal distribution in the size parameter is defined as:

$$\frac{dN}{d \ln x} = \frac{N}{\sqrt{2\pi} \ln \sigma} \cdot e^{-\frac{(\ln x - \ln \bar{x}_g)^2}{2 \ln^2 \sigma}} \quad (6.20)$$

Here,  $\bar{r}_g$  and  $\bar{x}_g$  denote medians. The subscript ‘ $g$ ’ stands for ‘geometric mean’, which is equal to the median in a lognormal distribution. The lognormal distribution is normalised so that it represents one aerosol.

$$\frac{dN}{d \ln x} = \frac{1}{\sqrt{2\pi} \ln \sigma_g} \cdot e^{-\frac{(\ln x - \ln \bar{x}_g)^2}{2 \ln^2 \sigma_g}} \quad (6.21)$$

In this formula,  $\sigma_g$  is the geometric standard deviation (not to be confused with  $\sigma_{\text{ext}}$ ). The integration of the extinction cross section over this lognormal distribution results in an average extinction cross section per aerosol as function of the median size parameter and the refractive index. Theoretically, the distribution is integrated from  $-\infty$  to  $\infty$  for  $\ln x$ . In practice, a cut-off size parameter is used at several (e.g. 4) standard deviations from the median at both sides.

$$\overline{\sigma_{\text{ext}}}(x_g, m) = \int_{-\infty}^{\infty} \sigma_{\text{ext}}(x, m) \cdot \frac{dN}{d \ln x}(x, x_g) \cdot d \ln x \quad (6.22)$$

The single-scattering albedo and the asymmetry parameter are averaged in a way analogue to Eqs. 6.7 and 6.8.

$$\bar{a}(x_g, m) = \frac{\int_{-\infty}^{\infty} a(x, m) \cdot \sigma_{\text{ext}}(x, m) \cdot \frac{dN}{d \ln x}(x, x_g) \cdot d \ln x}{\overline{\sigma_{\text{ext}}}(x_g, m)} \quad (6.23)$$

$$\bar{g}(x_g, m) = \frac{\int_{-\infty}^{\infty} g(x, m) \cdot a(x, m) \cdot \sigma_{\text{ext}}(x, m) \cdot \frac{dN}{d \ln x}(x, x_g) \cdot d \ln x}{\bar{a}(x_g, m) \cdot \overline{\sigma_{\text{ext}}}(x_g, m)} \quad (6.24)$$

The average dimensionless extinction efficiencies are defined in such a way that they are equal to the average extinction cross section divided by the average of the quantity by which it should be divided (average geometric cross section for  $\overline{\varepsilon_G}$ ).

$$\overline{\varepsilon_G} \equiv \frac{\overline{\sigma_{\text{ext}}}}{\pi r^2} = \frac{\overline{\sigma_{\text{ext}}}}{\pi \bar{r}_g^2 e^{\frac{4}{2} \ln^2 \sigma_g}} \quad (6.25)$$

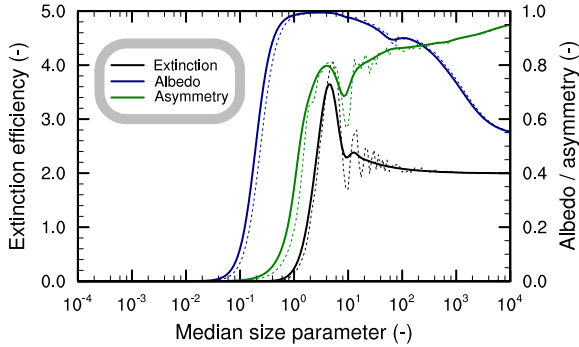


**Figure 6.5:** Pre-integrated extinction efficiency, single-scattering albedo and asymmetry parameter over lognormal modes with  $\sigma_g = 1.25$ . Properties of single aerosols are displayed in dotted lines. The refractive index is  $1.4 - 0.001i$ .

$$\overline{\varepsilon}_M \equiv \frac{\overline{\sigma_{\text{ext}}}}{\overline{m_a}} \rho_a \lambda = \frac{\overline{\sigma_{\text{ext}}} \lambda}{\frac{4}{3} \pi \overline{r_g}^3 e^{\frac{9}{2} \ln^2 \sigma_g}} = \frac{3\pi}{2 \overline{x_g} e^{\frac{5}{2} \ln^2 \sigma_g}} \overline{\varepsilon}_G \quad (6.26)$$

$$\overline{\varepsilon}_N \equiv \frac{\overline{\sigma_{\text{ext}}}}{\lambda^2} = \frac{\overline{x_g}^{-2} e^{\frac{4}{2} \ln^2 \sigma_g}}{4\pi} \overline{\varepsilon}_G \quad (6.27)$$

Here,  $\overline{Q}$  (without subscript ‘g’) is the arithmetic mean of a quantity  $Q$ . Figure 6.5 displays the pre-integrated optical properties for a lognormal distribution with  $\sigma_g = 1.25$  ( $m = 1.4 - 0.001i$ ). The integration averages out the interference pattern in the Mie-regime and shifts the graph to the left. The latter feature is because aerosols with  $x > x_g$  dominate the averaging, because of their greater absolute extinction cross sections.

### 6.3.2 Coupling to a model

The lookup table generated by the lookup table generator can be used by a model. Though this model can be of any type, we will refer to this model as a global circulation model (GCM). The toolbox contains a template file for an optics module that can be adapted to fit to a specific GCM. The mechanics of the optics module is displayed in Fig. 6.6. First, the input parameters of the lookup table are acquired. Then, the dimensionless optical properties are looked up from the table. Finally, the optical properties with the correct dimensions are calculated.

The refractive indices of the specific aerosol components are acquired from the refractive index database, using the wavelengths that are chosen by the GCM user. As these wavelengths do not change during the model run, this operation needs to be done only during model initialisation, after which the refractive index database is no longer needed. The database file in our toolbox contains refractive indices of sulphate, black carbon and sea salt from OPAC (Hess et al., 1998), those of organic matter and mineral dust from ECHAM-HAM (Kinne et al., 2003), and those of water from Segelstein (1981).



## 6.4 Applications

The Generic Aerosol Optics Toolbox is designed to be highly flexible and portable to various kinds of atmospheric models. Therefore, it can be applied in different fields of study. In climate research, the direct radiative effect of aerosols can be studied using our toolbox in a coupled climate model. This way, the radiative effect of aerosols and the impact on weather patterns can be investigated. On the smaller scale, the impact of absorbing aerosols on boundary-layer development can be investigated in large-eddy simulations or column models.

To show how the Generic Aerosol Optics Toolbox can be used in an applied study, we will present an application in a regional study on the direct radiative effect of aerosols (Savenije et al., 2012). We will show one numerical experiment from this study, without thoroughly analysing the results, because that is beyond the scope of this article. For this study, RACMO2 (van Meijgaard et al., 2008) and LOTOS-EUROS (Schaap et al., 2005) have been coupled for a more precise representation of the direct radiative effect of aerosols. LOTOS-EUROS is a regional transport model where the sources, sinks and transport of aerosols are modelled. To enable optical calculations, the aerosol number concentration and the aerosol hygroscopic growth have been calculated. Subsequently, the optical properties of the aerosols are calculated with our toolbox. The direct aerosol radiative effect is implemented in RACMO2 by accounting for the calculated aerosol optical properties in the radiation module.

When no coupling to LOTOS-EUROS or a similar model is applied, the direct radiative effect of aerosols in RACMO2 was parameterised according to climatologic aerosol optical depths from Tegen et al. (1997). With explicit representation of aerosols using LOTOS-EUROS, the temporal variability of the aerosol radiative effect can be more properly resolved. Therefore, the direct radiative effect of aerosols is represented more precisely with coupling to LOTOS-EUROS and using the Generic Aerosol Optics Toolbox than with the old parameterisation.

Figure 6.7 shows a study for one year from May 2008 to May 2009 with LOTOS-EUROS and RACMO2. Two simulations were performed, one with current emissions and one with estimated emissions from the 1990s. Since the 1990s, the air has become cleaner, so the aerosol optical depth is reduced up to 0.2, where the largest reduction is located in south-eastern Europe. As a result of the reduced AOD, the incoming shortwave radiation at clear-sky conditions is enhanced by up to  $10 \text{ Wm}^{-2}$  with the same spatial distribution. The enhanced radiation results in an increase of the average two-metre temperature up to  $0.4^\circ\text{C}$ . Like the changes of the AOD and the incoming shortwave radiation, the largest temperature increase is found in south-eastern Europe. However, the exact spatial distribution of the temperature increment is different from those of the AOD reduction and the shortwave radiation increment. The reason for this difference is that weather patterns change as a result of the direct aerosol effect. The effect of changing weather patterns may differ substantially for different simulated years, so these results should not be interpreted as the climatologic change. The influence of aerosols on weather patterns can be further investigated using our toolbox, but is beyond the scope of this article.

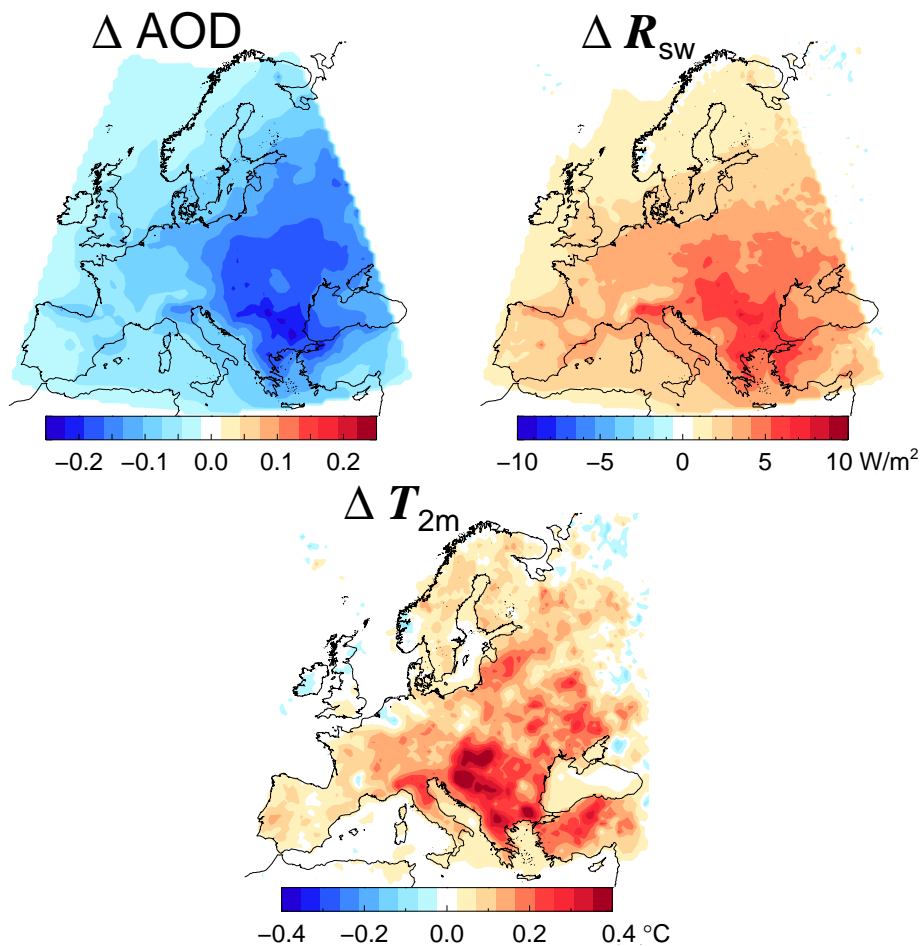


**Figure 6.7:** Application of the Generic Aerosol Optics Toolbox in LOTOS-EUROS and RACMO2, where the RACMO2 accounts for the direct radiative effect of aerosols. The concentration fields are imported from LOTOS-EUROS. Shown are the changes induced by reduced emissions compared to the 1990s. Upper left panel: Difference in aerosol optical depth. Upper right panel: Difference in clear-sky shortwave radiation. Lower panel: Difference in two-metre temperature.

## 6.5 Conclusions

The Generic Aerosol Optics Toolbox has been developed for implementation of the interaction between aerosols and radiation in models. The toolbox is developed in such a way that it can easily be adopted in different kinds of models, ranging from large-eddy simulations to global climate models. Given the concentration, the compositions and the size distribution of aerosols, the extinction coefficient, the single-scattering albedo and the asymmetry parameter can be calculated. The size distribution can be specified in a bin-scheme or with lognormal modes. The physics of Mie-scattering is used, which is a full physical description of the interaction between homogeneous spherical particles and electromagnetic radiation. The only critical assumption is that aerosols are assumed homogeneous and spherical, an assumption that is commonly made in atmospheric models.

The Generic Aerosol Optics Toolbox consists of a lookup table generator and coupling code for implementation in models. The lookup table generator enables the user to perform the optical calculations offline for lognormal aerosol distributions or for single size bins. Such a lookup table can be used for any number of model simulation and even by different models. The coupling code is responsible for the communication between the model and the lookup table and for the calculation of the effective medium of mixed aerosols.

The calculations have been evaluated for single aerosols and the characteristics of Mie-scattering are reproduced. For example, the limits for fine aerosols match the formulas postulated for Rayleigh scattering. Moreover, it has been observed that aerosols in a size range of  $0.4 - 1.0 \mu\text{m}$  scatter visible light the most efficiently per unit of aerosol mass. This characteristic has also been reproduced by our calculations.

The Generic Aerosol Optics Toolbox has been used in a coupled study with LOTOS-EUROS and RACMO2. This coupling allows accounting for radiative effect of the day-to-day variations of aerosol concentrations, allowing a sensitivity study. With such a sensitivity study with LOTOS-EUROS and RACMO2, it has been demonstrated that the reduction of aerosol emissions nowadays compared to the 1990s has a warming effect up to  $0.4^\circ\text{C}$  for the year from May 2008 to May 2009, with the largest change in south-eastern Europe.

# 7

---

General discussion and outlook

This chapter provides an overview of the most important findings in this thesis. Furthermore, a number of unsolved challenges is formulated for further investigation. Finally, it is evaluated to which extent the main objectives of this thesis have been accomplished.

## 7.1 General findings

The main research questions that were formulated in Sect. 1.3 were thoroughly analysed in chapters 3 to 6. Below, the main findings are summarised per research question. In short, the answers to the research questions are:

- **What are the main features of the European aerosol budget and what are the main sources of uncertainties in large-scale aerosol modelling?** Europe is a net exporter of anthropogenic aerosols. These aerosols are predominantly removed by wet deposition. The largest sources of uncertainties in the modelled mass concentration distributions and long-range transport are inaccurate emission estimates and the parameterisation of wet deposition.
- **How can a delayed gas-aerosol equilibrium for ammonium nitrate improve the match between modelled and observed ammonium nitrate concentrations?** For clear days in May 2008, a delay timescale up to two hours improves the match between the model and the observations. This delay timescale may depend on the meteorological circumstances.
- **How is the partitioning of nitrate between the gas and aerosol phase influenced by turbulent motions in a well-developed convective boundary layer?** Updrafts contain less aerosol ammonium nitrate than subsiding air. Therefore a temporal and horizontal spatial variability in the aerosol ammonium nitrate concentration is induced that is maximum around a third of the boundary layer height.
- **How can aerosol optics be implemented properly without taking too much computational time in such a way that the same module can easily be adapted to different models?** The optical properties of single aerosols or commonly-used size distributions of aerosols can be pre-calculated and stored in lookup tables. Together with a coupling module, these lookup tables can be used in any atmospheric model.

### 7.1.1 European aerosol budget and uncertainties

Our model simulations described in chapter 3 indicate that Europe is a net exporter of anthropogenic aerosols and a net importer of natural aerosols. Most of the anthropogenic aerosols are removed by wet deposition and most of the natural aerosols are removed by dry deposition. The largest uncertainties in the calculated European aerosol budget are due to inaccurate emissions and the parameterisation of wet deposition.

Uncertainties in aerosol emissions are related to uncertain emissions per unit of combusted fuel, aerosol speciation, condensable fraction of organic matter, and size distributions. Resuspension of previously deposited aerosols may be important but are not included in emission inventories. Poorly quantified or unknown pathways of organic aerosol formation is another source of uncertainty. The lack of resuspended aerosols in the model is an important reason for a slight but systematic underestimation of  $PM_{10}$  concentrations at ground level. Specific events, like the forest fires in western Russia in spring 2006, are not included in climatological emission inventories that are often used in model studies. Inclusion of specific emissions improved the match between model and observations substantially for a large part of Europe. Based on our simulations, we estimate that long-range transport from Russia can influence the aerosol concentrations in Europe to a significant extent.

Furthermore, a large systematic underestimation was found in the modelled aerosol optical depth compared to remote-sensing observations. This underestimation cannot be explained by a general underestimation of aerosol concentrations due to missing emissions, because the modelled concentrations at ground level are much closer to the observations. It is hypothesised that the model removes aerosols too efficiently at higher altitudes by in-cloud scavenging. Arbitrary down-scaling of in-cloud scavenging improves the match between modelled and observed aerosol optical depth without much deterioration of the match at ground level. This indicates that the efficiency of in-cloud scavenging is an important parameter, which should be investigated in more detail to improve modelled distributions of the aerosol optical depth.

### 7.1.2 Delay in ammonium nitrate partitioning

Ammonium nitrate aerosols undergoes a reversible phase transition to gas-phase ammonia and nitric acid under warm and dry conditions. This phase transition can reduce the concentration of aerosol ammonium nitrate at ground level on summer days. However, large-scale studies hardly investigate this phase transition, because most continuous measurements of ammonium nitrate poorly separate the gas and the aerosol phase, so the ability of large-scale models to correctly predict the partitioning of ammonium nitrate cannot be evaluated properly.

In chapter 4, we describe a case study that uses observations from the IMPACT campaign in which the gas and aerosol phase were sampled correctly (see Sect. 2.1 and chapter 4). This study shows that during a fair-weather period in May 2008, the observed daytime gas-phase fraction of ammonium nitrate is lower than the predicted thermodynamic equilibrium. This discrepancy can be explained by mixing of air from the upper boundary layer, where a larger fraction of ammonium nitrate resides in the aerosol phase due to a lower absolute temperature. When this air is transported to the surface, it will reduce the gas-phase fraction observed at the surface as long as the system does not instantaneously restore to the equilibrium. The model study of chapter 4 shows that a delay timescale of the gas-aerosol equilibrium up to two hours can substantially improve the match between modelled and observed partitioning at the surface.

Coarse-resolution models poorly resolve motions in the boundary layer, so explicit simulation of the partitioning of ammonium nitrate in the boundary layer is difficult in these models. It is demonstrated in chapter 4 how the partitioning at the surface can better be predicted in these models by calculating the equilibrium using the temperature and relative humidity at a higher altitude. For the beginning of May 2008, a representative altitude between 200 metres (night) and 600 metres (day) was found.

### 7.1.3 Influence on the partitioning of ammonium nitrate by turbulence

As explained above and in chapter 4, boundary-layer mixing influences the gas-aerosol partitioning of ammonium nitrate. In chapter 4, a single-column model was used and boundary-layer dynamics was parameterised with a k-diffusion model. This study has been extended in chapter 5 with a large-eddy simulation. A large-eddy simulation explicitly simulates turbulence and resolves updrafts and subsidence motions. Fluctuations in the gas-aerosol partitioning and their relationships with vertical motions are explicitly simulated in a large-eddy simulation, while a single-column model averages out these fluctuations. In continuous station measurements, these small-scale fluctuations are generally not resolved, because the average time of common station measurements is at least one hour. However, these fluctuations may be visible in airborne observations.

The simulations show that the horizontal variability in the partitioning is maximum when the gas-aerosol partitioning timescale is assumed half the turbulent timescale. This horizontal variability maximises at around one third of the boundary layer height. Furthermore, there is a continuous downward flux of aerosol nitrate and a continuous upward flux of gas-phase nitric acid. Maximum fluxes are calculated with an assumed partitioning timescale of half the turbulent timescale. Like for the horizontal variability, these fluxes peak around one third of the boundary layer height.

Because aerosol-nitrate-rich air originates from high altitudes and aerosol-nitrate-poor air originates from low altitudes, there is a negative correlation between the aerosol-nitrate concentration and the vertical wind. Because the vertical wind in a convective boundary layer is positively skewed (small strong updrafts accompanied with large areas with slow subsidence) and the negative correlation between vertical wind and aerosol nitrate concentration, a negative skewness for the aerosol nitrate concentration is modelled as long as the partitioning timescale is not assumed much longer than the turbulent timescale. At colder conditions, when a smaller fraction of ammonium nitrate aerosol outgasses at the surface, these dimensionless statistical properties of the aerosol nitrate concentration (correlation with vertical wind and skewness) do not change significantly.

### 7.1.4 Implementation of aerosol optics in models

Many aerosol studies include analysis on optical properties of aerosols. As calculations of aerosol optical properties are very complicated, model developers may

tend to simplify aerosol optics with parameterisations. To enhance the quality of aerosol optical calculations in models and to facilitate model intercomparison, a common toolbox for optical calculations on aerosols has been developed. This toolbox, presented in chapter 6, is generally applicable in atmospheric models that explicitly simulate aerosol size distributions.

The optical calculations implemented in the toolbox are based on Mie-scattering theory. As outlined in this theory, the optical properties of aerosols depend strongly on the aerosol size. The toolbox has been validated showing the well-known theory that aerosols in a size range from 0.4 to 1.0  $\mu\text{m}$  scatter visible radiation the most efficiently. Because of the sensitivity to the aerosol size, it is vital for models to correctly represent the aerosol size distribution for an adequate calculation of the aerosol optical properties.

The toolbox has been used in a study in which the regional transport model LOTOS-EUROS has been coupled to the regional climate model RACMO. Compared to a climatological parameterisation of the direct climate effect of aerosols, the coupled system with LOTOS-EUROS resulted in aerosol optical depths that correspond much better to observations. With this coupled system, the effect of reduced aerosol emissions compared to the 1990s has been quantified. As a result of the lower aerosol optical depth and the larger radiation flux to the surface, the yearly-averaged two-metre temperature in Europe increased up to 0.4°C.

## 7.2 Challenges

Our knowledge about aerosols and aerosol processes can be improved further by tackling issues that have been identified in this thesis. Most of these issues concern models. However, measurements remain essential, because models and model processes have to be validated with observations.

### 7.2.1 Wet removal of aerosols

In chapter 3, it is pointed out that the efficiency of in-cloud aerosol scavenging has to be scaled down substantially to improve the match between modelled and observed aerosol optical depth. It is also discussed that arbitrary down-scaling is not a final solution, because a sound parameterisation should be based on physical considerations. Evidently, in-cloud aerosol scavenging efficiently removes aerosol in a cloud, but it does not remove aerosols outside clouds. As clouds are usually smaller than a model grid cell, in-cloud scavenging causes aerosol concentrations within a grid cell to become non-uniform. These non-uniformities are not explicitly resolved in the model.

Our model, TM5, nowadays treats this issue by implementing a fixed timescale of mixing within one grid cell, so that the model can account implicitly for the segregation between the in-cloud and out-of-cloud fractions of a grid cell. However, this timescale of grid-cell mixing should depend on several factors, such as the size and shape of individual clouds. Mixing between the in-cloud and out-of-cloud fractions of a grid cell is expected to be faster if there are many small clouds

instead of a few big clouds, because in the latter case, the in-cloud and out-of-cloud fractions of the grid cell are more strongly separated. Also, the motions of the clouds can influence the efficiency of wet aerosol removal. Because wet removal is the most important aerosol removal mechanism, more attention to this process seems appropriate. With a detailed analysis of this process with a cloud resolving model, the parameterisation of wet removal in large-scale models, such as TM5, can be improved.

### 7.2.2 More dynamic aerosol modes

All representations of aerosols in models are based on substantial simplifications. As shown in Fig. 2.1 and the discussion on this figure in Sect. 2.2.1, the assumption of lognormal aerosol modes with a fixed geometric standard deviation leads to numeric diffusion after resolving a size-dependent process. Furthermore, the mixing state of aerosols is uncertain. All commonly-used aerosol representations in models implicitly assume a specific aerosol mixing state, which may not be correct. As explained in Sect. 1.3, the mixing state is important for the life cycle of aerosols.

These issues could be treated in a more sophisticated way by implementing a more dynamic aerosol mode system, for instance with a variable geometric standard deviation. The downside is that a more detailed description of the aerosol modes requires more variables and more computational time. The errors caused by numeric diffusion of modes and by wrongly-assumed mixing states are hard to quantify, because they may be masked by other model deficiencies. Moreover, experimental verification of these processes is extremely challenging, because the nature of aerosols is diverse and changes occur on short timescales.

### 7.2.3 Displacement between nitrate and chloride

The study on partitioning of semi-volatile aerosols in this thesis is limited to the ammonium-nitrate-sulphate system. Interaction with sodium chloride (sea salt) was not included in the analysis. It is shortly discussed in chapter 4 that experiments clearly show that nitrate can displace chloride in sea salt, influencing the ratio of gas and aerosol phase nitrate. However, most aerosol modules used in large-scale models represent sea salt as inert bulk material, so this acid displacement reaction is not included in those models. Though displacement of nitrate and chloride does not strongly influence aerosol concentrations in most regions over land, it can be important for the Netherlands.

Inclusion of sodium and chloride to the ammonium-nitrate-sulphate system adds significantly to the complexity. The reason is that with sodium, a second non-volatile ion is added to the system. The mixing state between sulphate and sodium significantly influences the partitioning of ammonium, nitrate and chloride. If sodium and sulphate reside on the same particles, they neutralise each other and less semi-volatile material is required to neutralise excess sodium or sulphate. If, on the other hand, sodium and sulphate reside on different particles, both have to be neutralised by semi-volatile material, increasing the aerosol-phase fraction

of these semi-volatile components. Modelling semi-volatile organic components is even more challenging, because the microphysical properties of organic components is versatile. Gas-aerosol partitioning of organic components and the influence of organics on the partitioning of ammonium nitrate may first be investigated in laboratory experiments.

## 7.2.4 Modelling the partitioning timescale

As highlighted in chapters 4 and 5, it is quite difficult to determine the timescale of gas-aerosol partitioning experimentally. Important factors determining the partitioning timescale are the aerosol size and the microphysical properties of the medium (e.g. viscosity). The relationship between the timescale of gas-aerosol partitioning and the aerosol size and microphysical properties has been defined in theory. However, the microphysical properties of aerosols are difficult to measure or to represent in models.

For an adequate estimate of the partitioning timescale in models, the relationship between the partitioning timescale and driving factors such as temperature, relative humidity and aerosol composition needs to be investigated. As pointed out in chapter 5, the partitioning timescale can indirectly be investigated by analysing fluctuations in observed concentrations of aerosol nitrate. However, this analysis requires measurements on homogeneous terrain. Since homogeneous conditions are difficult to acquire in reality, measurement of partitioning timescales may better be performed in a laboratory setting. Chapters 4 and 5 analysed a typical situation for the Netherlands. To further verify the findings of these chapters, similar measurement campaigns and accompanying model studies are needed for different pollution regimes and climatological conditions.

## 7.3 Perspective

The ultimate goal of this research is to quantify the aerosol budget in the Netherlands. We argue that a reliable quantitative analysis of the aerosol budget in the Netherlands is not yet possible with the current models and available data sets. However, important steps have been taken to improve our knowledge about aerosols and aerosol processes specifically relevant for the Dutch situation.

As the lifetime of aerosols is around one week, long-range transport contributes significantly to the local aerosol budget. Therefore, emission inventories and meteorological data for a large region are required to perform a model study on the local aerosol budget. Most continuous large-scale databases of meteorological data and emission estimates are at a resolution of 1 by 1 degree or even coarser, so the Netherlands are hardly resolved in these databases. Especially in the Netherlands, local aerosol concentrations are strongly influenced by heterogeneity in emissions and land use. As long as this heterogeneity is not resolved in global-scale data sets and in commonly-used global models, a proper model evaluation remains difficult.

A main message from this thesis is that the state-of-the-art of aerosol modelling is still at its infancy. However, given the growing information from more detailed

measurements and the enormous increase in computational power, there are many opportunities to make progress. Extension of measurement networks provides more observations that can be used for evaluating large-scale models. Well-designed intensive measurement campaigns can help modellers to unravel specific issues efficiently with case studies so that these specific issues can be parameterised more adequately in climate models. Furthermore, technological development on computers enables large-scale model calculations at a higher resolution. Modelling at a higher resolution not only provides more detailed results. It also eases the representation of small-scale processes.

# Bibliography

---

- Alessandrini, F., Back-Speier, I., Krappmann, D., Weichenmeier, I., Takenaka, S., Karg, E., Kloo, B., Schulz, H., Jakob, T., Mempel, M., and Behrendt, H.: Role of oxidative stress in ultrafine particle-induced exacerbation of allergic lung inflammation, *Am. J. Respir. Crit. Care Med.*, 179, 984–991, doi:10.1164/rccm.200807-1061OC, 2009.
- Alessandrini, F., Weichenmeier, I., van Miert, E., Takenaka, S., Karg, E., Blume, C., Mempel, M., Schulz, H., Bernard, A., and Behrendt, H.: Effects of ultrafine particles-induced oxidative stress on Clara cells in allergic lung inflammation, *Part. Fibre Toxicol.*, 7:11, doi:10.1186/1743-8977-7-11, 2010.
- Anderson, T. L., Covert, D. S., Marshall, S. F., Laucks, M. L., Charlson, R. J., Waggoner, A. P., Ogren, J. A., Caldow, R., Holm, R. L., Quant, F. R., Sem, G. J., Wiedensohler, A., Ahlquist, N. A., and Bates, T. S.: Performance characteristics of a high-sensitivity, three-wavelength, total scatter/backscatter nephelometer, *J. Atmos. Ocean. Tech.*, 13, 967–986, doi:10.1175/1520-0426(1996)013<0967:PCOAHS>2.0;2, 1996.
- Anderson, T. L., Charlson, R. J., Schwartz, S. E., Knutti, R., Boucher, O., Rodhe, H., and Heintzenberg, J.: Climate forcing by aerosols – a hazy picture, *Science*, 300, 1103–1104, doi:10.1126/science.1084777, 2003.
- Andres, R. J. and Kasgnoc, A. D.: A time-averaged inventory of subaerial volcanic sulfur emissions, *J. Geophys. Res.*, 103, 25251–25261, doi:10.1029/98JD02091, 1998.
- Ångström, A. K.: On the atmospheric transmission of sun radiation and on the dust in the air, *Geogr. Ann.*, 11, 156–166, 1929.
- Aspnes, D. E., Theeten, J. B., and Hottier, F.: Investigation of effective-medium models of microscopic surface roughness by spectroscopic ellipsometry, *Phys. Rev. B.*, 20, 3292–3302, doi:10.1103/PhysRevB.20.3292, 1979.
- Balkanski, Y. J., Jacob, D. J., Gardner, G. M., Graustein, W. C., and Turekian, K. K.: Transport and residence times of tropospheric aerosols inferred from a global three-dimensional simulation of  $^{210}\text{Pb}$ ., *J. Geophys. Res.*, 98, 20573–20586, doi:10.1029/93JD2456, 1993.

- Barber, P. W. and Hill, S. C.: Light scattering by particles: Computational Methods, Advanced series in applied physics, World Scientific, 2, 261 pp., 1990.
- Barnett, C. E.: Some applications of wave-length turbidimetry in the infrared, *J. Phys. Chem.*, 46(1), 69–75, doi:10.1021/j150415a009, 1942.
- Bauer, S. E., Wright, D. L., Koch, D., Lewis, E. R., McGraw, R., Chang, L.-S., Schwartz, S. E., and Ruedy, R.: MATRIX (Multiconfiguration Aerosol TRacker of mIXing state): an aerosol microphysical module for global atmospheric models, *Atmos. Chem. Phys.*, 8, 6003–6035, doi:10.5194/acp-8-6003-2008, 2008.
- Berkvens, P. J. F., Botchev, M. A., Lioen, W. M., and Verwer, J. G.: A Zooming Technique for Wind Transport of Air Pollution, in: Finite volumes for complex applications: problems and perspectives: international symposium, Duisburg, Germany, 499–506, 1999.
- Bernstein, J. A., Alexis, N., Barnes, C., Bernstein, I. L., Nel, A., Peden, D., Diaz-Sanchez, D., Tarlo, S. M., and Williams, P. B.: Health effects of air pollution, *J. Allergy Clin. Immunol.*, 114, 1116–1123, 2004.
- Bond, T. C., Streets, D. G., Yarber, K. F., Nelson, S. M., Woo, J.-H., and Klimont, Z.: A technology-based global inventory of black and organic carbon emissions from combustion, *J. Geophys. Res.*, 109, D14203, doi:10.1029/2003JD003697, 2004.
- Bond, T. C., Habib, G., and Bergstrom, R. W.: Limitations in the enhancement of visible light absorption due to mixing state, *J. Geophys. Res.*, 111, D20211, doi:10.1029/2006JD007315, 2006.
- Boucher, O.: On Aerosol Direct Shortwave Forcing and the Henyey-Greenstein Phase Function, *J. Atmos. Sci.*, 55, 128–134, doi:10.1175/1520-0469(1998)055<0128:OADSFA>2.0.CO;2, 1997.
- Bouwman, A. F., Lee, D. S., Asman, W. A. H., Dentener, F. J., van der Hoek, K. W., and Olivier, J. G. J.: A global high-resolution emission inventory for ammonia, *Global Biogeochem. Cy.*, 11(4), 561–587, doi:10.1029/97GB02266, 1997.
- Bregman, B., Segers, A., Krol, M., Meijer, E., and van Velthoven, P.: On the use of mass-conserving wind fields in chemistry-transport models, *Atmos. Chem. Phys.*, 3, 447–457, doi:10.5194/acp-3-447-2003, 2003.
- ten Brink, H. M., Plomp, A., Spoelstra, H., and van de Vate, J. F.: A high-resolution electrical mobility aerosol spectrometer (MAS), *J. Aerosol Sci.*, 14, 589–597, doi:10.1016/0021-8502(83)90064-2, 1983.
- ten Brink, H. M., Kruisz, C., Kos, G. P. A., and Berner, A.: Composition/size of the light-scattering aerosol in the Netherlands, *Atmos. Environ.*, 31, 3955–3962, doi:10.1016/S1352-2310(97)00232-X, 1997.

- ten Brink, H., Otjes, R., Jongeman, P., and Kos, G.: Monitoring of the ratio of nitrate to sulphate in size-segregated submicron aerosol in the Netherlands, *Atmos. Res.*, 92, 270–276, doi:10.1016/j.atmosres.2008.12.003, 2009.
- Brost, R. A., Delany, A. C., and Huebert, B. J.: Numerical Modeling of Concentrations of Fluxes of  $\text{HNO}_3$ ,  $\text{NH}_3$ , and  $\text{NH}_4\text{NO}_3$  near the Surface, *J. Geophys. Res.*, 93(D6), 7137–7152, doi: 10.1029/JD093iD06p07137, 1988.
- Brown, D. M., Wilson, M. R., MacNee, W., Stone, V., and Donaldson, K.: Size-dependent Proinflammatory Effects of Ultrafine Polystyrene Particles: A Role for Surface Area and Oxidative Stress in the Enhanced Activity of Ultrafines, *Toxicol. Appl. Pharm.*, 175, 191–199, doi:10.1006/taap.2001.9240, 2001.
- Bruggeman, D. A. G.: Berechnung verschiedener physikalischer Konstanten von heterogenen Substanzen, 1. Dielektrizitätskonstanten und Leitfähigkeiten der Mischkörper aus isotropen Substanzen, *Ann. Phys.*, 416, 636–664, doi:10.1002/andp.19354160802, 1935.
- Brunekreef, B. and Holgate, S. T.: Air pollution and health, *Lancet*, 360, 1233–1242, doi:10.1016/S0140-6736(02)11274-8, 2002.
- Buijsman, E., Maas, H. F. M., and Asman, W. A. H.: Anthropogenic  $\text{NH}_3$  emissions in Europe, *Atmos. Environ.*, 21, 1009–1022, doi:10.1016/0004-6981(87)90230-7, 1987.
- Canagaratna, M. R., Jayne, J. T., Jimenez, J. L., Allan, J. D., Alfarra, M. R., Zhang, Q., Qnasch, T. B., Drewnick, F., Coe, H., Middlebrook, A., Delia, A. E., Williams, L. R., Trimborn, A. M., Northway, M. J., DeCarlo, P. .F., Kolb, C. E., Davidovits, P., and Worsnop, D. R.: Chemical and microphysical characterization of ambient aerosols with the aerodyne aerosol mass spectrometer, *Mass Spectrom. Rev.*, 26, 185–222, doi:10.1002/mas.20115, 2007.
- Capaldo, K. P., Pilinis C., and Pandis, S. N.: A computationally efficient hybrid approach for dynamic gas/aerosol transfer in air quality models, *Atmos. Environ.*, 34, 3617–3627, doi:10.1016/S1352-2310(00)00092-3, 2000.
- Carslaw, K. S., Boucher, O., Spracklen, D. V., Mann, G. W., Rae, J. G. L., Woodward, S., and Kulmala, M.: A review of natural aerosol interactions and feedbacks within the Earth system, *Atmos. Chem. Phys.*, 10, 1701–1737, doi:10.5194/acp-10-1701-2010, 2010.
- Charlson, R. J., Schwartz, S. E., Hales, J. M., Cess, R. D., Coakley, J. A., Hansen, J. E., and Hofmann, D. J.: Climate forcing by anthropogenic aerosols, *Science*, 255, 423–430, doi:10.1126/science.255.5043.243, 1992.
- Chen, Y., Li, Q., Randerson, J. T., Lyons, E. A., Kahn, R. A., Nelson, D. L., and Diner, D. J.: The sensitivity of CO and aerosol transport to the temporal and vertical distribution of North American boreal fire emissions, *Atmos. Chem. Phys.*, 9, 6559–6580, doi:10.5194/acp-9-6559-2009, 2009.

- Cheng, Y. H. and Tsai, C. J.: Evaporation loss of ammonium nitrate particles during filter sampling, *J. Aerosol Sci.*, 28, 1553–1567, doi:10.1016/S0021-8502(97)00033-5, 1997.
- Chin, M., Rood, R. B., Lin, S.-J., Müller, J.-F., and Thompson, A. M.: Atmospheric sulfur cycle simulated in the global model GOCART: Model description and global properties, *J. Geophys. Res.*, 105, 24671–24687, 2000.
- Chung, S. H. and Seinfeld, J. H.: Climate response of direct radiative forcing of anthropogenic black carbon, *J. Geophys. Res.*, 110, D11102, doi:10.1029/2004JD005441, 2005.
- Cofala, J., Amann, M., and Mechler, R.: Scenarios of world anthropogenic emissions of air pollutants and methane up to 2030, Tech. rep., International Institute for Applied System Analysis (IIASA), Laxenburg, Austria, online available at: [http://www.iiasa.ac.at/rains/global\\_emiss/global\\_emiss.html](http://www.iiasa.ac.at/rains/global_emiss/global_emiss.html), (last access: 9-7-2009), 2005.
- Crosier, J., Allan, J. D., Coe, H., Bower, K. N., Formenti, P., and Williams, P. I.: Chemical Composition of summertime aerosol in the Po Valley (Italy), northern Adriatic and Black Sea, *Q. J. Roy. Meteorol. Soc.*, 133(S1), 61–75, doi:10.1002/qj.88, 2007.
- Cuijpers, J. W. M. and Duynkerke, P. G.: Large Eddy Simulation of Trade Wind Cumulus Clouds, *J. Atmos. Sci.*, 50, 3894–3907, doi:10.1175/1520-0469(1993)050<3894:LESOTW>2.0.CO;2, 1993.
- Dana, M. T. and Hales, J. M.: Statistical aspects of the washout of polydisperse aerosols, *Atmos. Environ.*, 10, 45–50, doi:10.1016/0004-6981(76)90258, 1976.
- Debye, P.: Der Lichtdruck auf Kugeln von beliebigem Material, *Ann. Phys.*, 335, 57–136, doi:10.1002/andp.19093351103, 1909.
- DeCarlo, P. F., Slowik, J. G., Worsnop, D. R., Davidovits, P., and Jimenez, J. L.: Particle morphology and density characterization by combined mobility and aerodynamic diameter measurements. Part 1: Theory, *Aerosol Sci. Technol.*, 38, 1185–1205, doi:10.1080/027868290903907, 2004.
- Dentener, F. and Crutzen, P. J.: A Three-dimensional Model of the global ammonia cycle, *J. Atmos. Chem.*, 19, 331–369, doi:10.1007/FG00694492, 1994.
- Dentener, F., Kinne, S., Bond, T., Boucher, O., Cofala, J., Generoso, S., Ginoux, P., Gong, S., Hoelzemann, J. J., Ito, A., Marelli, L., Penner, J. E., Putaud, J.-P., Textor, C., Schulz, M., van der Werf, G. R., and Wilson, J.: Emissions of primary aerosol and precursor gases in the years 2000 and 1750 prescribed data-sets for AeroCom, *Atmos. Chem. Phys.*, 6, 4321–4344, doi:10.5194/acp-6-4321-2006, 2006.

- 
- Dlugi, R., Berger, M., Zelger, M., Hofzumahaus, A., Siese, M., Holland, F., Wisthaler, A., Grabner, W., Hansel, A., Koppmann, R., Kramm, G., Möllmann-Coers, M., and Knaps, A.: Turbulent exchange and segregation of HO<sub>x</sub> and volatile organic compounds above a deciduous forest, *Atmos. Chem. Phys.*, 10, 6215–6235, doi:10.5194/acp-10-6215-2010, 2010.
- Dockery, D., Pope, C. A., Xu, X., Spengler, J. D., Ware, J. H., Fay, M. E., Ferris, B. G., and Speizer, F. E.: An association between air pollution and mortality in six US cities, *New Engl. J. Med.*, 329, 1753–1759, doi:10.1056/NEJM199312093292401, 1993.
- Drewnick, F., Hings, S. S., DeCarlo, P. F., Jayne, J. T., Gonin, M., Fuhrer, K., Weimer, S., Jimenez, J. L., Demerjian, K. L., Borrmann, S., Worsnop, and D. R.: A new time-of-flight aerosol mass spectrometer (TOF-AMS) – Instrument description and first field deployment, *Aerosol Sci. Technol.*, 39, 637–658, doi:10.1080/02786820500182040, 2005.
- Dosio, A.: Turbulent dispersion in the Atmospheric Convective Boundary Layer, Ph.D. thesis, Wageningen University, 2005.
- European Monitoring and Evaluation Programme: Hjellbrekke, A.-G., and Fjæraa, A. M.: Data report 2006: Acidifying and eutrophying compounds and particulate matter, Tech. rep., 2008.
- Farmer, D. K., Kimmel, J. R., Phillips, G., Docherty, K. S., Worsnop, D. R., Sueper, D., Nemitz, E., and Jimenez, J. L.: Eddy covariance measurements with high-resolution time-of-flight aerosol mass spectrometry: a new approach to chemically resolved aerosol fluxes, *Atmos. Chem. Phys.*, 4, 1275–1289, doi:10.5194/amt-4-1275-2011, 2011.
- Feng, Y. and Penner, J. E.: Global modeling of nitrate and ammonium: Interaction of aerosols and tropospheric chemistry, *J. Geophys. Res.*, 112, D01304, doi:10.1029/2005JD006404, 2007.
- Fisseha, R., Dommen, J., Gutzwiller, L., Weingartner, E., Gysel, M., Emmenegger, C., Kalberer, M., and Baltensperger, U.: Seasonal and diurnal characteristics of water soluble inorganic compounds in the gas and aerosol phase in the Zurich area, *Atmos. Chem. Phys.*, 6, 1895–1904, doi:10.5194/acp-6-1895-2006, 2006.
- Fountoukis, C. and Nenes, A.: ISORROPIA II: a computationally efficient thermodynamic equilibrium model for K<sup>+</sup>–Ca<sup>2+</sup>–Mg<sup>2+</sup>–NH<sub>4</sub><sup>+</sup>–Na<sup>+</sup>–SO<sub>4</sub><sup>2-</sup>–NO<sub>3</sub><sup>-</sup>–Cl<sup>-</sup>–H<sub>2</sub>O aerosols, *Atmos. Chem. Phys.*, 7, 4639–4659, doi:10.5194/acp-7-4639-2007, 2007.
- Fowler, D., Pilegaard, K., Sutton, M. A., Ambus, P., Raivonen, M., Duyzer, J., Simpson, D., Fagerli, H., Fuzzi, S., Schjoerring, J. K., Granier, C., Nefel, A., Isaksen, I. S. A., Laj, P., Maione, M., Monks, P. S., Burkhardt, J., Daemmgen, U., Neiryneck, J., Personne, E., Wichink-Kruit, R., Butterbach-Bahl, K., Flechard, C., Tuovinen, J. P., Coyle, M., Gerosa, G., Loubet, B.,

- Altmir, N., Gruenhage, L., Ammann, C., Cieslik, S., Paoletti, E., Mikkelsen, T. N., Ro-Poulsen, H., Cellier, P., Cape, J. N., Horváth, L., Loreto, F., Ninemets, Ü., Palmer, P. I., Rinne, J., Misztal, P., Nemitz, E., Nilsson, D., Pryor, S., Gallagher, M. W., Vesala, T., Skiba, U., Brüggemann, N., Zechmeister-Boltenstern, S., Williams, J., O'Dowd, C., Facchini, M. C., de Leeuw, G., Flossman, A., Chaumerliac, N., and Erisman, J. W.: Atmospheric composition change: Ecosystem-Atmosphere interactions, *Atmos. Environ.*, 43, 5193–5267, doi: 10.1016/j.atmosenv.2009.07.068, 2009.
- Ganzeveld, L., Lelieveld, J., and Roelofs, G.-J.: A dry deposition parameterization for sulfur oxides in a chemistry and general circulation model, *J. Geophys. Res.*, 103, 5679–5694, doi:10.1029/97JD03077, 1998.
- von Glasow, R.: Pollution meets sea salt, *Nat. Geosci.*, 1, 292–293, doi:10.1038/ngeo192, 2008.
- Gong, S. L.: A parameterization of sea-salt aerosol source function for sub- and super-micron particles, *Global Biogeochem. Cy.*, 17, 1097, doi:10.1029/2003GB002079, 2003.
- Gordon, M., Staebler, R. M., Liggio, J., Vlasenko, A., Li, S.-M., and Hayden, K.: Aerosol flux measurements above a mixed forest at Borden, Ontario, *Atmos. Chem. Phys.*, 11, 6773–6786, doi: 10.5194/acp-11-6773-2011, 2011.
- Guelle, W., Balkanski, Y. J., Schultz, M., Dulac, F., and Monfray, P.: Wet deposition in a global size-dependent aerosol transport model 1. Comparison of a 1 year  $^{210}\text{Pb}$  simulation with ground measurements, *J. Geophys. Res.*, 103, 28875–28891, 1998.
- Halmer, M. M., Schmincke, H.-U., and Graf, H.-F.: The annual volcanic gas input into the atmosphere, in particular into the stratosphere: a global data set for the past 100 years, *J. Volcanol. Geoth. Res.*, 115, 511–528, doi:10.1016/S0377-0273(01)00318-3, 2002.
- Hari, P. and Kulmala, M.: Station for Measuring Ecosystem-Atmosphere Relations (SMEAR II), *Boreal Environ. Res.*, 10, 315–322, 2005.
- Haywood, J. and Boucher, O.: Estimates of the direct and indirect radiative forcings due to tropospheric aerosols: a review, *Rev. Geophys.*, 38, 513–543, doi:10.1029/1999RG000078, 2000.
- Hecht, E.: *Optics*, Fourth edition, Addison-Wesley Publishing Co., Reading, Pennsylvania, 2003.
- van Heerwaarden, C. C. and Vilà-Guerau de Arellano, J.: Relative Humidity as an Indicator for Cloud Formation over Heterogeneous Land Surfaces, *J. Atmos. Sci.*, 65, 3263–3277, doi:10.1175/2008JAS2591.1, 2008.
- Hendriks, C., Kranenburg, R., Knenen, J., van Gijlsijk, R., Wichink Kruit, R., Segers, A., van der Gon, H. A. C., and Schaap, M.: The origin of ambient

- 
- Particulate Matter concentrations in the Netherlands, *Atmos. Environ.*, under review, 2012.
- Hess, M., Koepke, P., and Schult, I.: Optical Properties of Aerosols and Clouds: The Software Package OPAC, *B. Am. Meteorol. Soc.*, 79, 831–844, doi:10.1175/1520-0477(1998)079<0831:OPOAAC>2.0.CO;2, 1998.
- Heus, T., van Heerwaarden, C. C., Jonker, H. J. J., Siebesma, A. P., Axelsen, S., van den Dries, K., Geoffroy, O., Moene, A., Pino, D., de Roodeo, S. R., and Vilà-Guerau de Arellano, J.: Formulation of the Dutch Atmospheric Large-Eddy Simulation (DALES) and overview of its applications, *Geosci. Model Dev.*, 3, 415–444, doi:10.5194/gmd-3-415-2010, 2010.
- Hicks, B. B., Wesely, M. L., Coulter, R. L., Hart, R. L., Durham, J. L., Speer, R., and Stedman, D. H.: An experimental study of sulfur and NO<sub>x</sub> fluxes over grassland, *Bound. Lay. Meteorol.*, 34, 103–121, 1986.
- Hoek, G., Brunekreef, B., Goldbohm, S., Fischer, P., and van den Brandt, A.: Association between mortality and indicators of traffic-related air pollution in the Netherlands: a cohort study, *Lancet*, 360, 1203–1209, doi:10.1016/S0140-6736(02)11280-3, 2002.
- Holben, B. N., Tenré, D., Smirnov, A., Eck, T. F., Slutsker, I., Abuhassan, N., Newcomb, W. W., Schafer, J. S., Chatenet, B., Lavenu, F., Kaufman, Y. J., Vande Castle, J., Setzer, A., Markham, B., Clark, D., Frouin, R., Halthore, R., Karneli, A., O’Neill, N. T., Pietras, C., Pinker, R. T., Voss, K., and Zibordi, G.: An emerging ground-based aerosol climatology: Aerosol optical depth from AERONET, *J. Geophys. Res.*, 106, 12067–12097, 2001.
- Holtzlag, A. A. M. and Boville, B. A.: Local versus nonlocal boundary-layer diffusion in a global climate model, *J. Climate*, 6, 1825–1842, doi:10.1175/1520-0442(1993)006<1825:LVNBLD>2.0.CO;2, 1993.
- Hong, S.-Y. and Pan, H.-L.: Nonlocal boundary layer vertical diffusion in a Medium-Range Forecast model, *Mon. Weather Rev.*, 124, 2322–2339, doi:10.1175/1520-0493(1996)124<2322:NBLVDI>2.0.CO;2, 1996.
- Houweling, S., Dentener, F., and Lelieveld, J.: The impact of nonmethane hydrocarbon compounds on tropospheric photochemistry, *J. Geophys. Res.*, 103, 10673–10696, 1998.
- Huebert, B. J., Luke, W. T., Delany, A. C., and Brost, R. A.: Measurements of Concentrations and Dry Surface Fluxes of Atmospheric Nitrates in the Presence of Ammonia, *J. Geophys. Res.*, 93(D6), 7127–7136, doi:10.1029/JD093iD06p07127, 1988.
- Intergovernmental Panel on Climate Change: edited by: Nakicenovic, N., Akamo, J., Davis, G., de Vries, B., Fenhann, J., Gaffin, S., Gregory, K., Grübler, A., Jung, T. Y., Kram, T., La Rovere, E. L., Michaelis, L., Mori, S., Morita, T., Pepper, W., Pitcher, H., Price, L., Riaki, K., Roehrl, A., Rogner, H.-H., Sankovski,

- A., Schlesinger, M., Shukla, P., Smith, S., Swart, R., van Rooijen, S., Victor, N., and Dadi, Z.: Special report on Emissions Scenarios, 2000.
- Intergovernmental Panel on Climate Change, edited by: Solomon, S., Qin, D., Manning, M., Chen, Z., Marquis, M., Averyt, K. B., Tignor, M., and Miller, H. L.: Climate change 2007: The physical Science Basis, IPCC Fourth Assessment report (AR4), 2007.
- Jamnik, J., Kalmin, J. R., Kotomin, E. A., and Maier, J.: Generalised Maxwell-Garnett equation: application to electrical and chemical transport, *Phys. Chem. Chem. Phys.*, 8, 1310–1314, doi:10.1039/b514448p, 2006.
- Jarvis, P. G.: The interpretation of the variations in leaf water potentials and stomatal conductance found in canopies in the field, *Philos. Trans. R. Soc. Lond. B273*, 593–610, doi:10.1098/rstb.1976.0035, 1976.
- Justice, C. O., Vermote, E., Townshend, J., Defries, R., Royle, J. A., Hall, D., Salomonson, V., Privette, J. L., Riggs, G. A., Strahler, A. H., Lucht, W., Myneni, R. B., Knyazikhin, Y., Running, S. W., Nemanj, R. R., Wan, Z. M., Huete, A. R., van Leeuwen, W. J. D., Wolfe, R. E., Giglio, L., Muller, J.-P., Lewis, P., and Barnsley, M. J.: The Moderate Resolution Imaging Spectroradiometer (MODIS): Land Remote Sensing for Global Change Research, 36, 1228–1249, doi:10.1109/36.701075, 1998.
- Kahnert, M.: Modelling the optical and radiative properties of freshly emitted light absorbing carbon within an atmospheric chemical transport model, *Atmos. Chem. Phys.*, 10, 1403–1416, doi:10.5194/acp-10-1403-2010, 2010a.
- Kahnert, M.: Numerically exact computations of the optical properties of light absorbing carbon aggregates for wavelength of 200 nm–12.2  $\mu$ m, *Atmos. Chem. Phys.*, 10, 8319–8329, doi:10.5194/acp-10-8319-2010, 2010b.
- Kanakidou, M.: Aerosols in Global Models – Focus on Europe, in: *Regional Climate Variability and its Impacts in The Mediterranean Area*, chap. 4, Springer, The Netherlands, 143–154, 2007.
- Kanakidou, M., Seinfeld, J. H., Pandis, S. N., Barnes, I., Dentener, F. J., Facchini, M. C., Van Dingenen, R., Ervens, B., Nenes, A., Nielsen, C. J., Swietlicki, E., Putaud, J. P., Balkanski, Y., Fuzzi, S., Horth, J., Moortgat, G. K., Winterhalter, R., Myhre, C. E. L., Tsigaridis, K., Vignati, E., Stephanou, E. G., and Wilson, J.: Organic aerosol and global climate modelling: a review, *Atmos. Chem. Phys.*, 5, 1053–1123, doi:10.5194/acp-5-1053-2005, 2005.
- Kaufman, Y. J., Tanré, D., and Boucher, O.: A satellite view of aerosols in the climate system, *Nature*, 419, 215–223, doi:10.1038/nature01091, 2002.
- Kerkweg, A., Buchholz, J., Ganzeveld, L., Pozzer, A., Tost, H., and Jöckel, P.: Technical Note: An implementation of the dry removal processes DRY DEPosition and SEDImentation in the Modular Earth Submodel System (MESSy), *Atmos. Chem. Phys.*, 6, 4617–4632, doi:10.5194/acp-6-4617-2006, 2006.

- 
- Keuken, M. P., Schoonebeek, C. A. M., Vanwensveenlouter, A., and Slanina, J.: Simultaneous Sampling of  $\text{NH}_3$ ,  $\text{HNO}_3$ ,  $\text{HCl}$ ,  $\text{SO}_2$  and  $\text{H}_2\text{O}_2$  in Ambient Air by a Wet Annular Denuder System, *Atmos. Environ.*, 22, 2541–2548, doi:10.1016/0004-6981(88)90486-6, 1988.
- Khlystov, A., Wyers, G. P., and Slanina, J.: The Steam-Jet Aerosol Collector, *Atmos. Environ.*, 29, 2229–2234, doi:10.1016/1352-2310(95)00180-7, 1995.
- Kiehl, J. T. and Briegleb, B. P.: The relative roles of sulphate and greenhouse gases in climate forcing, *Science*, 260, 311–314, doi:10.1126/science.260.5106.311, 1993.
- Kinne, S., Lohmann, U., Feichter, J., Schultz, M., Timmreck, C., Ghan, S., Easter, R., Chin, M., Ginoux, P., Takemura, T., Tegen, I., Koch, D., Herzog, M., Penner, J., Pitari, G., Holben, B., Eck, T., Smirnov, A., Dubovik, O., Slutsker, I., Tanre, D., Tarnes, O., Mishchenko, M., Geogdzhayev, I., Chu, D. A., and Kaufman, Y.: Monthly averages of aerosol properties: A global comparison among models, satellite data and AERONET ground data, *J. Geophys. Res.*, 108, 2634, doi:10.1029/2001JD001253, 2003.
- Korhonen, H., Carslaw, K. S., Spracklen, D. V., Ridley, D. A., and Ström, J.: A global model study of processes controlling aerosol size distributions in the Arctic spring and summer, *J. Geophys. Res.*, 113, D08211, doi:10.1029/2007JD009114, 2008.
- Kramm, G. and Dlugi, R.: Modelling of the vertical fluxes of nitric acid, ammonia and ammonium nitrate, *J. Atmos. Chem.*, 18, 319–357, 1994.
- Krol, M. C. and van Wee, M.: Implications of variations in photodissociation rates for global tropospheric chemistry, *Atmos. Environ.*, 31, 1257–1273, doi:10.1016/S1352-2310(96)00323-8, 1997.
- Krol, M. C., Molemaker, M. J., and Vilà-Guerau de Arellano, J.: Effects of turbulence and heterogeneous emissions on photochemically active species in the convective boundary layer, *J. Geophys. Res.*, 105, 6871–6884, doi:10.1029/1999JD900958, 2000.
- Krol, M., Houweling, S., Bregman, B., van den Broek, M., Segers, A., van Velthoven, P., Peters, W., Dentener, F., and Bergamaschi, P.: The two-way nested global chemistry-transport zoom model TM5: algorithm and applications, *Atmos. Chem. Phys.*, 5, 417–432, doi:10.5194/acp-5-417-2005, 2005.
- Kulmala, M., Asmi, A., Lappalainen, H. K., Carslaw, K. S., Pöschl, U., Baltensperger, U., Hov, Ø., Brenquier, J.-L., Pandis, S. N., Facchini, M. C., Hansson, H.-C., Wiedensohler, A., and O’Dowd, C. D.: Introduction: European Integrated Project on Aerosol Cloud Climate and Air Quality interactions (EUCAARI) – integrating aerosol research from nano to global scales, *Atmos. Chem. Phys.*, 9, 2825–2841, doi:10.5194/acp-9-2825-2009, 2009.

- Landgraf, J. and Crutzen, P. J.: An efficient method for online calculations of photolysis and heating rates, *J. Atmos. Sci.*, 55, 863–878, doi:10.1175/1520-0469(1998)055<0863:AEMFOC>2.0.CO;2, 1998.
- Langner, J. and Rodhe, H.: A global Three-dimensional Model of the tropospheric Sulfur cycle, *J. Atmos. Chem.*, 13, 225–263, doi:10.1007/BF00058134, 1991.
- Lazaridis, M., Semb, A., Larssen, S., Hov, Ø., Hansen, J. E., Schaug, J., and Tørseth, K.: Measurements of particulate matter within the framework of the European Monitoring and Evaluation Programme (EMEP) 1. First results, *Sci. Total Environ.*, 285, 209–235, doi:10.1016/S0048-9697(01)00932-9, 2002.
- Lee, C. K.: Multifractal characteristics in air pollutant concentration time series, *Water Air Soil Pollut.*, 135, 389–409, doi:10.1023//A:1014768632318, 2002.
- Lee, Y. H. and Adams, P. J.: Evaluation of aerosol distributions in the GISS-TOMAS global aerosol microphysics model with remote sensing observations, *Atmos. Chem. Phys.*, 10, 2129–2144, doi:10.5194/acp-10-2129-2010, 2010.
- Li, N., Sioutas, C., Cho, A., Schmitz, D., Misra, C., Sempf, J., Wang, M., Oberley, T., Froines, J., and Nel, A.: Ultrafine particulate pollutants induce oxidative stress and mitochondrial damager, *Environ. Health Perspect.*, 111, 455–460, doi:10.1289/ehp.6000, 2002.
- van Loon, M., Vautard, R., Schaap, M., Bergström, R., Bessagnet, B., Brandt, J., Bultjes, P. J. H., Christensen, J. H., Cuvelier, C., Graff, A., Jonson, J. E., Krol, M., Langner, J., Roberts, P., Rouil, L., Stern, R., Tarrasón, L., Thunis, P., Vignati, E., White, L., and Wind, P.: Evaluation of long-term ozone simulations from seven regional air quality models and their ensemble, *Atmos. Environ.*, 41, 2083–2097, doi:10.1016/j.atmosenv.2006.10.073, 2007.
- Louis, J. F.: A parametric model of vertical eddy fluxes in the atmosphere, *Bound. Lay. Meteorol.*, 17, 187–202, doi:10.1007/FG00117978, 1979.
- Manders, A. M. M., Schaap, M., Querol, X., Albert, M. F. M. A., Vercauteren, J., Kuhlbusch, T. A. J., and Hoogerbrugge, R.: Sea salt concentrations across the European continent, *Atmos. Environ.*, 44, 2434–2442, doi:10.1016/j.atmosenv.2010.03.028, 2010.
- Madronich, S.: Photodissociation in the atmosphere. 1. Actinic flux and the effect of ground reflections and clouds, *J. Geophys. Res.*, 92, 9740–9752, doi:10.1029/JD092iD08p09740, 1987.
- Mahrt, L.: Boundary-layer moisture regimes, *Q. J. Roy. Meteorol. Soc.*, 177, 151–176, doi:10.1002/qj49711749708, 1991.
- Maxwell-Garnett, J. C.: Colours in metal glasses and in metallic films, *Philos. T. Roy. Soc. Lond. A*, 203, 385–420, doi:10.1098/rsta.1904.0024, 1904.

- 
- Mehlmann, A. and Warneck, P.: Atmospheric gaseous  $\text{HNO}_3$ , particulate nitrate, and aerosol size distribution of major ionic species at a rural site in Western Germany, *Atmos. Environ.*, 29, 2359–2373, doi:10.1016/1352-2310(95)00056-5, 1995.
- de Meij, A., Krol, M., Dentener, F., Vignati, E., Cuvelier, C., and Thunis, P.: The sensitivity of aerosol in Europe to two different emission inventories and temporal distribution of emissions, *Atmos. Chem. Phys.*, 6, 4287–4309, doi:10.5194/acp-6-4287-2006, 2006.
- van Meijgaard, E., van Ulft, B., van de Berg, W. J., Bosveld, F. C., van den Hurk, B., Lenderink, G., and Siebesma, A. P.: The KNMI regional atmospheric climate model RACMO, version 2.1, Tech. Rep. TR 302, KNMI, De Bilt, The Netherlands, 2008.
- Meng, Z. and Seinfeld, J. H.: Time scales to achieve atmospheric gas-aerosol equilibrium for volatile species, *Atmos. Environ.*, 30, 2889–2900, doi:10.1016/1352-2310(95)00493-9, 1996.
- Mensah, A. A., Holzinger, R., Otjes, R., Trimborn, A., Mentel, T. F., ten Brink, H., Henzing, B., and Kiendler-Scharr, A.: Aerosol chemical composition at Cabauw, the Netherlands as observed in two intensive periods in May 2008 and March 2009, *Atmos. Chem. Phys.*, 12, 4723–4742, doi:10.5194/acp-12-4723-2012, 2012.
- Mercado, L. M., Bellouin, N., Sitch, S., Boucher, O., Huntingford, C., Wild, M., and Cox, P. M.: Impact of changes in diffuse radiation on the global land carbon sink, *Nature*, 458, 1014–1017, doi:10.1038/nature07949, 2009.
- Metzger, S., Dentener, F., Krol, M., Jeuken, A., and Lelieveld, J.: Gas/aerosol partitioning 2: Global modeling results, *J. Geophys. Res.*, 107, 4313, doi:10.1029/2001JD001103, 2002a.
- Metzger, S., Dentener, F., Pandis, S., and Lelieveld, J.: Gas/aerosol partitioning 1: A computationally efficient model, *J. Geophys. Res.*, 107, 4312, doi:10.1029/2001JD001102, 2002b.
- Mie, G.: Beiträge zur Optik trüber Medien, speziell kolloidaler Metallösungen, *Ann. Phys.*, 330, 377–445, doi:10.1002/andp.19083300302, 1908.
- Millero, F. J.: Physicochemical controls on seawater, chap. 6.01, Elsevier, Amsterdam, The Netherlands, 1–21, 2004.
- Moeng, C.-H. and Rotunno, R.: Vertical-velocity skewness in the buoyancy-driven boundary layer, *J. Atmos. Sci.*, 47, 1149–1162, doi:10.1175/1520-0469(1990)047<1149:VVSITB>2.0.CO;2, 1990.
- Moosmüller, H. and Arnott, W. P.: Particle optics in the Rayleigh regime, *J. Air Waste Manage. Assoc.*, 59, 1028–1031, 2009.

- Morgan, W. T., Allan, J. D., Bower, K. N., Esselborn, M., Harris, B., Henzing, J. S., Highwood, E. J., Kiendler-Scharr, A., McMeeking, G. R., Mensah, A. A., Northway, M. J., Osborne, S., Williams, P. I., Krejci, R., and Coe, H.: Enhancement of the aerosol direct radiative effect by semi-volatile aerosol components: airborne measurements in North-Western Europe, *Atmos. Chem. Phys.*, 10, 8151–8171, doi:10.5194/acp-10-8151-2010, 2010.
- Morino, Y., Kondo, Y., Takegawa, N., Miyazaki, Y., Kita, K., Komazaki, Y., Fukuda, M., Miyakawa, T., Moteki, N., and Worsnop, D. R.: Partitioning of  $\text{HNO}_3$  and particulate nitrate over Tokyo: Effect of vertical mixing, *J. Geophys. Res.*, 111, D15215, doi:10.1029/2005JD006887, 2006.
- Moya, M., Ansari, A. S., and Pandis, S. N.: Partitioning of nitrate and ammonium between the gas and particulate phases during the 1997 IMADA-AVER study in Mexico City, *Atmos. Environ.*, 35, 1791–1804, doi:10.1016/S1352-2310(00)00292-2, 2001.
- Neftel, A., Blatter, A., Hesterberg, R., and Staffelbach, T.: Measurements of concentration gradients of  $\text{HNO}_2$  and  $\text{HNO}_3$  over a semi-natural ecosystem, *Atmos. Environ.*, 30(17), 3017–3025, doi:10.1016/1352-2310(96)00011-8, 1996.
- Nemitz, E. and Sutton, M. A.: Gas-particle interactions above a Dutch heathland: III. Modelling the influence of the  $\text{NH}_3$ - $\text{HNO}_3$ - $\text{NH}_4\text{NO}_3$  equilibrium on size-segregated particle fluxes, *Atmos. Chem. Phys.*, 4, 1025–1045, doi: 10.5194/acp-4-1025-2004, 2004.
- Nemitz, E., Sutton, M. A., Wyers, G. P., and Jongejan, P. A. C.: Gas-particle interactions above a Dutch heathland: I. Surface exchange fluxes of  $\text{NH}_3$ ,  $\text{SO}_2$ ,  $\text{HNO}_3$  and  $\text{HCl}$ , *Atmos. Chem. Phys.*, 4, 989–1005, doi: 10.5194/acp-4-989-2004, 2004a.
- Nemitz, E., Sutton, M. A., Wyers, G. P., Otjes, R. P., Mennen, M. G., van Putten, E. M., and Gallagher, M. W.: Gas-particle interactions above a Dutch heathland: II. Concentrations and surface exchange fluxes of atmospheric particles, *Atmos. Chem. Phys.*, 4, 1007–1024, doi:10.5194/acp-4-1007-2004, 2004b.
- Nemitz, E., Jimenez, J. L., Huffman, J. A., Ulbrich, I. M., Canagaratn, M. R., Worsnop, D. R., and Guenther, A. B.: An Eddy-Covariance System for the Measurement of Surface/Atmosphere Exchange Fluxes of Submicron Aerosol Chemical Species—First Application Above an Urban Area, *Aerosol. Sci. Technol.*, 8, doi:10.1080/02786820802227352, 2008.
- Nemitz, E., Phillips, G. J., Thomas, R., Di Marco, C. F., Tang, S., Coe, H., Allan, J., Harrison, R. M., and Fowler, D.: Nitrate Dynamics in UK Urban Environments, *European Aerosol Conference 2009*, Karlsruhe, Germany, 6–11 September 2009, Abstract T130A10, 2009.
- Nenes, A., Pandis, S. N., and Pilinis, C.: ISORROPIA: A new thermodynamic equilibrium model for multiphase multicomponent inorganic aerosols, *Aquat. Geochem.*, 4, 123–152, doi:10.1023/A:1009604003981, 1998.

- 
- Nieuwstadt, F. T. M. and Brost, R. A.: The Decay of Convective Turbulence, *J. Atmos. Sci.*, 43, 532–545, doi:10.1175/1520-0469(1986)043<0532%3ATDOCT>2.0.CO;2, 1986.
- Noh, Y., Chun, W. G., Hong, Y., and Raasch, S.: Improvement of the K-profile model for the planetary boundary layer based on large eddy simulation data, *Bound. Lay. Meteorol.*, 107, 401–427, doi:10.1023/A:1022146015946, 2003.
- van Oss, R., Duyzer, J., and Wyers, P.: The influence of gas-to-particle conversion on measurements of ammonia exchange over forest, *Atmos. Environ.*, 32(3), 465–471, doi: 10.1016/S1352-2310(97)00280-X, 1998.
- Ouwersloot, H. G., Vilà-Guerau de Arellano, J., van Heerwaarden, C. C., Ganzeveld, L. N., Krol, M. C., and Lelieveld, J.: On the segregation of chemical species in a clear boundary layer over heterogeneous land surfaces, *Atmos. Chem. Phys.*, 11, 10681–10704, doi:10.5194/acp-11-10681-2011, 2011.
- Pickering, K. E., Wang, Y., Tao, W.-K., Price, C., and Müller, J.-F.: Vertical distributions of lightning NO<sub>x</sub> for use in regional and global chemical transport models, *J. Geophys. Res.*, 103, 31203–31216, 1998.
- Pope, C. A., Dockery, D. W., and Schwartz, J.: Review of Epidemiological Evidence of Health Effects of Particulate Air Pollution, *Inhal. Toxicol.*, 7, 1–18, doi:10.3109/08958379509014267, 1995.
- Pope, C. A.: Epidemiology of the fine particulate air pollution and human health: biologic Mechanisms and who's at risk?, *Environ. Health Perspect.*, 108(Suppl 4), 713–723, doi:10.1289/ehp.00108s4713, 2000.
- Pöschl, U.: Atmospheric Aerosols: Composition, Transformation, Climate and Health Effects, *Angew. Chem. Int. Ed.*, 44, 7520–7540, doi:10.1002/anie.200501122, 2005.
- Prather, J.: Numerical Advection by Conservation of Second-Order Moments, *J. Geophys. Res.*, 91, 6671–6681, 1986.
- Pringle, K. J., Tost, H., Messina, S., Steil, B., Giannadaki, D., Nenes, A., Fountoukis, C., Stier, P., Vignati, E., and Lelieveld, J.: Description and evaluation of GMXe: a new aerosol submodel for global simulations (v1), *Geosci. Model Dev.*, 3, 391–412, doi:10.519/gmd-3-391-2010, 2010.
- Pugh, T. A. M., MacKenzie, A. R., Langford, B., Nemitz, E., Misztal, P. K., and Hewitt, C. N.: The influence of small-scale variations in isoprene concentrations on atmospheric chemistry over a tropical rainforest, *Atmos. Chem. Phys.*, 11, 4142–4134, doi:10.5194/acp-11-4121-2011, 2011.
- Putaud, J.-P., Raes, F., van Dingenen, R., Brüggemann, E., Facchini, M.-C., Decesari, S., Fuzzi, S., Gehrig, R., Hüglin, C., Laj, P., Lorbeer, G., Maenhaut, W., Mihalopoulos, N., Müller, K., Querol, X., Rodriguez, S., Schneider, J., Spindler, G., ten Brink, H., Tørseth, K., and Wiedensohler, A.: A European aerosol

- phenomenology-2: chemical characteristics of particulate matter at kerbside, urban, rural and background sites in Europe, *Atmos. Environ.*, 38, 2579–2595, doi:10.1016/j.atmosenv.2004.01.041, 2004.
- Randerson, J. T., van der Werf, G. R., Giglio, L., Collatz, G. J., and Kasibhatla, P. S.: Global Fire Emission Database, Version 2 (GFEDv2), Data set. Available on-line <http://daac.ornl.gov/> (last access 9-7-2009) from Oak Ridge National Laboratory Distributed Active Archive Center, Oak Ridge, Tennessee, USA, doi:10.3334/ORNLDAAC/834, 2006.
- Lord Rayleigh: On the light from the sky, its polarization and color, *Philos. Mag.*, 41, 107–120, 274–279, 1871.
- Roelofs, G.-J. and Lelieveld, J.: Distribution and budget of O<sub>3</sub> in the troposphere calculated with a chemistry general circulation model, *J. Geophys. Res.*, 100, 20983–20998, 1995.
- Rosenfeld, D., Lohmann, U., Raga, G. B., O’Dowd, C. D., Kulmala, M., Fuzzi, S., Reissell, A., and Andreae, M. O.: Flood or Drought: How Do Aerosols Affect Precipitation?, *Science*, 321, 1309–1313, doi:10.1126/science.1160606, 2008.
- Russchenberg, H. W. J., Bosveld, F., Swart, D., ten Brink, H., de Leeuw, G., Uijlenhoet, R., Arbesser-Rastburg, B., van der Marel, H., Lighthart, L., Boers, R., and Apituley, A.: Ground-based atmospheric remote sensing in The Netherlands; European outlook, *IEEE T. Commun.*, 2252–2258, doi:10.1093/ietcom/e88-b.6.2252, 2005.
- Russell, G. F. and Lerner, J. A.: A New Finite-Differencing Scheme for the Tracer Transport Equation, *J. Appl. Meteorol.*, 20, 1483–1498, doi:10.1175/1520-0450(1981)020<1483:ANFDSF>2.0.CO;2, 1981.
- Russell, P. B., Bergstrom, R. W., Shinozuka, Y., Clarke, A. D., DeCarlo, P. F., Jimenez, J. L., Livingston, J. M., Redemann, J., Dubovik, O., and Strawa, A.: Absorption Angstrom Exponent in AERONET and related data as an indicator of aerosol composition, *Atmos. Chem. Phys.*, 10, 1155–1169, doi:10.5194/acp-10-1155-2010, 2010.
- Ryder, J.: Emission, deposition and chemical conversion of atmospheric trace substances in and above vegetation canopies, *PhD Thesis*, University of Manchester, Manchester, 241 pp, 2010.
- Saarinén, J. J., Vartiainen, E. M., and Peiponen, K.-E.: On tailoring of nonlinear spectral properties of nanocomposites having Maxwell-Garnett or Bruggeman structure, *Opt. Rev.*, 10, 111–115, doi:10.1007/s10043-003-0111-y, 2003.
- Saarikoski, S., Sillanpää, M., Sofiev, M., Timonen, H., Saarnio, K., Teinilä, K., Karppinen, A., Kukkonen, J., and Hillamo, R.: Chemical composition of aerosols during a major biomass burning episode over northern Europe in spring 2006: Experimental and modelling assessments, *Atmos. Environ.*, 41, 3577–3589, doi:10.1016/j.atmosenv.2006.12.053, 2007.

- 
- von Salzen, K.: Piecewise log-normal approximation of size distributions for aerosol modelling, *Atmos. Chem. Phys.*, 6, 1351–1372, doi:10.5194/acp-6-1351-2006, 2006
- Santee, M. L., Read, W. G., Waters, J. W., Froidevaux, L., Manney, G. L., Flower, D. A., Jarnot, R. F., Harwood, R. S., and Peckham, G. E.: Interhemispheric Differences in Polar Stratospheric HNO<sub>3</sub>, H<sub>2</sub>O, ClO and O<sub>3</sub>, *Science*, 267, 849–852, doi:10.1126/science.267.5199.849, 1995.
- Savenije, M., van Ulft, L. H., van Meijgaard, E., Henzing, J. S., Aan de Brugh, J. M. J., Manders-Groot, A. A. M., and Schaap, M.: Two-way coupling of RACMO2 and LOTOS-EUROS: Implementation of the direct effect of aerosol on radiation, TNO report, 2012.
- Savéry, D. and Cloutier, G.: Modeling of the Acoustic Signal Backscattered by a Biphase Suspension: Application to the Characterization of Red Blood Cell Aggregation, *Acoustical Imaging*, 7, 289–295, doi:10.1007//0-306-47107-8\_40, 2002.
- Schaap, M., Müller, K., and ten Brink, H. M.: Constructing the European aerosol nitrate concentration Field from quality analysis data, *Atmos. Environ.*, 36, 1323–1335, doi:10.1016/S1352-231(01)00556-8, 2002.
- Schaap, M., van Loon, M., ten Brink, H. M., Dentener, F. J., and Bultjes, P. J. H.: Secondary inorganic aerosol simulations for Europe with special attention to nitrate, *Atmos. Chem. Phys.*, 4, 857–874, doi:10.5194/acp-4-857-2004, 2004a.
- Schaap, M., Spindler, G., Schultz, M., Acker, K., Maenhaut, W., Berner, A., Wiedprecht, W., Streit, N., Müller, K., Brüggemann, E., Chi, X., Putaud, J.-P., Hitznerberger, R., Puxbaum, H., Baltensperger, U., and ten Brink, H.: Artefacts in the sampling of nitrate studied in the “INTERCOMP” campaigns of EUROTRAC-AEROSOL, *Atmos. Environ.*, 38, 6487–6496, doi:10.1016/j.atmosenv.2004.08.026, 2004b.
- Schaap, M., Roemer, M., Sauter, F., Boersen, G., Timmermans, R., Bultjes, P. J. H., and Vermeulen, A. T.: LOTOS-EUROS documentation, available at: <http://www.lotos-euros.nl/doc/documentation.html> (last access: December 2011), 2005.
- Schaap, M., Weijers, E. P., Mooibroek, D., Nguyen, L., and Hoogerbrugge, R.: Composition and origin of Particulate Matter in the Netherlands. Results from the Dutch Research Programme on Particulate Matter, 2010.
- Schaap, M., Otjes, R. P., and Weijers, E. P.: Illustrating the benefit of using hourly monitoring data on secondary inorganic aerosol and its precursors for model evaluation, *Atmos. Chem. Phys.*, 11, 11041–11053, doi:10.5194/acp-11-11041-2011, 2011.
- Schumann, U: Large-Eddy Simulation of Turbulent Diffusion with Chemical Reactions in the Convective Boundary Layer, *Atmos. Environ.*, 23, 1713–1727, doi:10.1016/0004-6981(89)90056-5, 1989.

- Segelstein, D. J.: The complex refractive index of water, Master's thesis, University of Missouri-Kansas City, USA, 1981.
- Segers, A., Velthoven, P. V., Bregman, B., and Krol, M.: On the Computation of Mass Fluxes for Eulerian Transport Models from Spectral Meteorological Fields, in: ICCS'02: Proceedings of the International Conference on Computational Science-Part II, Springer-Verlag, London, UK, 767–776, 2002.
- Seibert, P. and Frank, A.: Source-receptor matrix calculation with a Lagrangian particle dispersion model in backward mode, *Atmos. Chem. Phys.*, 4, 51–63, doi:10.5194/acp-4-51-2004, 2004.
- Seinfeld, J. H.: Atmospheric Chemistry and Physics of Air Pollution, Wiley-Interscience, 1986.
- Sekiyama, T. T., Tanaka, T. Y., Shimizu, A., and Miyoshi, T.: Data assimilation of CALIPSO aerosol observations, *Atmos. Chem. Phys.*, 10, 39–49, doi:10.5194/acp-10-39-2010, 2010.
- Shiraiwa, M., Ammann, M., Koop, T., and Poschl, U.: Gas uptake and chemical aging of semi-solid organic aerosol particles, *P. Natl. Acad. Sci. USA*, 108(27), 11003–11008, doi:10.1073/pnas.1103045108, 2011.
- Sihto, S.-L., Kulmala, M., Kerminen, V.-M., Dal Maso, M., Petäjä, T., Riipinen, I., Korhonen, H., Arnold, F., Janson, R., Boy, M., Laaksonen, A., and Lehtinen, K. E. J.: Atmospheric sulphuric acid and aerosol formation: implications from atmospheric measurements for nucleation and early growth mechanisms, *Atmos. Chem. Phys.*, 6, 4079–4091, doi:10.5194/acp-6-4079-2006, 2006.
- Sihto, S.-L., Vuollekoski, H., Leppä, J., Riipinen, I., Kerminen, V.-M., Korhonen, H., Lehtinen, K. E. J., Boy, M., and Kulmala, M.: Aerosol dynamics simulations on the connection of sulphuric acid and new particle formation, *Atmos. Chem. Phys.*, 9, 2933–2947, doi:10.5194/acp-9-2933-2009, 2009.
- Slanina, J., ten Brink, H. M., Otjes, R. P., Even, A., Jongejan, P., Khlystov, A., Waijers-Ijpelaan, A., and Hu, M.: The continuous analysis of nitrate and ammonium in aerosols by the steam jet aerosol collector (SJAC): extension and validation of the methodology, *Atmos. Environ.*, 35, 2319–2330, doi:10.1016/S1352-2310(00)00556-2, 2001.
- Slinn, S. A. and Slinn, W. G. N.: Predictions for particle deposition on natural waters, *Atmos. Environ.*, 14, 1013–1016, doi:10.1016/0004-6981(80)90032-3, 1980.
- Sofiev, M., Vankevich, R., Lotjonen, M., Prank, M., Petukhov, V., Ermakova, T., Koskinen, J., and Kukkonen, J.: An operational system for the assimilation of the satellite information on wild-land fires for the needs of air quality modelling and forecasting, *Atmos. Chem. Phys.*, 9, 6833–6847, doi:10.5194/acp-9-6833-2009, 2009.

- 
- Steenefeld, G. J., van de Wiel, B. J. H., and Holtslag, A. A. M.: Diagnostic equations for the stable boundary layer height: Evaluation and dimensional analysis, *J. Appl. Meteorol. Clim.*, 46, 212–225, doi:10.1175/JAM2454.1, 2007.
- Stelson, A. W. and Seinfeld, J. H.: Relative humidity and temperature dependence of the ammonium nitrate dissociation constant, *Atmos. Environ.*, 16, 983–992, doi:10.1016/0004-6981(82)90184-6, 1982.
- Sternbeck, J., Sjödin, Å., and Andréasson, K.: Metal emissions from road traffic and the influence of resuspension – results from two tunnel studies, *Atmos. Environ.*, 36, 4735–4744, doi:10.1016/S1352-2310(02)00561-7, 2002.
- Stier, P., Feichter, J., Kinne, S., Kloster, S., Vignati, E., Wilson, J., Ganzeveld, L., Tegen, I., Werner, M., Balkanski, Y., Schulz, M., Boucher, O., Minikin, A., and Petzold, A.: The aerosol-climate model ECHAM5-HAM, *Atmos. Chem. Phys.*, 5, 1125–1156, doi:10.5194/acp-5-1125-2005, 2005.
- Stone, V. and Donaldson, K.: Small particles – Big problem, *Aerosol Soc. Newslett.*, 33, 12–14, 1998.
- Stratton, J. A. and Houghton, H. G.: A theoretical investigation of the transmissions of light through fog, *Phys. Rev.* 38, 159–165, doi:10.1103/PhysRev.38.159, 1931.
- Stull, R. B.: *An Introduction to Boundary Layer Meteorology*, Kluwer Academic Publishers, 1988.
- Sykes, R. L., Henn, D. S., Parker, S. F., and Lewellen, W. S.: Large-eddy simulation of a turbulent reacting plume, *Atmos. Environ.*, 26A, 2565–2574, doi:10.1016/0960-1686(92)90109-X, 1992.
- Takahama, S., Wittig, A. E., Vayenas, D. V., Davidson, C. I., and Pandis, S. M.: Modeling the diurnal variation of nitrate during the Pittsburgh Air Quality Study, *J. Geophys. Res.*, 109, D16S06, doi:10.1029/2003JD004149, 2004.
- Tang, I. N.: Chemical and size effects of hygroscopic aerosols on light scattering coefficients, *J. Geophys. Res.*, 101, 19245–19250, doi:10.1029/96JD03003, 1996.
- Tegen, I., Hollrig, P., Chin, M., Fung, I., Jacob, D., and Penner, J.: Contribution of different aerosol species to the global aerosol extinction optical thickness: Estimates from model results, *J. Geophys. Res.*, 102, 23895–23915, doi:10.1029/97JD01864, 1997.
- Tennekes, H. and Driedonks, A. G. M.: Basic entrainment equations for the Atmospheric boundary layer, *Bound. Lay. Meteorol.*, 20, 515–531, doi:10.1007/BF00122299, 1981.
- Textor, C., Schulz, M., Guibert, S., Kinne, S., Balkanski, Y., Bauer, S., Berntsen, T., Berglen, T., Boucher, O., Chin, M., Dentener, F., Diehl, T., Easter, R.,

- Feichter, H., Fillmore, D., Ghan, S., Ginoux, P., Gong, S., Grini, A., Hendricks, J., Horowitz, L., Huang, P., Isaksen, I., Iversen, I., Kloster, S., Koch, D., Kirkevåg, A., Kristjansson, J. E., Krol, M., Lauer, A., Lamarque, J. F., Liu, X., Montanaro, V., Myhre, G., Penner, J., Pitari, G., Reddy, S., Seland, Ø., Stier, P., Takemura, T., and Tie, X.: Analysis and quantification of the diversities of aerosol life cycles within AeroCom, *Atmos. Chem. Phys.*, 6, 1777–1813, doi:10.5194/acp-6-1777-2006, 2006.
- Thomas, R. M., Trebs, I., Otjes, R., Jongejan, P. A. C., ten Brink, H., Phillips, G., Kortner, M., Meixner, F. X., and Nemitz, E.: An automated analyzer to measure surface-atmosphere exchange fluxes of water soluble inorganic aerosol compounds and reactive trace gases, *Environ. Sci. Technol.*, 43, 1412–1418, doi:10.1021/es8019403, 2009.
- Tiedtke, M.: A Comprehensive Mass Flux Scheme for Cumulus Parameterization in Large-Scale Models, *Mon. Weather Rev.*, 117, 1779, doi:10.1175/1520-0493(1989)117<1779:ACMFSF>2.0.CO;2, 1989.
- Toon, O. B., Pollack, J. B., and Khare, B. N.: Optical-Constants of Several Atmospheric Aerosol Species – Ammonium-Sulfate, Aluminum-Oxide, and Sodium-Chloride, *J. Geophys. Res.*, 81, 5733–5748, doi:10.1029/JC081i033p05733, 1976.
- Trebs, I., Meixner, F. X., Slanina, J., Otjes, R., Jongejan, P., and Andreae, M. O.: Real-time measurements of ammonia, acidic trace gases and water-soluble inorganic aerosol species at a rural site in the Amazon Basin, *Atmos. Chem. Phys.*, 4, 967–987, doi:10.5194/acp-4-967-2004, 2004.
- Troen, I. B. and Mahrt, L.: A simple model of the atmospheric boundary layer; sensitivity to the surface evaporation, *Bound. Lay. Meteorol.*, 37, 129–148, doi:10.1007/BF00122760, 1986.
- Varutbangkul, V., Brechtel, F. J., Bahrein, R., Ng, N. L., Keywood, M. D., Kroll, J. H., Flagan, R. C., Seinfeld, J. H., Lee, A., and Goldstein, A. H.: Hygroscopic of secondary organic aerosols formed by oxidation of cycloalkanes, monoterpenes, sesquiterpenes, and related compounds, *Atmos. Chem. Phys.*, 6, 2367–2388, doi:10.5194/acp-6-2367-2006, 2006.
- Vecchi, R., Valli, G., Fermo, P., D’Alessandro, A., Pizzalunga, A., and Bernardoni, V.: Organic and inorganic sampling artefacts assessment, *Atmos. Environ.*, 43, 1713–1720, doi:10.1016/j.atmosenv.2008.12016, 2009.
- Vehkamäki, H., Kulmala, M., Napari, I., Lehtinen, K. E. J., Timmreck, C., Noppel, M., and Laaksonen, A.: An improved parameterization for sulfuric acid – water nucleation rates for tropospheric and stratospheric conditions, *J. Geophys. Res.*, 107, 4622, doi:10.1029/2002JD002184, 2002.
- Vestreng, V., Myhre, G., Fagerli, H., Reis, S., and Tarrasón, L.: Twenty-five years of continuous sulphur dioxide emission reduction in Europe, *Atmos. Chem. Phys.*, 7, 3663–3681, doi:10.5194/acp-7-3663-2007, 2007.

- 
- Vestreng, V., Ntziachristos, L., Semb, A., Reis, S. Isaksen, I. S. A., and Tarrasón, L.: Evolution of NO<sub>x</sub> emissions in Europe with focus on road transport control measures, *Atmos. Chem. Phys.*, 9, 1503–1520, doi:10.5194/acp-9-1503-2009, 2009.
- Vignati, E., Wilson, J., and Stier, P.: M7: An efficient size-resolved aerosol microphysics module for large-scale aerosol transport models, *J. Geophys. Res.*, 109, D22202, doi:10.1029/2003JD004485, 2004.
- Vignati, E., Facchini, M. C., Rinaldi, M., Scannell, C., Ceburnus, D., Sciare, J., Kanakidou, M., Myriokefalitakis, S., Dentener, F., and O'Dowd, C. D.: Global scale emission and distribution of sea-spray aerosol: Sea-salt and organic enrichment, *Atmos. Environ.*, 44, 670–677, doi:10.1016/j.atmosenv.2009.11.013, 2010a.
- Vignati, E., Karl, M., Krol, M., Wilson, J., Stier, P., and Cavalli, F.: Sources of uncertainties in modelling black carbon at the global scale, *Atmos. Chem. Phys.*, 10, 2595–2611, doi:10.5194/acp-10-2595-2010, 2010b.
- Vilà-Guerau de Arellano, J., Duynkerke, P. G., and Bultjes, P. J. H.: The divergence of the turbulent diffusion flux in the surface layer due to Chemical reactions: the NO-O<sub>3</sub>-NO<sub>2</sub> system, *Tellus*, 45B, 23–33, doi:10.1034/j.1600-0889.1993.00002.x, 1993a.
- Vilà-Guerau de Arellano, J., Duynkerke, P. G., Jonker, P. J., and Bultjes, P. J. H.: An Observational Study on the Effects of Time and Space Averaging in Photochemical Models, *Atmos. Environ.*, 27A, 353–362, doi:10.1016/0960-1686(93)90109-C, 1993b.
- Vilà-Guerau de Arellano, J., Kim, S.-W., Barth, M. C., and Patton, E. G.: Transport and chemical transformations influences by shallow cumulus over land, *Atmos. Chem. Phys.*, 5, 3219–3231, doi:10.5194/acp-5-3219-2005, 2005.
- Volkamer, R., Jizenez, J. L., San Martini, F., Dzepina, K., Zhang, Q., Salcedo, D., Molina, L. T., Worsnop, D. R., and Molina, M. J.: Secondary organic aerosol formation from anthropogenic air pollution: Rapid and higher than expected, *Geophys. Res. Lett.*, 33, LT17811, doi:10.1029/2006GL026899, 2006.
- van der Werf, G. R., Randerson, J. T., Giglio, L., Collatz, G. J., Kasibhatla, P. S., and Arellano Jr., A. F.: Interannual variability in global biomass burning emissions from 1997 to 2004, *Atmos. Chem. Phys.*, 6, 3423–3441, doi:10.5194/acp-6-3423-2006, 2006.
- White, W. H. and Roberts, P. T.: On the nature and origins of visibility-reducing aerosols in the Los Angeles air basin, *Atmos. Environ.*, 11, 803–812, doi:10.1016/0004-6981(77)90042-7, 1977.
- Wichink Kruit, R. J., van Pul, W. A. J., Otjes, R. P., Hofschreuder, P., Jacobs, A. F. G., and Holtslag, A. A. M.: Ammonia fluxes and derived canopy compensation points over non-fertilized agricultural grassland in The Netherlands

- using the new gradient ammonia – high accuracy – monitor (GRAHAM), *Atmos. Environ.*, 41, 1275–1287, doi:10.1016/j.atmosenv.2006.09.039, 2007.
- Wang, J., Hoffmann, A. A., Park, R. J., Jacob, D. J., and Martin, S. T.: Global distribution of solid and aqueous sulfate aerosols: Effect of the hysteresis of particle phase transition, *J. Geophys. Res.*, 103, D11206, doi:10.1029/2007JD009367, 2008.
- Wang, S. C. and Flagan, R. C.: Scanning electrical mobility spectrometer, *Aerosol Sci. Technol.*, 13, 230–240, doi:10.1080/02786829008959441, 1990.
- Weast, R. C.: *Handbook of Chemistry and Physics*, 66th edn., CRC Press, Florida, USA, 1985.
- Wehner, B., Siebert, H., Ansmann, A., Ditas, F., Seifert, P., Stratmann, F., Wiedensohler, A., Apituley, A., Shaw, R. A., Manninen, H. E., and Kulmala, M.: Observations of turbulence-induced new particle formation in the residual layer, *Atmos. Chem. Phys.*, 10, 4319–4330, doi:10.5194/acp-10-4319-2010, 2010.
- Weijers, E. P., Schaap, M., Nguyen, L., Matthijssen, J., Denier van der Gon, H. A. C., ten Brink, H. M., and Hoogerbrugge, R.: Anthropogenic and natural constituents in particulate matter in the Netherlands, *Atmos. Chem. Phys.*, 11, 2281–2294, doi:10.5194/acp-11-2281-2011, 2011.
- Wexler, A. S. and Seinfeld, J. H.: Analysis of aerosol ammonium nitrate departures from equilibrium during SCAQS, *Atmos. Environ.*, 26A, 579–591, doi:10.1016/0960-1686(92)90171-G, 1992.
- Wicker, L. J. and Skamarock, W. C.: Time splitting methods for elastic models using forward time schemes, *Mon. Weather Rev.*, 130, 2088–2097, doi:10.1175/1520-0493(2002)130<2088:TSMFEM>2.0.CO;2, 2002.
- Wiedensohler, A.: An approximation of the bipolar charge distribution for particles in the submicron size range, *J. Aerosol Sci.*, 19, 387–389, doi:10.1016/0021-8502(88)90278-9, 1988.
- Williams, J. E. and van Noije, T. P. C.: On the updating of the modified Carbon Bond Mechanism IV for use in global Chemistry Transport Models, Tech. Rep. TR 2008-02, KNMI, De Bilt, The Netherlands, 2008.
- Wilson, J., Cuvelier, C., and Raes, F.: A modeling study of global mixed aerosol fields, *J. Geophys. Res.*, 106, 34081–34108, 2001.
- Wolff, V., Trebs, I., Foken, T., and Meixner, F. V.: Exchange of reactive nitrogen compounds: concentrations and fluxes of total ammonium and total nitrate above a spruce canopy, *Biogeosciences*, 7, 1729–1744, doi:10.5194/bg-7-1729-2010, 2010.
- Wolff, V., Meixner, F. X., and Trebs, I.: Mixing ratios and exchange processes of ammonia-nitric acid-ammonium nitrate triad above a spruce forest canopy. In:

- H. Lacoste-Francid (Editor), *Earth Observations for Land-Atmosphere Interactions Science*, Frascati, Italy. European Space Agency, ESTEC, Noordwijk, The Netherlands, 2011.
- Wyers, G. P. and Duyzer, J. H.: Micrometeorological measurement of the dry deposition flux of sulphate and nitrate aerosols to coniferous forest, *Atmos. Environ.*, 31(3), 333–343, doi:10.1016/S1352-2310(96)00188-4, 1997.
- Yttri, K. E., Aas, W., Bjerke, A., Cape, J. N., Cavalli, F., Ceburnis, D., Dye, C., Emblico, L., Facchini, M. C., Forster, C., Hanssen, J. E., Hansson, H. C., Jennings, S. G., Maenhaut, W., Putaud, J. P., and Tørseth, K.: Elemental and organic carbon in PM<sub>10</sub>: a one year measurement campaign within the European Monitoring and Evaluation Programme EMEP, *Atmos. Chem. Phys.*, 7, 5711–5725, doi:10.5194/acp-7-5711-2007, 2007.
- Yu, S., Dennis, R., Roselle, S., Nenes, A., Walker, J., Eder, B., Schere, K., Swall, J., and Robarge, W.: An assessment of the ability of three-dimensional air quality models with current thermodynamic equilibrium models to predict aerosol NO<sub>3</sub><sup>-</sup>, *J. Geophys. Res.*, 10, D07S13, 1–22, doi:10.1029/2004JD004718, 2005.
- Yu, X.-Y., Lee, T., Ayres, B., Kreidenweis, S. M., Malm, W., and Collett, J. L. J.: Loss of fine particulate ammonium from denuded nylon filters, *Atmos. Environ.*, 40, 4797–4807, doi:10.1016/j.atmosenv.2006.03.061, 2006.
- Zhang, J., Charmeides, W. L., Weber, R., Cass, G., Orsini, D., Edgerton, E., Jongejan, P., and Slanina, J.: An evaluation of the thermodynamic equilibrium assumption for fine particulate composition: Nitrate and ammonium during the 1999 Atlanta Supersite experiment, *J. Geophys. Res.*, 108, 8414, doi:10.1029/2001JD001592, 2003.
- Zhang, X. and McMurry, P. H.: Evaporative losses of fine particulate nitrates during sampling, *Atmos. Environ.*, 26A, 3305–3312, doi:10.1016/0960-1686(92)90347-N, 1992.
- Zhange, Y., ten Brink, H. M., Slanina, J., and Wyers, G. P.: The influence of ammonium nitrate equilibrium on the measurement of exchange fluxes of ammonia and nitric acid. In G. J. Heij and J. W. Erisman (Editors), *Acid Rain Research: Do we have enough Answers?*, Elsevier Science B. V., 103–112, 1995.
- Zieger, P., Weingartner, E., Henzing, J., Moerman, M., de Leeuw, G., Mikkilä, J., Ehn, M., Petäjä, T., Clémer, K., van Roozendaal, M., Yilmaz, S., Frieß, U., Irie, H., Wagner, T., Shaiganfar, R., Beirle, S., Apituley, A., Wilson, K., and Baltensperger, U.: Comparison of ambient aerosol extinction coefficients obtained from in-situ, MAX-DOAS and LIDAR measurements at Cabauw, *Atmos. Chem. Phys.*, 11, 2603–2624, doi:10.5194/acp-11-2603-2011, 2011.



# Publications

---

- Aan de Brugh, J. M. J., Schaap, M., Vignati, E., Dentener, F., Kahnert, M., Sofiev, M., Huijnen, V., and Krol, M. C.: The European aerosol budget in 2006, *Atmos. Chem. Phys.*, 11, 1117–1139, doi:10.5194/acp-11-1117-2011, 2011.
- Aan de Brugh, J. M. J., Henzing, J. S., Schaap, M., Morgan, W. T., van Heerwaarden, C. C., Weijers, E.P., Coe, H., and Krol, M. C.: Modelling the partitioning of ammonium nitrate in the convective boundary layer, *Atmos. Chem. Phys.*, 12, 3005–3023, doi:10.5194/acp-12-3005-2012, 2012.
- Aan de Brugh, J. M. J., Ouwersloot, H. G., Vilà-Guerau de Arellano, J., and Krol, M. C.: A Large-Eddy Simulation of the Phase Transition of Ammonium Nitrate in a Convective Boundary Layer, *J. Geophys. Res.*, under review, 2012.
- Aan de Brugh, J. M. J., Schaap, M., Savenije, M., Henzing, J. S., Manders, A. M. M., Kahnert, M., and Krol, M. C.: The Generic Aerosol Optics Toolbox: an aerosol optics module for any atmospheric model, *Geosci. Model Dev. Discuss.*, in preparation, 2012.
- van Houselt, A., Gnielka, T., Aan de Brugh, J. M. J., Oncel, N., Kockmann, D., Heid, R., Bohnen, K.-P., Poelsema, B., and Zandvliet, H. J. W.: Peierls instability in Pt chains on Ge(001), *Surf. Sci.*, 602, 1731–1735, doi:10.1016/j.susc.2008.01.040, 2008.
- Thijssen, W. H. A., Strange, M., Aan de Brugh, J. M. J., and van Ruitenbeek, J. M.: Formation and properties of metal-oxygen atomic chains, *New J. Phys.*, 10, 033005, doi:10.1088/1367-2630/10/3/033005, 2008.



# Acknowledgements

---

A PhD programme is like a roller coaster. It starts with an uphill battle, slowly making progress without any noticeable change in the situation. After reaching the critical point, anything can happen in a wide spectrum between glorious triumph and bitter misery, logically ending up with a combination of both. And at the end, you feel at least four years older and an experience richer. Like a in a roller coaster, good guidance is essential for survival. Therefore, I would first like to thank my supervisors.

Maarten, bedankt dat ik de mogelijkheid heb gekregen om een promotie te doen. Ik wil je ook bedanken voor het leren van talloze wetenschappelijke vaardigheden, zoals het omgaan met onzekerheden en het wetenschappelijk schrijven. Zo ben ik ontwikkeld van een natuurkundige die gefrustreerd was over het feit dat TM5 geen quantummodel is, naar iemand die in staat is om zo ongeveer een artikel te schrijven.

Martijn, jij weet als geen ander mijn zelfvertrouwen omhoog te helpen door, waar mogelijk, te accentueren wat wel goed gaat. Na werkbeprekingen met jou krijg ik meer het idee dat het werk leuk is, dat ik het beter kan, en mijn papers worden er beter van. Ook heb ik bij jou veel persoonlijke steun gevonden in tijden dat het moeilijk ging. Jij weet je goed te verplaatsen in een AIO die nog niet alles zo perfect kan en weet.

Marina and Eduardo, I am glad to have you as paranymphs. Both of you have been a great support for me, both in good and in difficult times. I have the impression that you may know me even better than I know myself, even though you have never been in the same office as me. I am looking forward to seeing your defences. Eduardo, I never felt so at ease while discussing about depression cards or about bitter misery, as with you. Even planning a PhD-programme can be funny this way. Marina, I really appreciate the personal conversations we have had. I also appreciate your role in making the group more feminine in the beginning of 2010.

Ik wil graag de mensen van ons kantoortje in Atlas bedanken, hoe lang deze tijd ook in het verleden lijkt te liggen. Chiel, Joel, Daniëlle, Bram en Bart, bedankt voor alle interessante gesprekken en discussies over wolken, large-eddy simulaties, voetbal en vooral niet te veel over chemie. Jullie vormden de inspiratie voor mij om eens een keer echt te integreren in deze vakgroep door na mijn eerste paper iets met grenslagen te gaan doen.

Ik wil graag de mensen van ons kantoortje op Aqua bedanken. Niet dat dit kantoortje er nog staat, maar toch. Bert, Kees (dank God dat je er nog bent), Frits, Joel en Bart. Wederom bedankt over de gesprekken over andere onderwerpen dan chemie, zoals stadsklimaat en blauwe tuinslangen die symbool staan voor de Obukhovlengte.

Dan wil ik graag ons kamertje op Lumen bedanken: Miranda, Anneke, Natalie en Daniëlle. In plaats van oude beeldschermen en niet-werkende scanners hadden we zowaar planten in onze kamer, iets waar ik door mijn Y-chromosoom natuurlijk nooit het initiatief voor durfde te nemen. En eindelijk kwamen de kannen thee tenminste op.

Though I already mentioned quite a few of you as supervisor, paronymph or office mate in any of our buildings, I want to thank all the fellow people from the Meteorology and Air Quality group for the nice lunches, dinners, game evenings, pub visits and trips to Nijmegen and The Hague. Chiel, Jordi and Huug, thanks for infesting me with large-eddy simulations. It worked out and ended up as a chapter in this thesis. Michał, it was nice to bluff some Polish words with you. Dziękuję. Denica and Marie, it was to sing with you at the BBOS. Gert-Jan, you learned me a German that is much easier to use than the one that I failed to learn in secondary school. Now, I can finally try to talk to Joel.

Ik wil ook graag mijn collega's van TNO bedanken. Natuurlijk heb ik de meeste van jullie al geciteerd (een citatie is de grootst mogelijke dank in de wetenschappelijke wereld) en zullen ook veel van jullie zich aangesproken gaan voelen als ik het straks co-auteurs ga hebben. Monique, ik wil jou nog even speciaal bedanken. We zijn rond dezelfde tijd begonnen bij precies dezelfde begeleider binnen TNO, over andere aërosolen, maar wel allebei over aërosolen. Het was fijn om je te leren kennen en om er vervolgens achter te komen dat we na de interne verhuizing in dezelfde flexruimte terecht zijn gekomen. Ik kijk al uit naar jouw verdediging.

Nu ik toch bij TNO ben, kunnen jullie al helemaal niet ontbreken. Ik begin bij jou, Ina. Jij hebt heel veel voor mij betekend vanaf het moment dat je heb leren kennen. Jij hebt mij heel veel gesteund in de tijd van solliciteren en andere vormen van onzekerheden. Het is leuk om te zien hoe het contact met jou overslaat naar de andere secretaresses. Fijn om met jullie te lunchen en te wandelen door de botanische tuinen. Dit was ook niet mogelijk geweest als het niet zo goed had geklikt met jullie. Dus jullie allemaal, bedankt. Anke, ik wil jou nog even expliciet noemen, niet zozeer omdat je van onze groep bent, maar omdat ik soms vergeet dat het nog niet zo lang terug is dat je Marita kwam vervangen. Marita, ik voel me vereerd dat jij tussen je ziekte door nog een gaatje hebt weten te vinden om bij mijn afscheidsetentje te komen.

Dan wil ik graag ons renclubje bedanken, Anneke, Peter, Petra en alle mensen die een ook paar keer zijn meegeweest. Het rennen op maandag tijdens de lunch zorgt voor een betere fysieke en psychische gezondheid. Ook wil ik Marleen, Bram en Marjolein bedanken voor prettige samenwerking bij het organiseren van ons symposium. Nu heeft het lot bepaald dat mijn verdediging precies twee jaar na het symposium valt, op 22 februari. Ik mag van de wetenschap niet in symboliek geloven, dus ik laat de verdere theorieën maar achterwege.

I would like to thank the BBOS community. The BBOS is a good way to

---

get in touch with fellow PhD-students. Special thanks to Célia for her great effort in organising musical activities for the BBOS. Thanks also to everyone who participated in singing or playing with us. It is a great effort to perform songs with several voices with a such a small group. These activities makes the BBOS more like a community than just an event that takes place once a year.

I would like to thank everyone who was involved in the nice course in Hyytiälä (Finland). Thanks for persuading me to jump into the lake when leaving the sauna and for the suicidal adventure in the national park. O yes, and thanks for the knowledge about fluxes and new-particle formation. I also would like to thank the people that were involved in the nice course in Paphos (Cyprus). Thanks for the beach visits and going out in town. Special thanks to Ivar, Michał, Eduardo and Huug for one specific memorable evening. Also thanks for officially turning me into a boundary-layer meteorologist.

I would like to thank all the co-authors of my publications. Without your support, I could not have completed the papers and the PhD. I am pleased to have cooperated with such a various group of people.

I would like to thank Vivavoce. It was nice to make music together with you on Sundays. Thanks to you, I am no longer a Matthäus-Passion virgin. Finally. Thanks to WSKOV for making a lot of music and a lot of fun. Thanks Elysa, Sjoerd, Sanne, Josepa, Ab, Sylvia and Irene for the cooperation in the board in 2009 and for reading my minutes.

En hoe cliché het dan ook is. Ik wil natuurlijk vooral mijn vriendinnetje bedanken. Walinka, ik hou van jou. Kocham cię. Jij bent de belangrijkste reden dat ik mijn PhD heb overleefd. Daar kan geen enkel stom paper tegenop. Ook tof om samen te eten met je vriendinnen. Jullie zijn een gezellig groepje. Ik wil ook mijn ouders en mijn broer bedanken voor de leuke weekenden samen, de discussies over rennen, iPads en Magister, en voor de mentale steun gedurende deze periode.



# Index

---

- acid displacement, 49, 87, 140, 141
- AERONET, 31, 49, 118, 119
- aerosol optical depth, 47–51, 62–70, 121, 122, 132, 133, 137
- aging, 21, 23, 24
- air quality standards, 19, 40, 41
- ammonium nitrate, 26, 27, 44, 48, 72–75, 77, 78, 82–89, 94–96, 98–100, 103, 105–107, 109–116, 137, 138, 140, 141
- Ångström parameter, 48–51, 62–66, 69, 121, 122
- asymmetry parameter, 34, 35, 121, 122, 124–126, 129, 130
  
- boundary layer, 51, 54, 57, 60, 77, 84, 94, 95, 98, 107, 109, 137, 138
- budget, 26, 27, 40, 41, 55, 57–62, 69, 136, 141
- bulk aerosol approach, 31, 44, 76, 77
  
- climate, 19, 20, 40, 72, 98, 118
- coagulation, 21, 23, 43, 44
- column model, 36, 37, 72, 74, 76–82, 84–92, 137, 138
- concentrations, 21, 49–56, 69
- condensation, 20, 21, 23, 24, 43, 44, 80–82, 96
  
- dry deposition, 23, 25, 42, 44, 45
  
- effective-medium theory, 47, 80, 120, 121, 130, 131
- EMEP, 30, 48
- emission, 20–24, 45–47, 67–70, 136, 137
  
- extinction cross section, 34, 35, 121
- extinction efficiency, 122–127, 129–131
  
- flux, 99, 107–111, 116, 138
  
- health, 18, 40, 41
  
- ISORROPIA, 77, 78, 82–84, 101
  
- large-eddy simulation, 36, 37, 98, 99, 101, 102, 138
- large-scale models, 36, 37, 41, 94, 95, 119, 132, 133, 137–142
- lifetime, 25, 57, 58
- lognormal distribution, 32, 33, 43, 44, 129–131
- lookup table (optics), 47, 48, 130, 131
- lookup table generator, 127–129
  
- M7, 32, 42–44, 46
- MARGA, 75
- measurements, 30, 31, 48, 49, 73–76, 114, 115, 118, 119
- meteorological conditions, 42, 75, 84, 85, 102–105, 113
- Mie curve, 122–127, 130
- Mie regime, 125
- Mie theory, 34, 35, 47, 120, 139
- mixing state, 21, 23, 25, 26, 140, 141
- modal aerosol approach, 32, 33, 43, 44, 140
  
- nucleation, 23, 24, 43, 44, 47
  
- optics, 26, 27, 34–36, 47, 48, 78–82, 90–94, 118–134, 138, 139

- partitioning timescale, 77, 78, 84–89, 91, 92, 95, 99, 101, 102, 109–116, 137, 138, 141
- Rayleigh regime, 123, 125
- refractive index, 34, 78, 80, 120–122, 130, 131
- refractive index database, 47, 130, 131
- relative-humidity correction, 76, 90–94
- scattering coefficient, 90–92, 96
- single-scattering albedo, 34, 35, 121, 122, 124, 125, 129, 130
- size distribution, 18, 19, 21, 23–26, 30–36, 43, 45–48, 78–82, 96, 119, 140
- size parameter, 78, 122–127, 129–131
- skewness, 109–111, 114–116, 138
- SMPS, 30, 31, 75, 76, 78, 79
- TM5, 42, 70
- turbulence, 27, 98, 103, 105–107, 109, 110, 112–116, 138
- turbulent timescale, 99, 101–104, 110, 111, 116, 138
- wet deposition, 25, 42, 45, 64, 66, 67, 69, 136, 137, 139, 140



Netherlands Research School for the  
Socio-Economic and Natural Sciences of the Environment

# C E R T I F I C A T E

The Netherlands Research School for the  
Socio-Economic and Natural Sciences of the Environment  
(SENSE), declares that

***Joost Martinus Jacobus  
Aan de Brugh***

born on 23 March 1982 in Boxmeer, the Netherlands

has successfully fulfilled all requirements of the  
Educational Programme of SENSE.

Wageningen, 22 February 2013

the Chairman of the SENSE board

Prof. dr. Rik Leemans

the SENSE Director of Education

Dr. Ad van Dommelen

The SENSE Research School has been accredited by the Royal Netherlands Academy of Arts and Sciences (KNAW)



K O N I N K L I J K E N E D E R L A N D S E  
A K A D E M I E V A N W E T E N S C H A P P E N



The SENSE Research School declares that **Mr. Joost Aan de Brugh** has successfully fulfilled all requirements of the Educational PhD Programme of SENSE with a work load of 46 ECTS, including the following activities:

#### SENSE PhD Courses

- o Environmental Research in Context
- o Research Context Activity: Co-organizing WIMEK/SENSE Symposium on Modelling & Observing Earth Systems Compartments, Wageningen, 22 February 2011

#### Other PhD and Advanced MSc Courses

- o Biogeochemistry and -physics of the lower atmosphere
- o IDL (Interactive Data Language) Programming
- o Physics and chemistry of air pollution and their effects, Marie Curie-iLEAPS
- o Earth Science and Applications using Imaging Spectroscopy
- o Atmospheric dynamics
- o Atmospheric chemistry and air quality
- o Scientific Publishing
- o Scientific Writing
- o Career Assessment

#### Management and Didactic Skills Training

- o Assistant lecturer for the course 'Inleiding atmosfeer'
- o Development of graphical software for students and clients: A chemical box-model, an aerosol-dynamics box-model, a generic data processor and visualiser and statistics tool, and an aerosol size-distribution fitter

#### Oral Presentations

- o *The M7 aerosol model – Aerosols in the Netherlands*, BBOS autumn symposium, 22-24 October 2008, Texel, The Netherlands
- o *M7 in TM5*, TM meeting, 1-2 December 2008, Utrecht, The Netherlands
- o *TM5 budgets*, TM meeting, 8-9 June 2009, Ispra, Italy
- o *M7 development*, TM meeting, 7-8 December 2009, Wageningen, The Netherlands
- o *The European aerosol budget in 2006*, TM meeting, 21-22 June 2010, Heraklion, Crete
- o *Modelling the partitioning of ammonium nitrate in the convective boundary layer*, *BBOS BLT workshop, 27 May 2011, De Bilt, The Netherlands*
- o *Circulation and phase transition of ammonium nitrate in the convective boundary layer*, WIMEK/SENSE symposium 2012, 1 March 2012, Wageningen, The Netherlands

SENSE Coordinator PhD Education and Research

Mr. Johan Feenstra

This PhD-project was funded by TNO.

The project is supported by EU FP7 IP PEGASOS (FP7-ENV-2010/265148).

The model calculations presented in chapters 3 and 5 were supported by the National Computing Facilities Foundation (NCF).

Financial support from Wageningen University for printing this thesis is gratefully acknowledged.

The cover image is based on contents from:

<http://good-wallpapers.com/>

<http://worldskincolors.com/>

<http://www.clker.com/>



Printed by Gildeprint

